Technical Report

374

J. V. Evans

Ionospheric Backscatter Observations at Millstone Hill

ESRL

22 January 1965

Lincoln Laboratory

MASSACHUSETTS INSTITUTE OF TECHNOLOGY

Lexington, Massachusetts

MASSACHUSETTS INSTITUTE OF TECHNOLOGY

LINCOLN LABORATORY

IONOSPHERIC BACKSCATTER OBSERVATIONS
AT MILLSTONE HILL

J. V. EVANS

Group 31

TECHNICAL REPORT 374

22 JANUARY 1965

LEXINGTON   MASSACHUSETTS

ABSTRACT

Studies of the electron-density, electron and ion temperatures in the F-region were made by means of ground-based radar observations at the Millstone Hill Radar Observatory. A 70-meter parabolic antenna directed vertically and a 2.5-Mw pulse radar operating at 440 Mcps were employed for these measurements which were conducted for periods of 30 hours at approximately weekly intervals throughout 1963. Examination of the echo power as a function of height leads to a profile of electron density with height, provided the electron and ion temperatures are the same ($T_e = T_i$). Additional measurements of the spectra of the signals corresponding to different heights permit the ratio T_e/T_i to be determined and, where this is different from unity, the observed profile can then be corrected for the effect on the scattering introduced by the inequality in temperature.

Results of observations extending over a period of one year from February 1963 to January 1964 are presented. The ratio T_e/T_i achieved a maximum value ~2.0 to 2.6 at a height of about 300 km soon after dawn, irrespective of the season. There was little change in height dependence in this ratio throughout the daylight hours, and at sunset the ratio fell with a time constant of the order of an hour. At night T_e/T_i was occasionally close to unity, but more often a significant difference remained in the temperatures at all heights. Ion temperature increased with height at all times, but above 500 km this may be due in part to the presence of an unknown amount of He^+ ions, which considerably affects the interpretation of the signal spectra. Electron temperatures were largely independent of height above about 300 km. Evidence is presented of ionospheric heating during magnetically disturbed conditions, but it is shown that this is only of great importance at night.

TABLE OF CONTENTS

IONOSPHERIC BACKSCATTER OBSERVATIONS
AT MILLSTONE HILL

I. INTRODUCTION

In recent years the study of the upper part of the earth's ionosphere has received considerable impetus from the development of satellite and rocket methods of exploration. In the measurement of electron density, outstanding results have been obtained with the satellite Ariel and the top-side sounder Alouette. In addition, the rocket measurements made from Wallops Island, Virginia have been particularly successful.[1] Partly as a result of this work, and partly from the study of the drag on satellites produced by the neutral atmospheric constituents, early ideas concerning the behavior of this region have been abandoned. Until very recently it was widely believed that, above the peak of the F-region, O^+ was the principal ion over a wide range of heights. It was also thought that the temperatures of the ions T_i and electrons T_e were equal and independent of height, and that the electron-density distribution was wholly controlled by diffusion.[2-5] Thus the electron density would decrease with altitude with a scale height $H = k(T_e + T_i)/m_i g = 2kT_i/m_i g$, where k is Boltzmann's constant and m_i is the mass of atomic oxygen. In this model, H is not expected to vary significantly with height, and some rocket experiments supported this prediction. This model has given way to one more complex as a consequence of observations which show that: (a) the uppermost parts of the ionosphere con-sist of regions in which helium and hydrogen ions predominate,[6-9] (b) the electron and ion temperatures need not be the same,[10-14] (c) charge exchange between O^+ and H^+ (Ref. 15) governs the proton distribution, and diffusive equilibrium of the separate constituents may not be established until heights of 700 km are reached.[16]

The results obtained by the topside sounder Alouette indicate that very rarely does the upper F-region electron density exhibit constant scale height H (Refs. 17 and 18). This result is interpreted as indicating that one or more of the above effects operate at most latitudes. In addition, this satellite has shown that the equatorial anomaly observed with ground-based iono-sondes extends into the upper F-region over a range of geomagnetic latitudes of at least ±20° (Refs. 19 and 20). Over these regions, and possibly others, the geomagnetic field plays a signif-icant role in governing the electron-density distribution. Theoretical attempts to account for this control have recently been made,[21-24] but it cannot yet be claimed that all the features are understood.[19]

At high latitudes geomagnetic control may disappear but significant fluxes of precipitating particles may contribute to the ionization, particularly in the auroral zones. It seems, there-fore, that only in temperate latitudes is the F-region likely to be largely uninfluenced either by geomagnetic control of diffusion or additional sources of ionization from the Van Allen belts.

In these latitudes an understanding of the behavior of the ionospheric F-layer could perhaps be derived from observations in which the following quantities are measured simultaneously as functions of height: (a) electron density; (b) electron temperature; (c) ion temperature; (d) ion composition; (e) neutral density; (f) neutral temperature; (g) neutral composition; and (h) the incident solar radiation. At the present time many of these quantities are being measured individually by means of satellites, but it is often difficult from these data to extract the separate dependence of, for example, the electron temperature on height, local time, latitude (and longitude) and variations in the solar flux.[25] Thus, rockets appear to provide the best means of making these measurements, but so far none have been equipped to measure simultaneously more than three of the quantities involved. Further, in order to observe temporal variations, repeated rocket launchings are required involving considerable effort and expenditure.

One relatively inexpensive ground-based method can provide measurements of the quantities (a) through (d), but being a radio method it is insensitive to the quantities (e) through (h). This method is the radar incoherent backscatter technique discussed by Gordon[26] and employed to study the ionosphere, first by Bowles[27, 28] and later by Pineo, et al.[29, 30] The backscatter facility in its present form came into operation in January 1963, and this report presents the results of the first year of operation. In Sec. II we review briefly the theory of the method. A detailed account of the incoherent backscatter radar facility at the Millstone Hill Radar Observatory is provided in Sec. III, the observational methods are presented in Sec. IV, and reduction procedures are presented in Sec. V.

II. THEORY

A. Electron-Density Distribution

In 1958, Gordon[26] pointed out that if a very powerful radar beam were directed at the ionosphere, a weak but detectable echo from the free electrons there might be obtained. The intensity of the echo can be computed by assuming that the electrons scatter independently with a scattering cross section σ_c given by the square of the classical radius $r_e = (e^2/mc^2)$. Some confusion has arisen because this cross section is defined as that which scatters energy into unit solid angle, whereas, in radar calculations, it is customary to normalize the cross section to correspond to power reflected into 4π solid angle.[31] Hence the radar cross section σ_e is expected to be $4\pi\sigma_c$ ($\sim 10^{-28}$ m^2). For a volume containing N electrons, the phase of the N reflected waves will be independent and the powers should add to give an average scattered power proportional to $N\sigma_e$. Because at any given height the electrons completely fill the radar beam, the echo power should vary with range R only as $1/R^2$, not $1/R^4$ as for conventional (i.e., "point") targets. For observations conducted in the zenith it may be shown that the echo power P_r is given in[32-34]

$$P_r = \frac{P_t \eta_r^2 ct N\sigma\lambda^2}{64\pi^2 h^2} \int_\Theta G^2(\Theta) \sin\Theta \, d\Theta \quad , \tag{1}$$

where P_t is the transmitter power, η_r is the efficiency of the waveguide or feeder system, c is the velocity of light, τ is the pulse length, λ is the radio wavelength and h is the height to the pulse center. $G(\Theta)$ is the antenna gain over a lossless isotropic radiator, assuming that the antenna pattern is cylindrically symmetrical about its axis, and Θ is the angle subtended in any

direction from this axis. The electron cross section σ is usually different from $\sigma_e = (4\pi\sigma_c)$ for reasons which will be given. For a typical parabolic antenna, Evans[33] has shown that Eq. (1) can be reduced to

$$P_r = 0.74 \; \frac{P_t \eta_r^2 c\tau N\sigma A_o}{16\pi h^2} \quad , \tag{2}$$

where A_o is the effective antenna aperture. From Eq. (2) we see that, for the detection of a given density N at a given height h, the radar designer can adjust only the product $P_t \tau A_o$. If, however, it is necessary to obtain a given height resolution $\Delta h = c\tau/2$, one has no choice but to employ both a high transmitter power P_t and large effective aperture A_o to obtain useful results. One of the largest systems so far constructed (at Arecibo, Puerto Rico) employs the same transmitter power P_t as the Millstone Hill radar, but has a value of A_o which is 20 times that at Millstone.[35] If the electron density were independent of height, the Arecibo radar could be expected to detect echoes four times higher than Millstone, but in practice this ratio will be more nearly two times.

B. Signal Spectra

Bowles[28] was first to discover that the Doppler width of the reflected signals was considerably less than expected for a model of the scattering in which it is assumed that each electron contributes a signal with a Doppler shift proportional to the component of its velocity in a direction to the radar. Bowles correctly attributed this behavior to the role played by the ions in the plasma. Subsequent theoretical papers by Fejer[36] and others[37-39] have shown that when the radar wavelength λ is greater than $4\pi\lambda_D$, where λ_D is the Debye length ($= \sqrt{kT/4\pi Ne^2}$), the simple model above must be replaced by one in which the collective behavior of the electrons and ions is considered. The motions of the ions govern fluctuations in the electron density (with a scale of λ_D), and these fluctuations constitute small changes in the refractive index. When the radar wavelength is significantly larger than the size of these fluctuations, they must be thought of as the scattering centers and not the individual electrons. The situation becomes more complex when observations are conducted in directions normal or nearly normal to the magnetic-field lines, for then the gyrorotation of the ions causes the ion motions to be ordered. This case has been considered by Fejer[40] and others,[41-44] and experimental verification of the narrowing of the spectrum has been reported by Pineo, et al.[45] As magnetic effects play no part in observations at the Millstone Hill observatory, they will not be discussed further here.

In the theory developed by Fejer[36] it is assumed that both electrons and ions have Boltzmann energy distributions and that collisions are infrequent and may be neglected. Then, if it is further assumed that only singly charged ions of mass m_i are present, the shape of the echo spectrum takes the form shown in Fig. 1. It is clear from this figure that the echo power frequency spectrum is a function of both the electron temperature T_e and ion temperature T_i; hence, by determining the shape of the spectrum, the ratio T_e/T_i can be determined. If, in addition, m_i is known then T_i can be obtained from the total width of the spectra. The first observations of the spectrum shapes from which these quantities were extracted were reported by Evans[11] and Pineo and Hynek.[12] Subsequently, further measurements have been reported by Evans and Loewenthal,[46] and Evans.[47,48]

3

C. Electron Cross Section

The cross section of the electrons σ is proportional to the area under the curve in Fig. 1 and, as such, depends upon the ratio T_e/T_i. This dependence has been considered by Bunneman[49] and others.[50,51] Bunneman gives for σ the expression:

$$\sigma = \sigma_e \left\{ 1 - \frac{1}{1 + \left(\frac{4\pi\lambda_D}{\lambda}\right)^2} \cdot \frac{1}{\left[1 + \left(\frac{4\pi\lambda_D}{\lambda}\right)^2\right]\left[1 + \left(\frac{4\pi\lambda_D}{\lambda}\right)^2 + \frac{T_e}{T_i}\right]} \right\} . \tag{3}$$

Thus, for very short wavelengths, $4\pi\lambda_D \gg \lambda$, $\sigma \to \sigma_e$. In the ionosphere, at heights presently being studied by this technique, the Debye length λ_D is of the order of a few millimeters, and for these radars $\lambda \geqslant 4\pi\lambda_D$. When $\lambda \gg 4\pi\lambda_D$, Eq. (3) becomes:

$$\sigma = \sigma_e \left\{ 1/[1 + (T_e/T_i)] \right\} \quad , \tag{4}$$

and thus the highest cross section that can be expected (under conditions of thermal equilibrium) is $\sigma = 0.5\,\sigma_e$ ($= 0.499 \times 10^{-28} m^2$).

If T_e/T_i is a function of altitude h, the electron-density profile N(h) can only be determined from Eq. (2) if the height dependence of σ is known. This complication was not immediately recognized and some published backscatter profiles of electron density are now thought to be in error. This difficulty has caused Bowles,[52] operating at 50 Mcps, and Greenhow, et al.,[34] operating at 398 Mcps, to adopt a method of deriving an electron-density profile from measurements of the Faraday rotation of the radio waves in place of the echo power. This technique is difficult to implement at frequencies above 100 Mcps where the amount of rotation is small.

In the measurements to be described, the echo power P_r has been obtained as a function of height, and N(h) obtained from Eq. (2) by determining the variation of σ with height. This is accomplished by simultaneous measurements of the signal spectra corresponding to different heights from which T_e/T_i can be obtained. The height dependences of T_e/T_i and T_i are, of course, of interest in their own right, and much of the report is devoted to observations of these quantities.

D. Mixtures of Ions

As the ion mass m_i enters the equations in the form $(m_i)^{1/2}$, it seems that O^+ and N^+ (or O_2^+, N_2^+ and NO^+) could be considered for all practical purposes as identical, in that it would not be possible experimentally to distinguish one from the other. Below about 200 km it is expected that significant concentrations of several of these ions exist, and Petit[53] has considered the experimental accuracy required to determine the ratio of the heavier to the lighter ions. Observations conducted at the Millstone Hill observatory during 1963 are restricted to a height range of approximately 200 to 750 km. The lower limit is set by ground clutter echoes, and the upper limit by the strength of the signals. Over much of this height range O^+ is expected to predominate.[54,55] However, above about 750 km by day and perhaps 500 km at night, H^+ and H_e^+ ions become important constituents.[56,57] Their presence can modify the scattering considerably by changing the shape of the signal spectra. Figure 2 shows the influence of increasing the amount of He^+ in an O^+/He^+ mixture on the shape of the spectra for the case $T_e/T_i = 2.0$. It is clear that the presence of large amounts of He^+ (e.g., 50 percent) can be recognized readily.

However, if only small amounts of He^+ are present, the spectra might be interpreted as indicating an erroneously high value of T_i and low value of T_e/T_i. Moorecroft[58] has considered how the quantities T_e, T_i and the ratio between the percentages of He^+, H^+ and O^+ ions might be extracted from spectrum observations. In principle, it is possible to perform such an analysis provided that: (1) the measurements can be made to a very high degree of precision; and (2) it is possible to remove some ambiguities in the interpretation by observations conducted at higher and lower altitudes. In practice, where pulsed radar observations are made one must consider also the distortion of the theoretical spectra by the finite width of the transmitter pulses, and in any radar system there will be some further smoothing due to the finite width of the filters employed in the spectrum analyzer. Considerable effort has been made to compute these effects for the Millstone Hill Radar Observatory (Sec. V).

III. EQUIPMENT

A. General

The Millstone Hill Radar Observatory is located in Westford, Massachusetts (71.5°W, 42.6°N). The parameters of the ionospheric radar are listed in Table I. The antenna (Fig. 3) is a 70-meter parabola directed vertically. The feed system is a circular horn coupled to a turnstile junction. A pair of opposite ports are connected into remotely adjustable shorts allowing any mode of polarization to be radiated. In practice, circularly polarized waves of one sense are transmitted and the opposite sense received. The transmitter is coupled to another port of the turnstile junction by a waveguide, and the receiver is similarly coupled to the fourth port. The transmitter and receiver frequencies are controlled by synthesizing all the needed oscillator frequencies from a single frequency standard.

B. Receiver

The first amplifier in the receiver is a Zenith electron-beam parametric amplifier which is synchronously pumped (at 880 Mcps). This amplifier normally introduces additional noise due to an unwanted side-band or image. However, by employing a pump frequency which is precisely twice the radar frequency (i.e., synchronously pumping), the image can be removed.

TABLE I
PARAMETERS OF IONOSPHERIC RADAR

Antenna	70-meter fixed parabola
Polarization	Circular
Effective aperture A_o	1600 m^2
Frequency f	440 Mcps
Transmitter power P_t	2.5 Mw
Transmitter pulse lengths τ	0.1-, 0.5- and 1.0-msec pulses used
Pulse repetition frequency	50 cps
Receiver bandwidth b	25 kcps
System temperature T_s	~200°K (monitored continuously)
Post detector integration	~20 db

Unfortunately, the phase information of the signal is then destroyed; that is, it becomes impossible to observe at the output of the receiver if the signal spectrum is asymmetric, for the amplifier now operates both in the conventional way and as a side-band exchanger. The statistical fluctuations of the noise at the output terminals of the receiver are also changed so that, after n independent samples, the rms temperature fluctuation is $\pm\sqrt{2}T_S/\sqrt{n}$ instead of $\pm T_S/\sqrt{n}$ as in the case of a conventional amplifier with system temperature T_S. These disadvantages are outweighed by the rapid recovery of the amplifier following the transmitter pulse, its complete stability, and the fact that it cannot be destroyed by moderate amounts of transmitter power.

C. Echo Power Integration

The electron-density profiles are obtained from measurements in which the echo power as a function of height is determined. This is accomplished by placing in the receiver a filter whose bandwidth (25 kcps) is sufficient to accommodate all the frequency components of the reflected signal. The output of this filter is connected to a square-law detector which provides a voltage proportional to the input power. This voltage, in turn, is sampled by a digital voltmeter at intervals of 200 μsec and assigned one of 256 possible levels. The digital numbers representing these voltages are continuously summed in the CG 24 computer to form a plot of the integrated echo power vs delay over the time-base. This integration process is continued usually for periods of 10 to 20 minutes, thereby reducing the fluctuation in power by at least 20 db (to ±3°K). Figure 4 provides an example of a plot of integrated power vs delay. A resolution of 100 μsec (15 km) is achieved by making the interpulse period an odd number of 100-μsec intervals and interlacing two time-bases sampled at 200-μsec intervals.

D. Spectrum Analyzer

The signal spectra are explored by a bank of 24 filters. The outputs of the filters are rectified with linear detectors, and these voltages are then summed by carefully constructed analog integrators. The filters are driven by a wide-band (50-kcps) amplifier which is normally switched off, and gated on for a part of the time-base equal to the length of the transmitter pulse (0.5 or 1.0 msec). The delay t between this gated portion and the time at which the transmitter pulse is radiated determines the height at which the signal spectrum is being explored. In order to calibrate the gains of the filter channels, the detectors, and to remove any influence of the earlier stages of the receiver on the shape of the spectra, a second gated portion of the time-base is applied to the filter bank. This second portion is equal in width to the first, but at a delay corresponding to a height from which no detectable signal is expected. The outputs of the detectors are switched to store the voltages corresponding to this second gate in another set of 24 integrators. Thus the first set stores signal plus noise and the second set only noise; by taking a ratio between the two sets equipment effects can be eliminated. Because the oscillations of the filters must be allowed to decay completely before the second pulse is applied, this compensation scheme imposes restrictions on the maximum prf, which cannot be more than 50 cps for the present filters. Throughout 1963, single-pole filters were employed having identical bandpass characteristics with a half-power width of 500 cps and center-to-center spacing of 480 cps.

Both halves of the spectrum should be identical. (Even if asymmetry were to exist, it would be destroyed by the receiver.) Thus, only one half is normally measured and either the

upper or lower side band can readily be selected for spectral analysis. The integrators have a self time constant of several hours. At the end of a 5-minute integration period, the receiver pulses to the filter bank are removed and the 48 stored voltages are automatically sampled in turn and measured by means of a 14-bit digital voltmeter. These voltages, together with the time, are recorded on a punched paper tape.

IV. OBSERVING PROCEDURES

A. General

Observations were made at intervals of about one week throughout 1963. Each period of observation usually commenced near 0900[*] and ended at about 1700 on the following day. In this way the daytime behavior was observed twice during any one run. Typically, in any one hour the equipment was operated as shown in Table II.

<table>
<tr><td colspan="3">TABLE II
TYPICAL EQUIPMENT OPERATION SEQUENCE</td></tr>
<tr><td>Pulse Length
(msec)</td><td>Computer Integration
(min.)</td><td>Spectrum Delay
(msec)</td></tr>
<tr><td>0.1</td><td>10</td><td>—</td></tr>
<tr><td>0.5</td><td>15</td><td>1.5, 2.0, 2.5</td></tr>
<tr><td>1.0</td><td>15</td><td>3.0, 4.0, 5.0</td></tr>
<tr><td>0</td><td>5</td><td>(and 6.0)</td></tr>
</table>

The sums of echo power formed in the computer (e.g., Fig. 4) were recorded on magnetic tape for later analysis. Spectrum measurements at any one delay (Table II) normally occupy 5 minutes, thus to explore the full range of heights takes almost an hour. During the daytime in summer, useful measurements were obtained with a delay of 6 msec, but in winter at nighttime there was insufficient signal strength to make measurements beyond about 3 msec. At the end of each hour, the RF drive to the transmitter was removed and the measurements repeated as a check on the proper operation of the equipment in the absence of a signal. The voltage outputs of the integrators were recorded in binary fashion on a punched paper tape for later analysis. It is also possible to record the receiver IF signals for spectrum analysis at a later time; this can be useful when it is required to determine the behavior more rapidly than once per hour.

If the electron-to-ion temperature T_e/T_i is known (from the signal spectra), the electron density at that height can be determined from absolute power measurements. These require that the effective antenna aperture A_o, the transmitter power P_t, and the receiver system temperature T_s be determined.

Antenna aperture is measured by observing the radio source in Cygnus A which requires a repositioning of the feed so that the beam is directed toward the south by 2° from the zenith. The transmitter power is continuously monitored by means of power meters which are connected to couplers inserted into the waveguide. The system temperature T_s is determined in the following way. A gas discharge tube providing a 10,000°K noise source is coupled to the

---

*Time periods are EST unless otherwise indicated.

7

receiver via a 20-db coupler and ignited for 2 msec at the end of each sweep of the time-base. A 100°K rise in system temperature can then be observed in the plot of integrated receiver output power vs delay formed in the computer (Fig. 4). If the 20-db coupler is placed before the TR cavity, any deterioration in the performance of the TR tube can be recognized.

Accuracy in determining the antenna efficiency and system temperature is governed chiefly by the uncertainty in the noise source used as a reference. Several such noise sources have been employed but are usually observed to differ by the order of ±1 db. A comparable error may exist in the determination of the transmitter power P_t. Hence, for the most part, the absolute value of the echo power is <u>not</u> used to determine the electron density; instead, the profiles are assigned an absolute scale from ionosonde measurements in which f_oF2 is determined. The ionosonde is located within 1 km of the backscatter radar.

B. Choice of Pulse Length (Profile Measurements)

The echo power profile represents the convolution of the shape of the pulse $\Delta h = c\tau/2$ with the true electron-density profile N(h). In order to minimize the distortion of the profile introduced by the pulse, the shortest value of pulse length τ compatible with achieving sufficient echo power [Eq. (2)] is used. For the Millstone Hill apparatus this is 100 μsec. The thickness of the F-layer between points of half-maximum density is of the order of 100 km or more (Fig. 5). The resolution afforded by 100-μsec pulses (15 km) is adequate to explore the main features of the profile, but features having small height extent (e.g., the F1 ledge) are lost.

During the 0.5- and 1-msec pulse measurements the region above 400-km altitude is explored with better signal-to-noise ratio (though poorer resolution). Fortunately, in these regions the scale height is comparable to the pulse length, and serious distortion of the profile is not introduced.

C. Choice of Pulse Length (Spectrum Measurements)

The height resolution achieved in the spectrum measurements is considerably poorer than that for the density measurements as a consequence of the need to employ long pulses in order to minimize the distortion of the spectra. For 0.5-msec pulses the height resolution is approximately 75 km, and the width of the pulse (2 kcps) is of the order of one-fifth the width of the spectra (10 kcps). If a higher operating frequency were employed, signal spectra would be proportionally wider and shorter pulses could be used. However, in this case, the ratio $\lambda/4\pi\lambda_D$ would approach unity at a lower height and thereby restrict the vertical extent of the measurements. One solution of this dilemma seems to be to employ an antenna directed at a low elevation angle and to restrict the vertical extent of the pulse by the obliquity of the path.

For a pulse of length τ sec and a spectrum delay t sec between the leading edge of the transmitter pulse and the receiver gate (of width τ sec), the lowest height from which echoes are received is $(c/2)(t-\tau)$ km, and the uppermost height is $(c/2)(t+\tau)$ km. The combined action of the finite width of the pulse and the equal width of the receiver gate is to "weight" the electrons distributed between these heights in a triangular fashion, those at $(c/2)t$ km affecting the spectrum the most. Actually, it is not the electron-density distribution but the echo power P_r which is given this weighting by the receiver gate. As P_r is decreasing with delay t (for most delays), the effective center of the pulse is somewhat lower than ct/2. Allowance is made for this by computing the <u>effective height</u> of the pulse as a function of delay t, from the observed echo power P_r, vs height measurements.

8

V. DATA ANALYSIS

A. Profile Measurements

Plots of echo power vs delay (Fig. 4) are recorded on magnetic tape and later analyzed by the computer in the following way. First the mean noise level is established from the values of about 20 points near the center of the time-base, and this mean is then subtracted from all the points. Mean power of the noise calibration pulse (Fig. 4) is next established and used to define the absolute level of the echo power. Echo power is then scaled up in proportion to the square of the height to obtain an electron-density profile $N'(h)$ which is printed out later. The computer normalizes the electron-density profile to the peak value and plots it as a function of height (Fig. 5). Smooth curves are drawn through these plots by hand, and a single density profile is extracted from the plots of the 0.1-, 0.5- and 1.0-msec pulse observations in the same hour. Figure 6 presents an example of such a combined profile and has been published previously.[46] At this point the profile $N'(h)$ may differ from the true profile $N(h)$ if σ is a function of height but, as Fig. 6 shows, the error is not extremely large. Thus, by assigning the value for f_oF2 observed on the ionosonde to the point of peak electron density, an absolute scale is established which enables the approximate value of the plasma frequency f_p at all other heights to be estimated. This is necessary in order to interpret the spectrum measurements accurately.

Later, when the values for T_e/T_i have been obtained as a function of height (Fig. 7), a first-order correction can be applied using Eq. (4) to obtain the true density profile $N(h)$. Figure 8 shows the corrected version of the profile shown in Fig. 6 after adjustment, to allow for the temperature inequality shown in Fig. 7.

B. Spectrum Measurements

The punched paper tape on which the 48 integrator voltages have been recorded is later analyzed by the computer. All the values are squared and a ratio is then taken of each of the values of the 24 signal-plus-noise to the 24 noise powers to obtain the signal-to-noise power at each frequency. By subtracting one from these ratios the signal spectrum is obtained. Corrections are applied to remove systematic differences between the integrators in each pair. These corrections are obtained by taking a mean of all the ratios observed during the runs when the transmitter is not radiating (Sec. IV).

In order to analyze the spectrum measurements it is simply necessary to compare each measured spectrum with a set of theoretical spectra to find which agrees best. Because the electron-to-ion temperature ratio T_e/T_i controls the ratio x between the power in the wing to that at the center frequency, this quantity (x) is scaled from the records. A second quantity f, the frequency difference between the center and a point of half peak power, is also scaled and for a given ion mass m_i may be regarded as a measure of the ion temperature T_i. The effect of the transmitter pulse and the frequency resolution of the receiver spectrum analyzer must be allowed for, and in order to do this it has been necessary to compute a large number of theoretical spectra (e.g., Fig. 1). These spectra were then convolved, first with the spectral distribution of the power in the transmitter pulse, and second with the power-vs-frequency response of one of the filters in the receiver. The effect of the convolution on theoretical spectra corresponding to given values of T_i and T_e/T_i is to lower x and increase f as shown in Fig. 9.

A third effect, which has not so far been taken into consideration, is the action of the receiver gate on the shape of the spectra. As mentioned previously, the receiver gate is necessary to define the height interval from which echoes are received. The effective height of the pulse center is defined by a weighted distribution of echo power within this gate, and this quantity is calculated. However, the distortion introduced by the receiver gate in the shape of the signal spectra was not included in the initial theoretical calculations. From more recent computations, it appears that when the gate width is made equal to the pulse length the spectrum shape is changed only by a further lowering of the wing, and hence the ratio is reduced. It seems, therefore, that the neglect of this effect will not in any way influence the values of T_i reported herein, but T_e and T_e/T_i may be underestimated by 10 to 20 percent. This is probably comparable with the experimental error at most heights up to 500 km and less than the experimental error above 500 km.

The solid lines in Fig. 9 represent a spectrum analysis chart used for 1-msec pulse observations at a height where the plasma frequency f_p is close to 5 Mcps. The need to specify the plasma frequency stems from the fact that, as the radio wavelength λ approaches $4\pi\lambda_D$ ($\lambda_D = \sqrt{kT_e/4\pi Ne^2}$), the spectrum shape changes rapidly. This is illustrated in Fig. 10 where spectrum charts for a 1-msec pulse at 2.5- and 1.0-Mcps plasma frequency f_p have been superimposed. Thus, at the wavelength (68 cm) employed here, the shape of the spectrum depends upon T_e, T_i and the density N (which then specifies the Debye length). This accounts for the need to obtain an approximate profile before performing the spectrum analysis reduction. Charts such as Figs. 9 and 10 have been prepared for 1.0-msec pulses for f_p = 1.0, 1.5, 2.0 and 5.0 Mcps, and for 0.5-msec pulses at 2.5 and 5.0 Mcps. Above f_p = 5.0 Mcps, $\lambda \gg 4\pi\lambda_D$ and no further changes in the spectrum shapes occur. This was tested by computing the spectrum shapes for f_p = 10 Mcps. All charts discussed so far assume that O^+ is the only ion present.

The values of T_e/T_i corresponding to the measurements shown in Fig. 6 are shown in Fig. 7, and the separate dependence of T_e and T_i on this occasion is shown in Fig. 11.

It is possible that above 500 km appreciable amounts of He^+ were present at the time these measurements were made.[9] The distribution of He^+ ions has been discussed on theoretical grounds,[56, 57] but unfortunately there is inadequate experimental evidence at this time to verify the accuracy of these models. What evidence is available is somewhat contradictory as Gringauz, et al.[59] find a complete transition from O^+ to He^+ over the height range 520 to 620 km. The theory[56] and the experimental results of Taylor, et al.[9] indicate a more gradual transition. At no time during the course of the backscatter measurements have spectra been obtained that definitely indicate the presence of He^+ ions, though the spectra obtained for the uppermost heights (750 km by day, 500 km by night) are uncertain due to the low signal-to-noise ratio, and perhaps as much as 30 percent He^+ might be undetected (Fig. 2). Figure 12 shows that the measurements made on 2 July at 720-km equivalent height are consistent with theoretical spectra computed for a plasma containing no He^+ (i.e., 100 percent O^+) or one containing as much as 20 percent He^+. Unfortunately, as Fig. 13 shows, the presence of even small amounts of He^+ requires a significant change in the interpretation of the results. In the specific example shown in Fig. 12, it is not possible to distinguish experimentally between two extreme cases: namely, (1) wholly O^+, T_e/T_i = 1.14, T_e = 2320°K, T_i = 2040°K; and (2) 80 percent O^+, 20 percent He, T_e/T_i = 1.4, T_e = 1960°K, T_i = 1410°K. These diverging interpretations are indicated in Fig. 11.

10

On a theoretical analysis of the behavior of the electron and ion temperatures in the upper F-region, it is possible to decide between the two possible curves shown in Fig. 11. Geisler and Bowhill,[60] who have performed such an analysis, show that by far the most important parameter is the very high thermal conductivity of the electron gas above about 400 to 500 km. Thus, T_e is expected to be isothermal above this height almost irrespective of the behavior of T_i or the neutral temperature T_n. If this is correct, the solid curve of Fig. 11 (100 percent O^+) would appear to be closest to the true situation, and the restriction of analyzing the results on the assumption that O^+ predominates may be deemed to be in order, where the results show that T_e is isothermal at the greatest heights.

In principle, it should be possible to determine the ratio O^+/He^+ by careful measurement of the slope of the spectrum near the point of half peak intensity (Fig. 2). In the measurements described here, this slope has been set largely by the distortion introduced by the transmitter pulse and receiver filter characteristics. It is hoped that by using improved filters in the receiver spectrum analyzer this problem can be minimized.

In summary it may be said that the interpretation of the spectra corresponding to heights of more than 500 km is uncertain at the present time owing to the likely presence of He^+ ions. Despite this, Fig. 11 shows clearly that T_i increases markedly with height as distinct from the neutral temperature T_n, which is widely thought to be independent of height above 300 km (Ref. 61). Either this view is incorrect, or $T_i \geqslant T_n$ above 300 km as Dalgarno[62] and Hanson[63] have suggested.

VI. ACCURACY OF RESULTS

A. Profile Measurements

Systematic errors have occurred during the course of the profile measurements due to poor recovery of the TR tube. Unfortunately, this condition is usually not recognized during an operation as it is masked by the ionospheric echo. When this malfunction has been very severe it may be recognized in the analyzed profiles by the fact that (for 1-msec pulses) N(h) becomes negative near 700 km. Many of the measurements made in 1963 suffered because of this trouble. In October, provision was made to monitor the recovery of the TR tube and the first stages of the receiver by switching the receiver off-tune sufficiently (50 kcps) to place the echo outside the receiver pass band. When not too severe, the effect of the TR tube trouble has been to cause a systematic underestimation of N(h) which increases with height. An example of this behavior is given in Fig. 14 in which a backscatter profile obtained on 12 July is compared with a density curve obtained from the results of the topside sounder Alouette (Van Zandt, private communication). It can be seen that serious error is encountered above 500-km height.

Unfortunately, the fact that this was a continuing difficulty was not recognized until October. Earlier attempts to effect a cure were always short-lived as a result of changes in the characteristics of the discharge tubes as they aged. Since October, it is believed that the density profiles are of comparable accuracy to those shown in Fig. 8. However, prior to October it was not always possible to determine whether or not the results for a given day were accurate or not, unless the malfunction was particularly severe. Thus the values for the density above 500 km by day and about 350 km at night should be accepted with some caution.

The random errors of measurement increase rapidly with height (Fig. 5) because: (1) at the uppermost heights the echo power is obtained as the difference between two large uncertain

numbers, and (2) in computing the profile N'(h) these differences are scaled in proportion to $(h)^2$. The profile measurements depend upon the determination of the total echo power in a wide filter, thus they can always be conducted to heights at which the spectrum measurements are unusable. Thus, when the equipment is operating properly, the upward extent of the profile measurements is curtailed by the absence of good spectrum results and not by the errors in the profiles themselves. The agreement between the rocket and backscatter measurements shown in Fig. 8 suggests that on this occasion there were no serious sources of error in the profile measurements. However, we note that if the uppermost spectra (Fig. 12) are interpreted as indicating the presence of 20 percent He^+, the ratio T_e/T_i would be raised to 1:4 and, as a result, the backscatter curve would be adjusted to agree completely with the rocket results (full line) at 720 km. Evidently the interpretation of the spectra can constitute one of the major sources of error in profile measurements.

Below the peak of the F-region, ground clutter echoes restrict the lowest measurements to about 200 km. These echoes are caused by horizontal radiation from the antenna feedhorn. It is possible that steps could be taken to reduce these echoes, but the resolution obtainable in the spectrum measurements would be inadequate to explore this region, as T_e/T_i, T_i, and the ion mixture all change rapidly with height. It is planned to use an oblique incidence radar operating at 1295 Mcps to explore the region 100- to 300-km height.

B. Spectrum Measurements

Each spectrum measurement occupies a period of five minutes during which time 15,000 pulses are averaged. When the signals are stronger than the noise (at low heights), the error in each point is set simply by the uncertainty in the signal power corresponding to this number of samples (±1 percent). When the signal is less than the noise, the signal-to-noise power ratio will be $\sqrt{2}$ times the uncertainty in the noise level (i.e., $\pm\sqrt{2}$ percent). When the spectra are later scaled, the determination of the ratio x is always more difficult than the half width f, since this is a ratio between two like numbers. The error in x might be expected to be about $\sqrt{2}$ times that in a single point (i.e., ±2 percent noise/signal power ratio at low signal levels).

In practice, when the signal power is weak, systematic errors are introduced by low-level interference of various forms. Airborne altimeters and search radars appear to be the worst offenders. In the profile measurements these interfering signals raise the absolute noise level but do not systematically distort the profiles, as they are not synchronized to our repetition frequency. However, in the spectrum measurements they will reduce the apparent signal-to-noise ratio over a limited frequency range. These interfering signals appear at different frequencies in an unpredictable fashion and, as a rule, useful spectra are not obtained when the signal-to-noise power ratio is less than 0.2.

We have already discussed the effect of an ion mixture on the interpretation of the spectra. The poorest spectra corresponding to the uppermost heights are in fact those for which this problem arises. At present, the interpretation of the spectra above 500-km height must be regarded as uncertain.

VII. OBSERVATIONS IN 1963

A. General

This report is intended to give a full account of the Millstone Hill ionospheric radar and the backscatter results obtained in 1963. The results presented in Sec. V have been published previously, together with other measurements made in July, to demonstrate the utility of the method.[46]

Table III lists the dates and times when observations were made. From 28 February onward, the receiver was operated with the synchronously pumped electron-beam parametric amplifier as first stage. No other major modifications to the equipment were made during the report period, although numerous minor changes were incorporated to improve reliability and performance. Radar equipment failures occurred on few occasions and were the least troublesome cause of lost observing time.

Combinations of human and equipmental errors in operation of the CG 24 computer caused all profile results for eight consecutive weeks in May and June to be destroyed and, in addition, some shorter periods later in the year were also lost (see Table III). The next most serious trouble was caused by various kinds of external radio interference, which resulted in the loss of some observation time and in the reduction of the accuracy of results obtained during much of the remaining time.

B. Reduction Procedure

The data gathered in this program were analyzed according to the methods outlined in Sec. V. A complete electron-density profile is obtained together with the height dependence of T_e and T_i approximately every hour of observing time. In order to reduce this large amount of data to manageable proportions, the electron-density plots are presented as diagrams in which contours of constant critical frequency are drawn as functions of altitude and time.

One difficulty in presenting the diurnal variation of the temperature is that the equivalent heights of the spectra vary throughout the day as a consequence of changes in the shape of the layer. Hence, any given delay does not correspond to a given fixed height. Thus it has proved convenient to present the temperature results as contours of constant T_e/T_i, T_e and T_i on diagrams having height as ordinate and time as abscissa.

In principle it would be possible to prepare these diagrams for each day, but in practice the large gaps introduced by loss of data through one cause or another make it preferable to average many days' data into a single plot. The diurnal and seasonal behavior were considered the most important characteristics to study. Consequently, the results have been used to construct mean plots showing the behavior averaged over each calendar month. In order to do this, the day is treated as 24 separate hourly intervals, and a mean taken of all the results obtained in each given hour over a given month. In the case of the electron-density profiles it is first necessary to adjust all the profiles to their mean height before computing the mean shape. The mean profile is then accorded the average value of the density at its peak. When the day-to-day critical frequency is subject to rapid change (e.g., during the equinoctial periods), some difficulty can be encountered in constructing the diurnal plots if records are missing for parts of certain days. Thus, gaps are left on several of these plots where there are insufficient data to make meaningful averages.

Date	Start Time (EST)	End Time (EST)	Comments	Date	Start Time (EST)	End Time (EST)	Comments
1963				1963			
4/5 Feb	1100	1700	2100–0400 receiver malfunction, no data; diode parametric amplifier in use	16/17 Aug	0830	1550	Severe interference; NO PROFILE DATA 2000–0500
19/20 Feb	1100	1615	Electron-beam parametric amplifier used	23/24 Aug	0900	1640	NO PROFILE DATA 0100–0600
28 Feb/1 Mar	1030	1600	Electron-beam parametric amplifier synchronously pumped	29/30 Aug	1100	1100	
7/8 Mar	1230	1700		6/7 Sept	0820	1540	
14/15 Mar	1040	1600	1300–1700 on 14 Mar, NO DATA (transmitter malfunction)	13/14 Sept	0915	1600	Strong auroral interference; NO PROFILE DATA 0000–1600
20/21 Mar	0930	1400		20 Sept	0740	1600	
28 Mar	0500	1915		21/22 Sept	0840	0700	Interference; NO PROFILE DATA 0000–0600
4/5 Apr	0930	1415		27 Sept	0740	1600	
10/11 Apr	0920	1550		28/29 Sept	0740	0800	TR trouble severe; NO PROFILE DATA 2000–0800
17/18 Apr	1210	1815		4/5 Oct	1100	1540	Digital voltmeter failed; all spectrum data recorded and processed on 29/30 Oct
25/26 Apr	1140	1315	NO PROFILE RESULTS	18/19 Oct	0840	1530	NO PROFILE DATA 1000–1530 on 19 Oct
2/3 May	0740	1200	NO PROFILE RESULTS	25/26 Oct	0850	1530	Several equipment malfunctions; NO PROFILE DATA 0400–0930
10/11 May	1550	1800	NO PROFILE RESULTS	1/2 Nov	1130	1650	NO PROFILE DATA 0100–0530
31 May/1 June	1015	1600	NO PROFILE RESULTS	7/8 Nov	1000	1700	NO PROFILE DATA 1900–0600
7/8 June	1000	1540	NO PROFILE RESULTS	14/15 Nov	1045	1620	
14/15 June	0840	1600	NO PROFILE RESULTS	21/22 Nov	0930	1640	
21/22 June	0830	1600	NO PROFILE RESULTS	29/30 Nov	0910	1715	
28/29 June	0930	1530	NO PROFILE RESULTS until 0600, 29 June	6 Dec	0930	1300	Punch failure caused loss of spectrum data obtained after 1300
7/8 July	0900	1230		13/14 Dec	0930	1630	NO PROFILE DATA 1935–0010
11/12 July	0800	1530		20/21 Dec	1030	1715	NO PROFILE DATA 0240–0720
19 July	0830	1940		27/28 Dec	0920	1645	
21 July	0820	1940	Severe interference 0800–1400; NO PROFILE DATA 0900–1300	1964			
26/27 July	0800	1600		3/4 Jan	0910	1600	NO SPECTRUM DATA 0030–1015
2/3 Aug	0840	1600	TR trouble severe; NO PROFILE DATA 0100–0500	10/11 Jan	0930	1630	NO SPECTRUM DATA 1400–1630 on 11 Jan
9/10 Aug	0810	1620	Severe interference; NO PROFILE DATA 2000–2300	17/18 Jan	1000	1650	NO SPECTRUM DATA 1000–1500 on 17 Jan

14

No large changes in the height behavior of the ratio T_e/T_i were encountered as a function of date; hence, some saving in reduction time was achieved by taking a mean of the uncorrected $N'(h)$ profiles and correcting this using the mean T_e/T_i curve obtained for that month.

The quality of the spectrum results varied markedly with altitude, time of day, and depending on whether or not any radio interference was present. This is accounted for in the computations of the mean temperatures by weighting the values of T_e, T_i and T_e/T_i, one, two, or three times according to the confidence that could be placed in the corresponding spectrum. This weighting is somewhat arbitrary, but does serve to bring the mean values for T_e and T_i closer to the values obtained from the best spectra. Thus a weighted mean is obtained for the values of T_e, T_e/T_i, and T_i obtained in each hour, in each month, for each given delay. This mean is assigned the weighted mean equivalent height. For each hour a plot is then constructed of T_e and T_i as a function of height, and smooth curves are drawn through the points because no sharp discontinuities in either of these temperatures would be physically plausible. In this way the effects of single spurious points are minimized unless they happen to be uppermost. In constructing these curves, greatest weight is given to the points representing the average of the largest number of determinations. Finally, a new determination of the ratio T_e/T_i with altitude is obtained from these smooth T_e and T_i curves and compared with the weighted mean values. Usually good agreement would be found, but where there is a difference the T_e/T_i curve derived from the two temperature curves is followed instead of the original points.

No effort was made during the data-taking operations to synchronize the measurements to fixed times; hence, it is assumed that the average values are representative of conditions at the midpoint of each hour, and they are plotted accordingly.

Where the electron-density profiles were destroyed, or otherwise missing, the spectrum measurements could still be analyzed if the approximate critical frequency at the corresponding height could be estimated. To do this, it was assumed that the plasma frequency was the same, on the day for which it was missing, as actually observed on the nearest date at that hour. It is believed that the errors inherent in this procedure are not sufficient to cause serious inaccuracy in interpretation of the spectra.

VIII. ELECTRON-DENSITY MEASUREMENTS

Figures 15(a) through (j) show results of the electron-density determinations. The months of May and June are missing for the reasons mentioned previously (see Sec. VII). Other months have gaps where the paucity of data makes it difficult to construct meaningful average profiles. No attempt has been made to smooth the plots shown in Figs. 15(a) through (j), instead the values for each hourly interval have simply been joined by straight lines. The main features of these plots are discussed briefly here.

There is little summer-winter difference in the density at the maximum of the layer because sunspot minimum conditions were being approached at this time. The highest midday critical frequency observed was 7.0 Mcps in November, and the lowest was 5.0 Mcps in July and August. Millstone Hill is located under the "winter spur" of high latitude ionization but this is not pronounced near sunspot minimum.[64] The critical frequency rises rapidly at dawn and usually reaches a maximum near noon or a little before. In all months, h_{max} is lowest at about 2 to 3 hours after sunrise (around 0700 to 0900) and then has a value lying between 220 and 230 km. As the day advances, h_{max} rises almost linearly to about 310 km which it reaches a little after midnight. At sunrise, h_{max} decreases rapidly.

In summer and the equinoctial months, the shape of the layer is roughly constant throughout the major part of the day. The rise in h_{max} causes the layer as a whole to increase in height until sunset. During the evening the shape of the layer changes, but remains roughly constant during the early morning hours — when the whole layer can be seen to be disappearing. In winter (e.g., November) there is no time when the layer shape is not changing.

A prominent feature of the variation of f_oF2 on the east coast of the United States is a large increase occurring at sunset. Often f_oF2 will then exceed its value at any other time of the day. In summer months (e.g., July) the noon and evening maxima may be separated by as much as 10 hours, but in the equinoxes (March and October) this is reduced to about 6 hours. The evening increase is absent in winter. Cause of the evening increase is very evident from inspection of the results for July and August. At 650-km altitude, density begins to decrease 2 to 3 hours before the evening increase reaches its peak. A similar decrease in density takes place at lower heights, somewhat delayed after that at 650 km. Evidently ionization moves downward and piles up at h_{max}. The reason for the downward motion of ionization at this time is thought to be the large fall in T_e at sunset, which causes the equilibrium scale height H to decrease rapidly. Similar behavior was observed during the eclipse of 20 July 1963 (Ref. 47). Increases of f_oF2 during eclipses have been shown[65] to depend upon the eclipse being total at F1 region heights, and the magnetic dip being large ($I \geq 60°$). We suggest that this latter condition is most important for observing an evening increase. When I is large, fast photoelectrons can travel upward to great heights during the daytime, and thus give rise to high values for the exospheric electron temperature. Also, the downward diffusion (which depends upon the dip angle I according to $\sin^2 I$) can be rapid at sunset.

In a separate paper,[48] the appearance of the midlatitude evening increase in f_oF2 will be discussed in some detail. The absence of the effect in winter can be attributed to the more gradual and less extensive fall in T_e at sunset. Also, less ionization is available above h_{max} to participate in downward diffusion. At sunspot maximum, the effect is less pronounced but does serve to maintain high values of f_oF2 almost until midnight. This change between sunspot minimum and maximum can be attributed to reduction in the temperature difference $T_e - T_i$, thought to occur at sunspot maximum as a consequence of the higher electron density.[66] The effect of the magnetic declination on the effect reported by Eyfrig,[67, 68] if real, must now be interpreted as evidence for electrodynamic drifts which either oppose or assist the downward diffusion induced by the temperature change.

Systematic increases in f_oF2 are observed at night during winter months (November, December and January). These increases all begin between midnight and 0200, well before local sunrise. There is some evidence for an increase in f_oF2 in March beginning at 0400 — again before sunrise. We can exclude the possibility that this is a consequence of freshly created ionization, perhaps produced by cosmic rays precipitating into the atmosphere. If this were the case we should expect a pronounced increase in T_e at this time. As we shall see, T_e usually decreases during these periods, and this can be explained as a result of the inability of the nighttime heat source (to be discussed) to maintain the same temperature in the presence of additional ionization.

It also seems unlikely that this phenomenon is identical in nature to the summer evening increase. On the basis of such a model, it would be exceedingly difficult to explain why the increase occurs in the early hours of the morning, and why large decreases in T_e and T_i which

could give rise to such an effect are not seen. Nor can the increase in f_oF2 be attributed simply to a large change in the shape of the layer, which causes a redistribution of ionization in which more electrons appear at the peak. The increase observed at the peak is evident at other levels above and below h_{max}.

The regular evening decrease in density appears to be arrested near 2300 in these winter months, and the density at all levels then increases reaching peaks at about 0230 in the 400- to 500-km region and at about 0400 at h_{max}. This suggests an influx of ionization from great heights, which must commence near 2300 and persist for several hours. The phenomenon is common at midlatitude stations in winter at sunspot minimum. It so happens that the evening increase discussed above is most pronounced at these same stations in summer at sunspot minimum. We suggest that the early morning winter increase is a consequence of the late evening increase that occurs in the summer (southern) hemisphere. Without needing to invoke actual transport of ionization from one hemisphere to another as proposed by Rothwell,[69] a plausible explanation (though highly speculative) can be offered. We suppose that above about 400 km the electron temperature along a field line is approximately constant as a result of the high thermal conductivity of the electrons. During the northern winter evening hours, a large region of the exosphere must be warmed from the southern foot of the field line where the sun has not set. When the sun does set, the temperature along the whole field line may decrease giving rise almost immediately to a pronounced increase in f_oF2 in the summer hemisphere and to a considerably smaller increase in the winter hemisphere at some later time. This idea has been discussed in more detail elsewhere.[70]

The total electron content of the ionosphere can be determined by Faraday rotation measurements. The two-frequency moon-reflection measurements are probably most accurate.[71] At temperate latitudes in winter, the daytime ratio n_a/n_b of the number n_a of electrons above $h_{max}F2$ to the number below n_b is approximately 2.5 to 1, and at sunspot minimum the summer day ratio is about twice this.[72] We are not in a position to test these values as the profiles do not extend to either sufficiently low or sufficiently high altitudes. However, it is clear that, although f_oF2 decreases from winter to summer, the density at a height of say 600 km increases from winter to summer. Thus the scale height H of the ionization above $h_{max}F2$ is larger in summer than winter, and this causes the increase in the ratio n_a/n_b.

IX. ION-TEMPERATURE MEASUREMENTS

Plots were constructed by drawing smooth temperature curves for each hourly interval and plotting as points the height at which a given temperature occurred; these points were then joined with straight lines. Fluctuations occur in these plots as a result of experimental errors, and a better presentation can be obtained by drawing smooth curves to follow the general behavior of the lines in these plots. These smoothed plots are shown in Figs. 16(a) through (l). It was frequently difficult to decide to what extent the original curves should be smoothed, and it is likely that some real variations have been lost in this process. Nevertheless, the smoothed plots do retain the main features of the diurnal behavior. The values for heights above 500 km are possibly too large as a result of the influence on the spectra of He^+ ions, and as such must be accepted with caution.

The principal features of these plots are the rapid increase in T_i at dawn, and somewhat less rapid decrease at sunset. These changes occurred at all heights above about 250 km.

During the daytime the ion temperatures show an increase of about 2°/km in the height range 250 to 500 km, irrespective of season. Above 500 km, T_i increases by more than 2°/km in the daytime, suggesting that the ion temperature is converging toward the electron temperature. At night, T_i increases by about 1°/km up to about 500 km, and usually by less above this height. There is evidence in some of the plots for sudden decreases of T_i during the hours of darkness (during the winter months), and these appear to be associated with increases in density at that time. Seasonal variations of T_i will be discussed later (Sec. XII).

X. ELECTRON-TEMPERATURE MEASUREMENTS

Figures 17(a) through (l) show determinations of the electron temperature. These plots were constructed in the same manner as those for the ion temperature. It is at once evident that $T_e > T_i$ at all heights most of the time. Like the ion temperature, T_e shows a rapid increase at dawn and less rapid decrease at sunset. There is some tendency for the electron temperature (at say 300-km altitude) to reach its highest value at about 2 to 3 hours after sunrise, but there are no large changes in T_e at this altitude during the major part of the day. Unlike T_i, the electron temperature increases rapidly with height ($\sim 2°$/km) up to about 400 km and then becomes almost isothermal in the daytime. The influence of neglected He^+ ions will be to overestimate T_i but underestimate T_e/T_i, thus T_e is likely to be the quantity least in error. Despite this, we feel the fact that the region above 500 km appears isothermal suggests that the spectra have been properly interpreted for the most part; i.e., little He^+ is present during the daytime at these altitudes.

Nighttime increases in T_e appear to have taken place during some of the months. A clear example is that at 0200 to 0300 in March. In winter months the spectra were usually poor because of the low electron density. Partly as a result of this, and also because of real fluctuations in T_e with time, it has been difficult to construct the nighttime behavior in the winter months (e.g., February). Precisely because the electron density is low during these months, the electron temperature can be raised considerably by only a small heat flux.

XI. MEASUREMENTS OF ELECTRON-TO-ION TEMPERATURE RATIO

Plots of the ratio of T_e/T_i are shown in Figs. 18(a) through (l). The highest value of the ratio is usually encountered at about 350- to 400-km altitude shortly before noon. Often there is a second maximum about noon or later. In most months these maxima have a value of 2.2 or 2.4, and the highest ratio at this altitude was 3.0 in March. During the daytime, $T_e/T_i \gtrsim 1.6$ at all altitudes under observation; hence, there are no violent changes in the ratio with altitude. The ratio T_e/T_i increases initially with altitude because T_e is rising faster than T_i, but subsequently decreases as T_e becomes nearly isothermal and T_i begins to increase rapidly. It is believed that these values of T_e/T_i are correct to ±20 percent up to about 500 km. Above this altitude, the presence of He^+ ions (particularly at night) may cause the spectra to be interpreted as indicating too low a value of T_e/T_i.

Although there is a clear increase in T_e/T_i at sunrise and a corresponding decrease at sunset, very rarely is thermal equilibrium completely established at night. Because T_i and T_e tend to vary during the night, their ratio T_e/T_i often provides a clearer indication of nighttime heating. Instances of such heating are evident in March (near 0300), in May (near 0300), in June (near 0200), in October (near midnight), and in January 1964 (near 2100). Even at times

18

other than near these definite nighttime increases, only during the summer months is T_e/T_i ever as low as 1.2. A more typical ratio would be 1.6, but the marked fluctuations of T_e/T_i at night, particularly during the winter months, make it difficult to construct meaningful plots.

The possibility of very large values of T_e/T_i occurring at sunrise at certain heights has been raised by Dalgarno.[62] Evidence of this during May must be discounted, as there is reason to believe there was appreciable heating during the early morning hours in this month. If an effect associated with sunrise does occur, it might be expected chiefly in the winter months when the predawn electron density is lowest, yet it does not seem to have been observed. This implies that the local heating assumption invoked by Dalgarno[62] does not hold in the ionosphere.

XII. AVERAGE DAYTIME-TEMPERATURE BEHAVIOR

In most months, fairly stable temperature conditions seem to exist throughout the major part of the day. Accordingly, a period of 6 or 7 hours was selected during the middle of the day in each month when the temperatures appeared to change least, and mean temperature profiles were constructed for these periods. These profiles are shown in Figs. 19(a) through (l) where, in general, the behavior of T_e and T_i with height does not have any very marked seasonal dependence, though some changes can be observed.

Seasonal variations in T_i are shown in Fig. 20 where the monthly mean values for 300, 400 and 500 km extracted from Figs. 19(a) through (l) are plotted. It can be seen that T_i increases from about 960°K in midwinter to about 1050°K in midsummer at 300 km. At 400 km the variation is about the same, i.e., from 1020° to 1160°K, but the winter-to-summer variation at 500 km is much larger — approximately 240°K. At 300-km altitude, the values of T_i obtained here are probably close to the neutral temperature T_n. However, satellite results indicate that T_n is a maximum in the equinoxes[73] and not in the summer as found for T_i. It is possible that some of the fluctuation of the points in Fig. 20 is significant, but there seems no way of testing this at the present time. The possibility that the summer increase in T_i is a consequence of the summer measurements being made on magnetically disturbed days has been investigated. The magnetic character figure A_p is plotted in Fig. 21 for all the days on which measurements were made; also shown is the monthly mean. It can be seen that there is no correlation between the mean monthly temperatures and the mean values for A_p. This probably signifies that the largest part of the variation in Fig. 20 is simply a seasonal one, and a more careful test needs to be made to determine whether or not there are any changes during disturbed conditions. Such a test is described in Sec. XIV. Also, it can be seen from Fig. 20 that the solar ultraviolet flux as characterized by the sun's radio radiation at 10.7 cm ($S_{10.7}$) was roughly constant throughout 1963, so that the summer increase in T_i cannot be ascribed to changes in the intensity of the solar ultraviolet. It would seem that this is simply a consequence of the reduced solar zenith distance in summer.

The seasonal dependence in the electron temperature is shown in Fig. 22 for 300- and 500-km altitude. The scatter of the points for the electron temperature is larger than that for T_i, making interpretation more difficult. It is clear, however, that T_e is at a minimum in the winter months and at a maximum in the late spring to early summer. It is probable that there is a second smaller maximum in the late summer. The difference between maximum and minimum is ~500° to 600°. The variation of the maximum value of T_e/T_i is also shown in Fig. 22, and it seems clear that it is this variation which gives rise to the two maxima in T_e.

The seasonal variation in T_i can readily be accounted for by the variation of the sun's zenith distance provided it is assumed that $T_i \geq T_n$ above 300 km. A simple explanation can also be offered for the variation in T_e/T_i. At first sight it would seem that T_e/T_i should peak in the summer, because the electron density is then least at the peak of the F2 layer and the fast photoelectrons should be able to traverse the peak with less energy loss than in the winter. However, an opposing effect exists, namely that the thickness of the layer is at maximum in summer,[74] and perhaps this more than offsets the change in density at the peak.

XIII. AVERAGE NIGHTTIME-TEMPERATURE BEHAVIOR

Daytime behavior is usually fairly stable and, by taking an average over several hours, we have been able to identify certain seasonal trends. Nighttime behavior, on the other hand, seems erratic (particularly in the winter months); hence, averages have been taken not simply as a means of reducing experimental errors but in order to gain a better understanding of the average behavior. These nighttime averages are shown in Figs. 23(a) through (l). Considerable variability exists from month to month reflecting the random changes within the month, and also the reduced experimental accuracy at night when the signals are weak. Despite this, some regularities can be discerned.

Below 300 km, T_i and T_e/T_i are usually found to be increasing, but above this height T_i usually increases by less than 1°/km. T_e/T_i does not change by very large amounts with height, but may exhibit a maximum of 350- to 400-km altitude. Because T_e/T_i does not change markedly with height, the curve for T_e tends to follow the curve for T_i.

Figure 24 shows the variation of T_e, T_i, and T_e/T_i at 350-km altitude. If any nighttime heating agency is active throughout the year without any significant change in flux, it would be expected that T_e/T_i would be a minimum in summer when the electron density N is highest (since the heat loss from electrons to ions proceeds at a rate proportional to N^2).[63] This appears to be the case — the lowest values of T_e/T_i being observed in July. The ion temperature shows a pronounced peak in September, and one is reminded that this was the month that was most magnetically disturbed (Fig. 21). The electron temperature is also large in this month, and it is tempting to conclude that there is a heat source whose magnitude depends upon the magnetic character figure A_p but that the daytime temperatures are insensitive to this source, as solar ultraviolet is much larger.

XIV. TEMPERATURE EFFECTS ASSOCIATED WITH MAGNETICALLY DISTURBED CONDITIONS

We have been concerned in this study principally with determining the normal daily and seasonal behavior of the quantities measured; hence, magnetic disturbance effects have not been examined in detail. It is, however, important to assess to what extent magnetic disturbances may have played a part in controlling the results. We have already concluded that during the daytime T_e and T_i are insensitive to disturbances as characterized by the figure A_p. Also we have seen that T_e and T_i apparently increase on disturbed nights, but this conclusion rests on the high values observed at night in September — the most-disturbed month. To test these conclusions we have divided September into the quietest days ($A_p \leq 14$) and most-disturbed days ($A_p \geq 19$). The average values of A_p for the two groups were 11 and 67, respectively. The mean-temperature-vs-height dependence for the two groups is shown in Figs. 25 and 26. As

20

far as can be determined, T_e is the same on both the quiet and disturbed days in the daytime though, below 400 km, T_i was about 100° higher on the disturbed day. At night, however, extremely large differences appear. Above 350 km, T_e is raised over 800°K and T_i by about 200°K. We have discussed elsewhere[75] the behavior of the temperature on individual days in this month, and will here only summarize the results. For the daytime period (1000 to 1500) there seemed little significant change in T_i at any height, but a decrease in T_e on disturbed days (Table IV). At night, T_i and T_e increased at all heights during disturbed conditions. The average increase in T_i per unit increase of the K_p index, $\Delta T_i / \Delta K_p \sim 190°$ (Table IV) and $\Delta T_e / \Delta K_p$, was twice as large. Also given in Table IV are the temperature increases as functions of the three-hour index a_p. It seemed from the scatter of the results that the temperature was more closely related to A_p than K_p, though there were insufficient data to be certain of this.

The values of $\Delta T_e / \Delta K_p$ given in Table IV presumably depend to a very large extent upon the electron density, and hence would be expected to exhibit both diurnal and seasonal changes — even if K_p is a proper index to employ as a measure of the heat flux. For example, we should expect quite small heat fluxes to raise T_e considerably at night in winter but not in summer.

Evans and Taylor[71] observed from Faraday rotation measurements that during the night in winter the F2 region scale height increases with magnetic activity (as indicated by the K_p index). Apparently this scale height increase is the result of increased electron and ion temperatures. It is not clear whether heating by hydromagnetic waves (as suggested by Dessler[76]), by electric fields,[77] or by particle precipitation is the responsible agency.

Heating of the neutral constituent by an agency correlated with K_p or a_p has been reported by several workers.[78-83] The time resolution in these measurements, which are based on the observed drag on artificial earth satellites, is inadequate to show diurnal changes. Jacchia and Slowey[84] find $\Delta T_n / \Delta K_p \sim 35°K$ for $K_p \leqslant 5$. For $K_p > 5$, there is better correlation with the a_p index and $\Delta T_n / \Delta a_p = 1°K$. Since our September results were obtained at times when K_p was mostly <5, we would expect closest agreement between these satellite results and the values for $\Delta T_i / \Delta K_p$ at 300 km. The large difference in daytime and nighttime values for this quantity suggests that either (a) the heat flux associated with disturbed conditions is absent during the daytime, or (b) it cannot be detected during daytime in the presence of the much larger ultraviolet flux from the sun. In either case, it may be that the variation of T_n with magnetic conditions observed from satellite results is largely a nighttime phenomenon. The nature of this heat source remains to be determined, but it seems evident that measurements of T_e and T_i over a wide range of height, made with a time resolution far superior to the present determinations of T_n, should contribute significantly.

XV. SCALE HEIGHT OF UPPER F-REGION

Throughout most of the daytime hours, the electron-density distribution above h_{max} exhibits almost constant scale height H up to about 500 to 600 km. The value of the scale height has been obtained from the mean profiles by determining at what height the electron density falls by e^{-1} from its value at 350 km. This quantity has a value of the order of 100 to 150 km, and is therefore approximately equivalent to the scale height at 400- to 425-km altitude. The values for the mean scale height have been plotted in Figs. 27(a) through (j). No values are given for May and June because no electron-density profiles were obtained in these months.

TABLE IV					
FRACTIONAL INCREASES IN TEMPERATURE AT VARIOUS HEIGHTS					
Daytime					
Index	300 km	400 km	500 km	600 km	Mean of All Heights
$\Delta T_i/\Delta A_p$	1.4	0.7	−4.5	−2.1	−1.1
$\Delta T_i/\Delta a_p$	1.1	−0.2	−5.1	−2.3	−2.2
$\Delta T_i/\Delta K_p$	20	10	−31	−11	−3
$\Delta T_e/\Delta A_p$	−15.2	−24.8	−21.7	−19.1	−20.2
$\Delta T_e/\Delta a_p$	−12.5	−22.0	−19.6	−19.8	−18.5
$\Delta T_e/\Delta K_p$	−46	−123	−76	−80	−81
Nighttime					
$\Delta T_i/\Delta A_p$	9.5	7.6	6.4	−	7.8
$\Delta T_i/\Delta a_p$	23.1	20.9	20.0	−	21.3
$\Delta T_i/\Delta K_p$	195	186	185	−	189
$\Delta T_e/\Delta A_p$	15.2	16.3	13.2	−	14.9
$\Delta T_e/\Delta a_p$	43.6	43.1	45.6	−	44.1
$\Delta T_e/\Delta K_p$	378	367	422	−	389

Under conditions of diffusive equilibrium, when the electron and ion temperatures T_e and T_i are changing with height, H is given in

$$-\frac{1}{H} = \frac{d}{dz} (\log N) = -\frac{m_i g}{k(T_i + T_e)} - \frac{1}{T_i + T_e} \cdot \frac{d}{dz} (T_i + T_e) \quad , \tag{5}$$

in which z is geopotential altitude [$z = hR_e/(R_e + h)$, where h is the true altitude and R_e the earth's radius]. The difference between true height h and geopotential altitude z can be allowed for approximately by taking the value for g (868 cm sec^{-2} at 400 km).

Using the above expression and assuming that O^+ is the principal ion ($m_i = 2.65 \times 10^{-23}$ gm), we have computed the expected scale height at 400 km for the average temperatures, and these values are also shown in Figs. 27(a) through (j). In several months (e.g., November) the agreement seems excellent; there is a tendency, however, for the daytime observed values to lie below the computed ones, particularly in the early part of the year. It is possible that this arises as a consequence of the fact that the mean ion mass is less than that of atomic oxygen. However, the agreement in October and November suggests that this is not the case, and a more likely explanation is that in some months the density profiles are in error as a result of the TR recovery problem discussed previously (Sec. VI-A). In particular, it is known that this problem was severe during some days in July. It would seem, therefore, that the upper part of the F-region is in diffusive equilibrium and that O^+ is the principal ion up to about 500 km both by day and by night.

This is an important result; it implies, for instance, that the evening increase in f_oF2 observed in the summer months is simply a consequence of cooling of the ionosphere, causing a lowering of the equilibrium scale height. It seems quite unnecessary to invoke electrodynamic drift motions to explain this phenomenon though, on the basis of the results presented here, one cannot exclude the possibility of such drift motions provided they are small.

XVI. HEAT FLUX Q_{350}

A second quantity extracted from the data and presented in Figs. 28(a) through (j) is the heat flux Q defined in

$$T_e - T_i = \frac{2 \times 10^6 Q T_e^{3/2}}{N^2} \quad , \tag{6}$$

where Q is the energy input to the electron gas (ev cm^{-3} sec^{-1}), and N is the electron density. This expression has been derived by Dalgarno, et al.,[85] and Hanson,[63] and specifies the heat input required to maintain a given temperature difference $T_e - T_i$ at an altitude (above 300 km) where the electron gas is cooled entirely by coulomb encounters with atomic oxygen ions. Since T_e, T_i, and N are known we can compute Q as a function of time and height. However, it has been shown[46] that during the day, when $T_e > T_i$ at all heights, the altitude variation of Q is determined chiefly by the variation of N^2 in Eq. (6). That is, Q decreases with a scale height about half that for the electron density. At night this is not necessarily true, and Q may show a peak where T_e/T_i reaches a maximum ($\sim$350 km). Accordingly, Q has been computed for a fixed height of 350 km both for daytime and nighttime. In the summer months, Q_{350} is found to increase almost linearly throughout the day and to reach a peak of the order of 500 to 600 ev cm^{-3} sec^{-1} near sunset. This is accounted for by the rise of the whole layer throughout the day,

causing the electron density N at 350 km to increase. In the winter months the peak shifts to the middle of the day, as the density at 350 km is greatest at that time.

It should be stressed that these daytime values of Q do not represent the total heat flux into any cell of the electron gas at 350-km altitude. They represent the heat lost in such a cell to the ions. A considerably larger amount of heat is conducted to other altitudes.

The flux Q_{350} is most accurately measured when $T_e - T_i$ is large; hence, the greatest uncertainty lies in values obtained during the summer at night. Despite this, small fluxes in the range 10 to 50 ev cm^{-3} sec^{-1} are found at night in all months; there seems to be no significant seasonal variation. These fluxes are of the order of one tenth or less of the daytime fluxes but are entirely adequate to cause pronounced effects, especially in winter, when there is a large diurnal change in N^2.

It is possible that more than one agency contributes to this nighttime heating, but for want of better evidence we presume there is a single source whose intensity is correlated with K_p. During the daytime, the peak in T_e/T_i is about 100 to 150 km higher than the peak of the layer h_{max}. At night, during those months where the T_e/T_i plot shows a peak, the height difference is usually less than 50 km. Evidently the nighttime heating must occur in the vicinity of 300 km in order that T_e/T_i and N can both have peaks near this altitude. By contrast, the daytime absorption of solar ultraviolet takes place chiefly at heights below 250 km.

XVII. DISCUSSION

A. High Values for Electron Temperature

The possible difference between the temperature of the electrons T_e and the neutral gas temperature T_n seems to have been considered quantitatively only recently. Hanson and Johnson[86] outlined the physical processes involved, and their work has been summarized by Bourdeau and Bauer.[87] More recently, Hanson,[63] Dalgarno, et al.,[85] and Dalgarno[62] have discussed the problem anew.

Photoelectrons with a wide range of energies (5 to 50 ev) are produced by the incident solar flux. The first step in any calculation of $T_e - T_n$ consists of estimating the number of photoelectrons produced as a function of height and their average energy. In view of the many possible excitation reactions, this is perhaps one of the most uncertain steps in the computation. Next, it is necessary to investigate the mechanisms by which the fast electrons may lose their energy; these too are a function of height. At low levels the electrons rapidly lose energy by inelastic collisions with the neutral gas. Important are the excitation of the ^1D state of atomic oxygen and also the excitation of molecular nitrogen into vibrational states. These effects should rapidly reduce the electron energy to a little less than 2 ev. At this energy level a fast photoelectron is finally slowed to thermal speeds by coulomb interaction with other electrons. This latter effect raises the temperature of the electron gas as a whole.

Proceeding upward in height, the number density of neutral particles decreases and a larger fraction of the excess energy is given to the electron gas via coulomb encounters. In this region (above 300 km) the temperature difference no longer depends linearly upon the energy of the photoelectrons, as those with more than about 10 ev can escape along the field lines to the conjugate point.[63] Thus, heating efficiency (of the electron gas by the fast electrons) appears to increase with height in a rather uncertain manner. At these heights the electron gas loses energy primarily to the (oxygen) ions via elastic collisions, and the temperature difference will be as shown in Eq. (6).[63, 85]

Dalgarno, et al.,[85] ignore transport of heat either by thermal conduction or by the fast photoelectrons, and assume that the heat Q given to the electrons at any height is determined by absorption of solar ultraviolet radiation at that height. Hanson[63] considers upward transport of energetic electrons (which could contribute considerably to the value of Q above 300 km) but is unable to reach very firm conclusions. Two other points which Hanson[63] raises are (1) the electrons have high thermal conductivity and might be expected to maintain a constant temperature more or less independent of the atmospheric temperature above 600 km, and (2) the ions will be in good thermal contact with the neutral particles at low altitudes but, as the collision frequency falls with height, they may assume the electron temperature (above about 750 km). Dalgarno[62] supports this latter prediction.

Both Dalgarno, et al.,[85] and Hanson[63] anticipate that the largest difference between the electron and neutral temperatures should occur near 220 km, and Brace, et al.,[13] have provided some experimental evidence in support of this. On the other hand, the results presented here indicate the largest difference lies between 350 and 600 km.

In a more recent attack on the problem,[60] attempts were made to include thermal conduction and an upward flux of fast photoelectrons. It was assumed that the thermal conductivity of the electrons was so much greater than that of the ions, that the latter could be neglected. Thus, electrons at heights above 300 km are heated by (1) heat conducted from below, and (2) an upward flux of fast photoelectrons. They lose heat partly by conduction to other heights and partly in coulomb counters with ions. The ions are presumed to lose heat solely by collisions with the neutral particles. This model has been able to account satisfactorily for the behavior of T_e and T_i observed during the daytime at midlatitudes in summer at sunspot minimum.[60] Figure 29 shows a comparison of the temperatures given in Fig. 11 with temperatures deduced by Geisler and Bowhill[60] according to the model. The agreement is considered quite good in view of the many uncertain quantities remaining in the theory. Geisler and Bowhill[60] report, however, that the thermal conductivity of the electrons is so great that many other parameters (e.g., the electron-density distribution) can be changed without significantly influencing the results. It seems therefore that a theoretical understanding of the behavior of the electron and ion temperatures in the ionosphere is now at hand. This seems to be a demonstration of the power of the theoretical method to provide the correct answer once it is known.

B. Ionospheric Anomalies

The summer evening increases in f_oF2 have been explained as a result of this work.[48] It has been shown to be simply a consequence of the cooling of the exospheric electron temperature at sunset. We have suggested[70] that the nocturnal increase in f_oF2 observed in winter is the consequence of the same phenomenon to an observer in the winter hemisphere. This latter proposal lacks a theoretical treatment of the problem of temperature distribution along a field line when one foot is sunlit and the other is in shadow. Hence, it cannot be regarded as other than speculative at the present time.

The major temperate latitude ionospheric anomaly, the so-called "winter anomaly" of higher midday winter f_oF2 values than summer, has not been explained. Wright[88] has argued that "winter anomaly" is an improper description since it can be shown that summer behavior is anomalous. In part, the seasonal anomaly can be explained as a result of an expansion of the F-region in summer, leading to a scale height H above h_{max} that is higher in summer than in

winter. Observations of Faraday rotation of moon-reflected radar signals yield values for the total electron content of the ionosphere.[89, 71, 72] These show that the anomaly in the total content is much less pronounced than in the value for the peak of the layer. Nevertheless, an anomaly does remain.

The results presented here show that the seasonal anomaly cannot be satisfactorily explained as a consequence of large seasonal changes in the ionospheric temperature which might either (1) violently expand the region as suggested by Appleton,[90] or (2) change the rates of recombination.[91] Presumably the reason for the anomaly must be sought in seasonal changes in the loss rates governing the disappearance of electrons at F-region heights. These changes could be realized by changing the composition of the atmosphere.[88, 92-94]

XVIII. CONCLUSIONS

The operation of the Millstone Hill ionospheric radar has been described, and results of about 1500 hours of observation throughout 1963 have been presented. Several hitherto unexplained features of the behavior of the F-region are now understood as a result of this work. The results reported herein apply to conditions at sunspot minimum. It is currently thought that conditions should be substantially different at sunspot maximum. In particular, it is believed that the temperature difference $T_e - T_i$ will be much less.[60, 66, 70] This prediction remains to be tested. Also, at sunspot maximum it seems likely that heating associated with magnetically disturbed conditions will be much more common. The nature of the nighttime heat source remains to be established. We do not yet know whether the high temperatures observed in September were the result of an increase in the intensity of the nighttime agent, or of yet a third source of ionospheric heating.

Many other opportunities presented by the development of the backscatter technique remain to be explored. A more careful examination of the uppermost spectra shall be conducted to determine the ratio of the numbers of O^+ to He^+ ions. This, in turn, will lead to temperature values at heights which are less uncertain than those presented here. The region below 240 km remains to be explored effectively. In this region, N, T_e, T_i and the ratios of the numbers of ions all change rapidly with height. It is unlikely that, even were there no problem with ground clutter echoes, our existing radar could satisfactorily examine this region. (This is also true of the Arecibo Ionospheric Observatory.) We intend, therefore, to use a radar operating at 1295 Mcps with a beam directed obliquely (at 20° elevation) to explore the E and F1 regions.

Other groups employing the incoherent scatter technique exist in several countries: e.g., at Prince Albert in Canada; at Nancay in France; at Malvern in England; as well as the Arecibo Ionospheric Observatory in Puerto Rico, and the Jicamarca Ionospheric Radar in Peru. Many useful results should emerge from this work.

ACKNOWLEDGMENTS

REFERENCES

1. R. E. Bourdeau, Space Sci. Rev. 1, 683 (1963).

2. F. S. Johnson, J. Geophys. Res. 65, 2571 (1960).

3. W. B. Hanson and D. D. McKibbin, J. Geophys. Res. 66, 1667 (1961).

4. J. E. Jackson and S. J. Bauer, J. Geophys. Res. 66, 3055 (1961).

5. S. J. Bauer and R. E. Bourdeau, J. Atmos. Sci. 19, 218 (1962).

6. M. Nicolet, J. Geophys. Res. 66, 2263 (1962).

7. W. B. Hanson, J. Geophys. Res. 67, 183 (1962).

8. R. E. Bourdeau, et al., J. Geophys. Res. 67, 467 (1962).

9. M. A. Taylor, et al., J. Geophys. Res. 68, 5339 (1963).

10. N. W. Spencer, L. H. Brace and G. R. Carignan, J. Geophys. Res. 67, 157 (1962).

11. J. V. Evans, J. Geophys. Res. 67, 4914 (1962).

12. V. C. Pineo and D. P. Hynek, J. Geophys. Res. 67, 5119 (1962).

13. L. H. Brace, N. W. Spencer and G. R. Carignan, J. Geophys. Res. 68, 5397 (1963).

14. A. F. Nagy, et al., J. Geophys. Res. 68, 6401 (1963).

15. W. B. Hanson, T. N. L. Patterson and S. S. Degaonkar, J. Geophys. Res. 68, 6203 (1963).

16. S. J. Bauer, J. Geophys. Res. 69, 553 (1964).

17. J. W. King, et al., Document RRS/IM 94, Radio Research Station, Slough, England (1963).

18. S. J. Bauer and L. J. Blumle, J. Geophys. Res. 69, 3613 (1964).

19. J. W. King, et al., Document RRS/IM 112, Radio Research Station, Slough, England (1963).

20. G. E. K. Lockwood and G. L. Nelms, J. Atmos. Terrest. Phys. 26, 569 (1964).

21. P. C. Kendall, J. Atmos. Terrest. Phys. 24, 805 (1962).

22. Ibid., 25, 87 (1963).

23. H. A. Rishbeth, A. J. Lyon and M. Peart, J. Geophys. Res. 68, 2559 (1963).

24. R. A. Goldberg, P. C. Kendall and E. R. Schmerling, J. Geophys. Res. 69, 417 (1964).

25. P. J. Bowen, et al., Proc. Roy. Soc. (London) A281, 526 (1964).

26. W. E. Gordon, Proc. IRE 46, 1824 (1958).

27. K. L. Bowles, Phys. Rev. Letters 1, 454 (1958).

28. _____, J. Research Natl. Bur. Standards 65D, 1 (1961).

29. V. C. Pineo, L. G. Kraft and H. W. Briscoe, J. Geophys. Res. 65, 1620 (1960).

30. Ibid., 65, 2629 (1960).

31. V. C. Pineo and H. W. Briscoe, J. Geophys. Res. 66, 3965 (1961).

32. K. L. Bowles, G. R. Ochs and J. L. Green, J. Research Natl. Bur. Standards 66D, 395 (1962).

33. J. V. Evans, "Studies of the F-Region by the Incoherent Backscatter Method," Technical Report 274, Lincoln Laboratory, M. I. T. (24 July 1962), DDC 292730.

34. J. S. Greenhow, H. K. Sutcliffe and C. D. Watkins, J. Atmos. Terrest. Phys. 25, 197 (1963).

35. W. E. Gordon, Trans. IEEE, PTGMIL MIL-8, 206 (1964).

36. J. A. Fejer, Can. J. Phys. 38, 1114 (1960).

37. J. P. Dougherty and D. T. Farley, Proc. Roy. Soc. (London) A259, 79 (1960).

38. E. E. Salpeter, Phys. Rev. 120, 1528 (1960).

39. _____ , J. Geophys. Res. 65, 1851 (1960).

40. J. A. Fejer, Can. J. Phys. 39, 716 (1961).

41. D. T. Farley, J. P. Dougherty and D. W. Barron, Proc. Roy. Soc. (London) A263, 238 (1961).

42. T. Hagfors, J. Geophys. Res. 66, 1699 (1961).

43. E. E. Salpeter, J. Geophys. Res. 66, 982 (1961).

44. J. Renau, M. Camnitz and W. Flood, J. Geophys. Res. 66, 2703 (1961).

45. V. C. Pineo, D. P. Hynek and G. M. Millman, J. Geophys. Res. 68, 2695 (1963).

46. J. V. Evans and M. Loewenthal, Planet. Space Sci. 12, 915 (1964).

47. J. V. Evans, J. Geophys. Res. 70, 131 (1965).

48. _____ , "The Cause of the Mid-Latitude Evening Increase in $f_o F2$," J. Geophys. Res. 70 (1965) (in press).

49. O. Bunneman, J. Geophys. Res. 67, 2050 (1962).

50. E. E. Salpeter, J. Geophys. Res. 68, 1321 (1963).

51. D. R. Moorecroft, J. Geophys. Res. 68, 4870 (1963).

52. K. L. Bowles, paper presented at 14th International URSI Meeting, Tokyo, September 1963.

53. M. Petit, Compt. rend. 255, 2804 (1962).

54. S. M. Poloskov, Space Research I, edited by H. K. Kallmann-Bijl (North Holland Publishing Co., Amsterdam, 1960), p. 95.

55. V. G. Istomin, Planet. Space Sci. 9, 179 (1962).

56. S. J. Bauer, Nature 197, 36 (1963).

57. G. Kockarts and M. Nicolet, Ann. de Geophys. 19, 370 (1963).

58. D. R. Moorecroft, J. Geophys. Res. 69, 955 (1964).

59. K. I. Gringauz, et al., An. USSR Geoficicheskaya Sekt. 151, 560 (1963).

60. J. E. Geisler and S. A. Bowhill, paper presented at the Fall URSI Meeting, Urbana, Ill., 1964.

61. F. S. Johnson, The Satellite Environment Handbook, edited by F. S. Johnson (Stanford University Press, Stanford, 1961), p. 9.

62. A. Dalgarno, Technical Report 63-11-N, Geophysics Corporation of America (1963).

63. W. B. Hanson, Space Research III, edited by W. Priester (North Holland Publishing Co., Amsterdam, 1963), p. 282.

64. J. O. Thomas, J. Geophys. Res. 68, 2707 (1963).

65. J. V. Evans, J. Geophys. Res. 70, 733 (1965).

66. R. E. Bourdeau, paper presented at the COSPAR Meeting in Florence, May 1964.

67. R. W. Eyfrig, J. Geophys. Res. 68, 2529 (1963).

68. _____ , Ann. de Geophys. 19, 102 (1963).

69. P. Rothwell, J. Phys. Soc. Japan 17, Suppl. 1A, 263 (1962).

70. J. V. Evans, "The Cause of the Mid-Latitude Winter Night Increase in $f_o F2$," in preparation.

71. J. V. Evans and G. N. Taylor, Proc. Roy. Soc. (London) A263, 189 (1961).

72. G. N. Taylor, Proc. Roy. Soc. (London) A279, 497 (1964).

73. H. K. Paetzold, Space Research IV, edited by P. Muller (Wiley, New York, 1964), p. 271.

74. J.W. Wright, Electron Density Distributions in Ionosphere and Exosphere, edited by E. Thrane (North Holland Publishing Co., Amsterdam, 1964), p. 186.

75. J.V. Evans, "Mid-Latitude Ionosphere Temperatures on Magnetically Quiet and Disturbed Days," submitted to J. Geophys. Res. (1965).

76. A.J. Dessler, J. Geophys. Res. 64, 397 (1959).

77. L.R. Megill and N.P. Carleton, J. Geophys. Res. 69, 101 (1964).

78. L.G. Jacchia, Nature 183, 1662 (1959).

79. _____ _, Space Research III, edited by W. Priester (North Holland Publishing Co., Amsterdam, 1963), p. 3.

80. G.V. Groves, Space Research I, edited by H.K. Kallmann-Bijl (North Holland Publishing Co., Amsterdam, 1961), p. 715.

81. L.G. Jacchia and J. Slowey, Special Report 84, Smithsonian Astrophysical Observatory (1962).

82. _____ , Special Report 125, Smithsonian Astrophysical Observatory (1963).

83. _____ , J. Geophys. Res. 69, 905 (1964).

84. _____ , J. Geophys. Res. 69, 4145 (1964).

85. A. Dalgarno, M.B. McElroy and R.J. Moffet, Planet. Space Sci. 11, 463 (1963).

86. W.B. Hanson and F.S. Johnson, Les Congres et Collogues de l'Université de Liege 20, 390 (1961).

87. R.E. Bourdeau and S.J. Bauer, Space Research III, edited by W. Priester (North Holland Publishing Co., Amsterdam, 1963), p. 173.

88. J.W. Wright, J. Geophys. Res. 68, 4379 (1963).

89. J.V. Evans, J. Atmos. Terrest. Phys. 11, 259 (1957).

90. E.V. Appleton, Nature 136, 52 (1935).

91. O. Burkard, Geofisica Pura E Applicata 48, 57 (1961).

92. G.A.M. King, Planet. Space Sci. 9, 95 (1962).

93. _____ , J. Atmos. Sci. 21, 231 (1963).

94. J.M. Bullen, J. Atmos. Terrest. Phys. 26, 559 (1964).
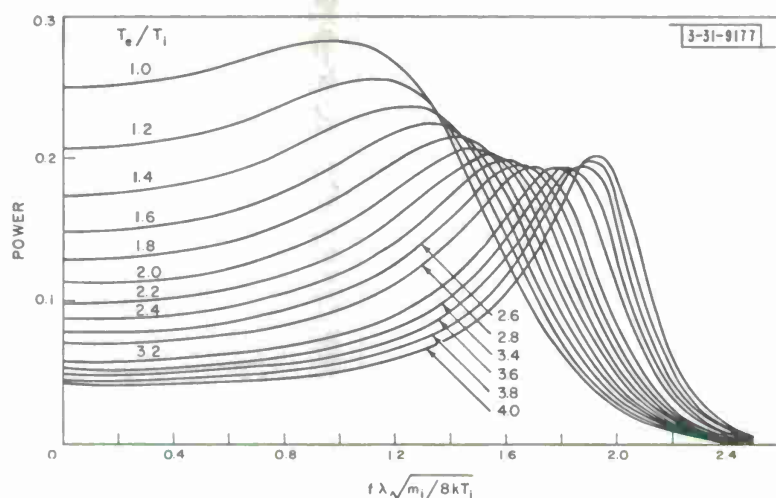
Fig. 1.   Theoretical spectra of ionospheric backscatter signals computed for various values of electron-to-ion temperature ratio T_e/T_i.   Spectra are symmetrical about center frequency.   It has been assumed that the mass m_i of the ions is that of O^+. Abscissa is Doppler shift f normalized by multiplying by radio wavelength λ and a term inversely proportional to velocity of sound for ions.
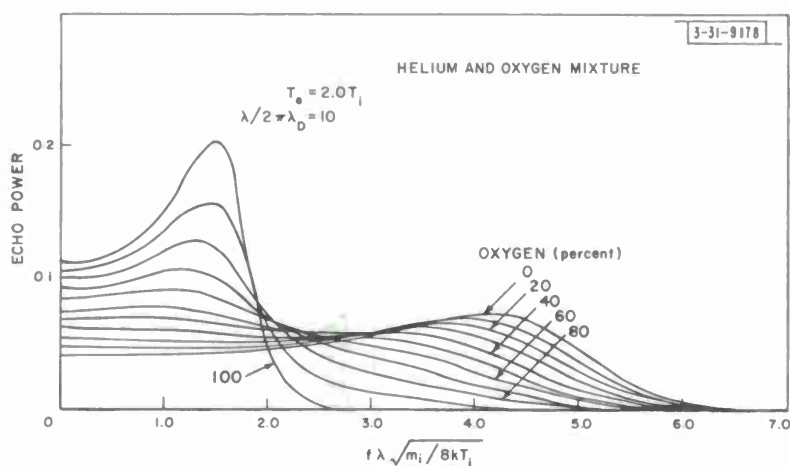
Fig. 2.   Effect on spectrum in which $T_e/T_i = 2.0$ as progressively larger amounts of He^+ ions are introduced into an O^+/He^+ mixture.   Abscissa same as Fig. 1, and m_i represents the mass of the heavier constituent (O^+).

31
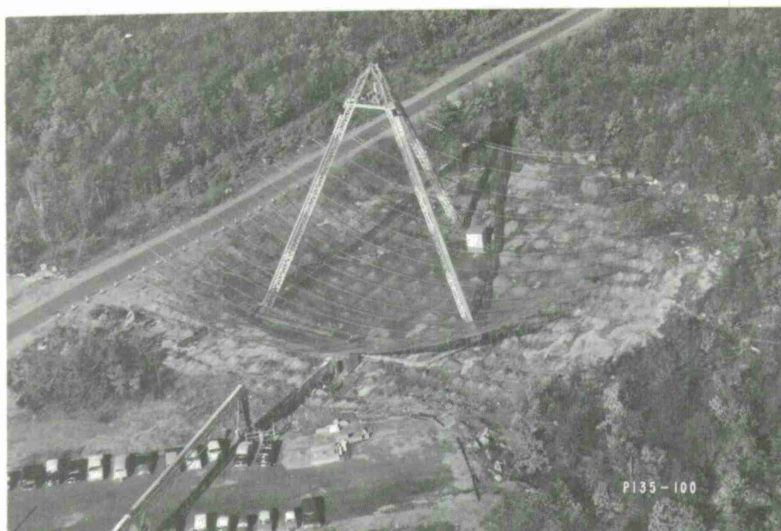
Fig. 3. The 70-meter parabola employed at Millstone Hill Radar Observatory for ionospheric studies. Tripod structure supports feedhorn and turnstile junction. Left-hand waveguide connects turnstile junction to transmitter (in building off the picture), and right-hand waveguide connects junction to first stages of receiver housed in lower hut.
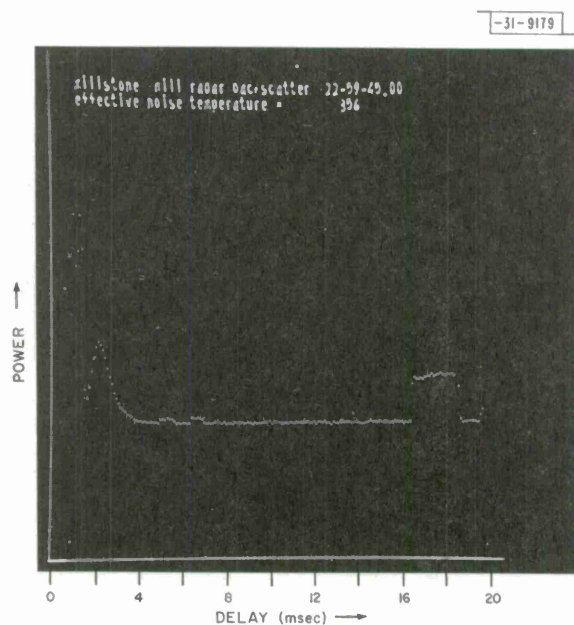
Fig. 4. A cathode-ray-tube display presenting result of integration over a time base performed in computer. In this measurement, pulse length was 0.5 msec and points representing averaged output power are at 100-μsec intervals. Following receiver suppression (extreme left) are first some ground clutter echoes and second the echo from the ionosphere. Beyond ionospheric echo are echoes from two satellites that chanced to traverse the beam during this measurement. Large pulse at right is introduced into receiver to calibrate scale and corresponds to an increase in system temperature of 100°K.
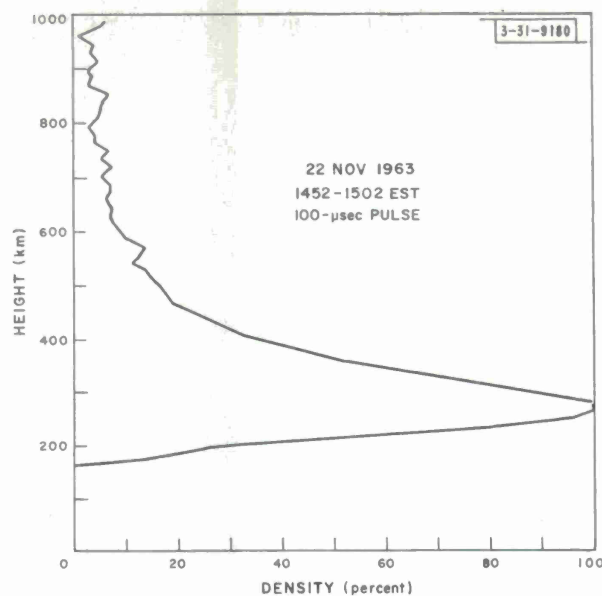
Fig. 5. Plot produced by computer of electron density N'(h) vs height. Computer draws straight lines between measured points which are at 15-km height intervals. Fluctuations observed above 500-km height are errors due to noise and not true variations in electron density. Below 200 km, receiver was suppressed against ground clutter echoes.
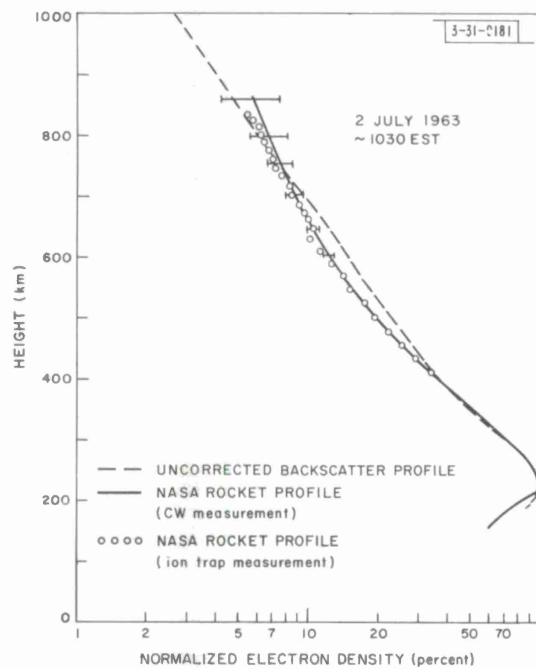
Fig. 6. Example of combined electron-density profile obtained from plots (e.g., Fig. 5) for 0.1-, 0.5- and 1.0-msec pulses. These partic-ular measurements were made at same time as rocket was launched from Wallops Island, Virginia. Difference between rocket and backscatter profile is largely due to fact that σ has been assumed constant to ob-tain this profile.

33
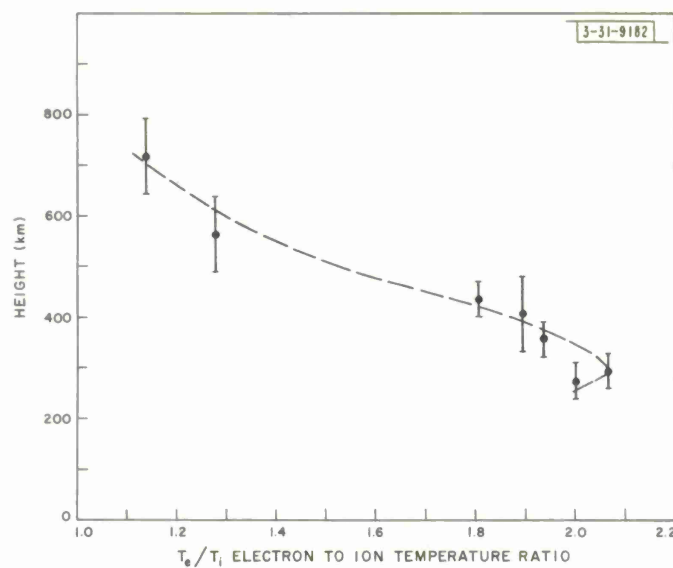
Fig. 7. Variation of electron-to-ion temperature ratio T_e/T_i obtained from spectra measured during period 0834 to 1005 EST on 2 July 1963.
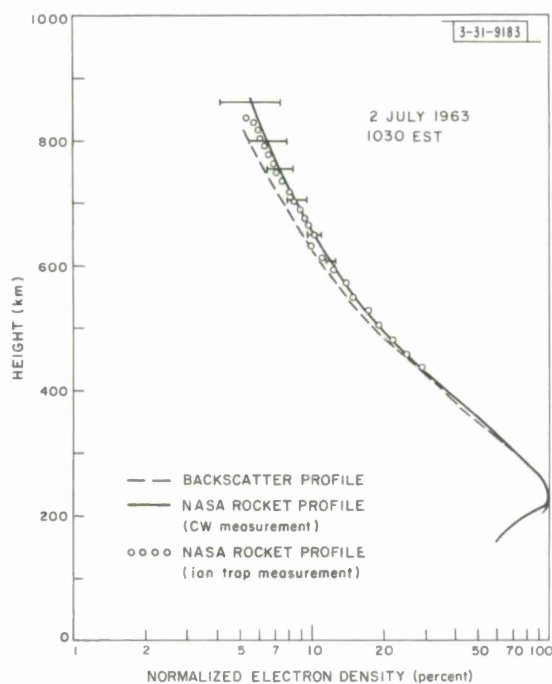
Fig. 8. Backscatter electron-density profile (Fig. 6) after correcting for variation of electron cross section σ, with height according to Eq. (4) and results for T_e/T_i presented in Fig. 7. Rocket measurements were made at 0922, but ground clutter echoes obscured F-region peak in backscatter measurement until 1030.

34
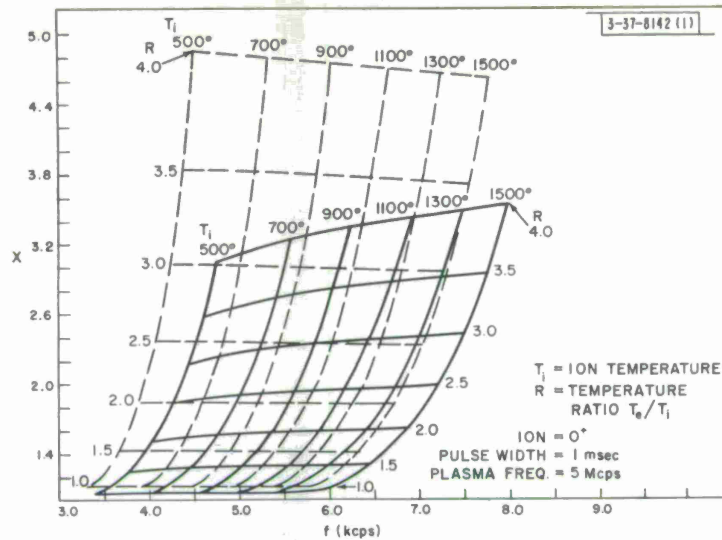
Fig. 9. Plots showing variation of contours of constant T_e/T_i (= R) and T_i as functions of scaled quantities f and x. Ordinate x is the ratio between peak echo power in the wing (Fig. 1) to that at center frequency, and f is Doppler shift of a point of half peak intensity. Dotted lines show values in absence of equipmental effects, whereas solid lines show change in x and f when spectral distortion introduced by transmitter pulses and receiver filters is allowed for.
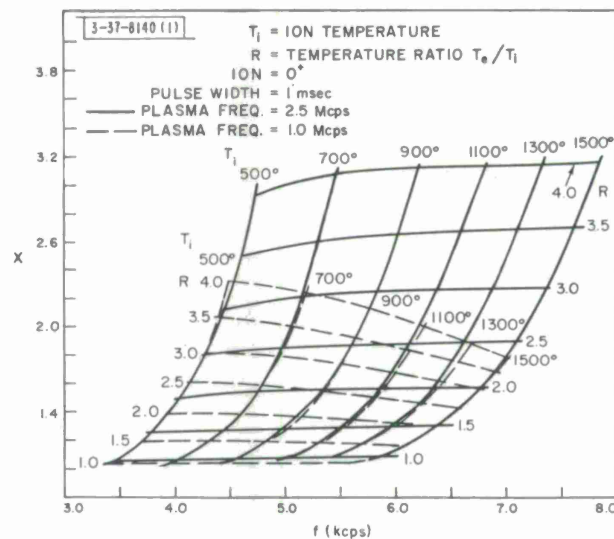
Fig. 10. Two spectrum analysis charts similar to full lines in Fig. 9 are here superimposed to illustrate dependence of spectrum shapes upon electron density N (specified in terms of a plasma frequency f_p). Density N enters because equations contain ratio of radar wavelength λ to $4\pi\lambda_D$ where λ_D is Debye length $(= \sqrt{kT_e/4\pi Ne^2})$.
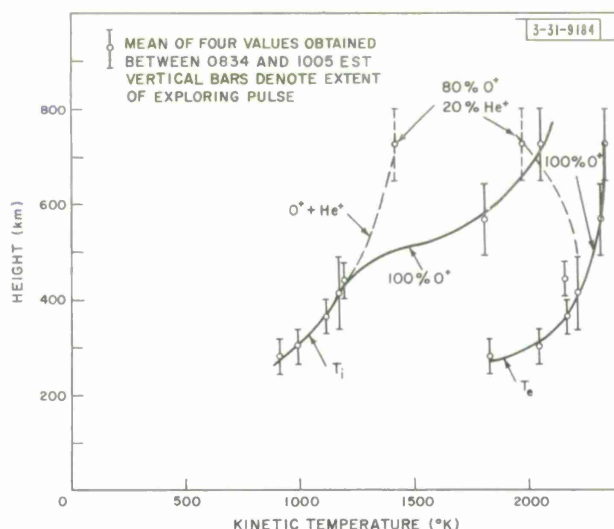
Fig. 11. Variation of electron (T_e) and ion (T_i) temperatures observed on 2 July 1963. Solid lines denote values deduced on assumption that only O^+ ions are present at all heights. Dotted lines indicate how temperature might vary if percentage of He^+ ions becomes significant above 500 km and increases to value of 20 percent of total at 720 km.
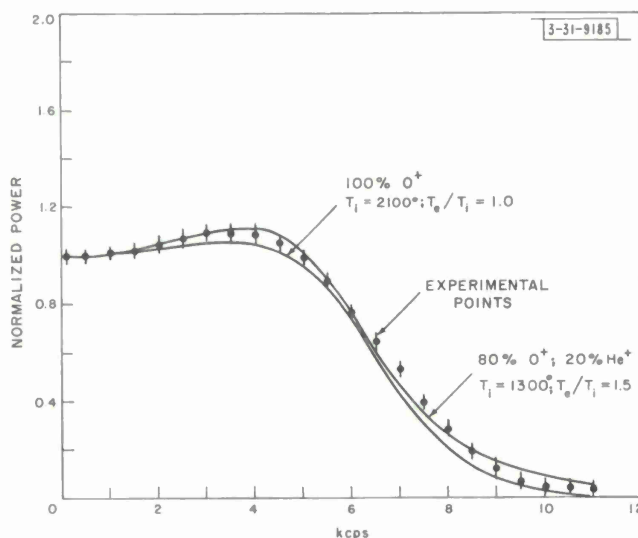
Fig. 12. Mean of all experimental profiles obtained at greatest height (720 km) during period 0834 to 1005 on 2 July 1963 is here compared with closest fitting precomputed curves for an O^+ gas and mixture containing 80 percent O^+, 20 percent He^+. A better fit could be obtained by adjusting theoretical curves so that for O^+, $T_i = 2040°$ and $T_e/T_i = 1.14$, and for O^+/He^+, $T_i = 1400°$ and $T_e/T_i = 1.40$. When this is done, solutions are experimentally indistinguishable.
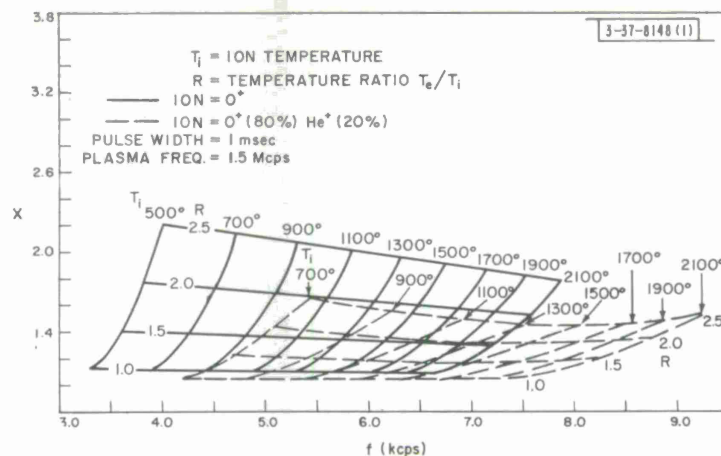
Fig. 13. Spectrum analysis chart for f_p = 1.5 Mcps and different ion compositions. Solid lines represent wholly O^+ ions in absence of equipmental effects; dotted lines denote 80/20 percent mixture of O^+/He^+ ions observed using a 1-msec pulse. If x and f are the only quantities scaled from the records, widely differing values of T_e/T_i can be obtained depending upon whether or not He^+ ions are assumed present.
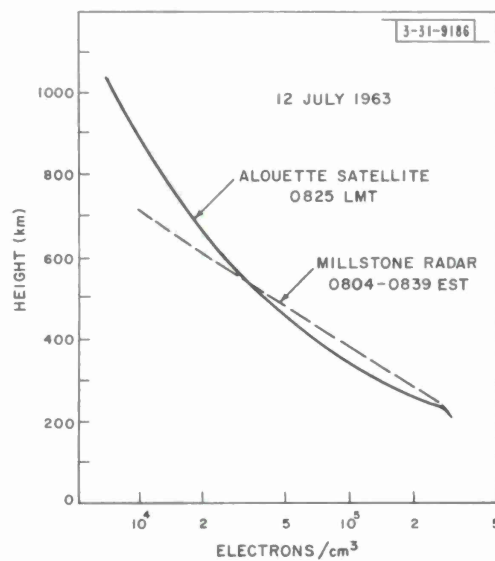
Fig. 14. Comparison between electron-density profile obtained by the Alouette satellite and backscatter radar on the morning of 12 July. Large discrepancy in two profiles above 500 km is attributed to improper recovery of receiver TR at this time. (The Alouette profile was kindly provided by Dr. T.E. Van Zandt.)
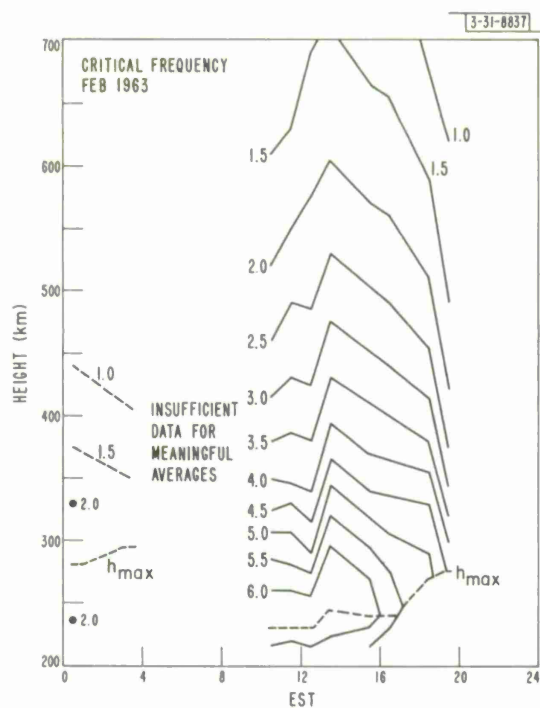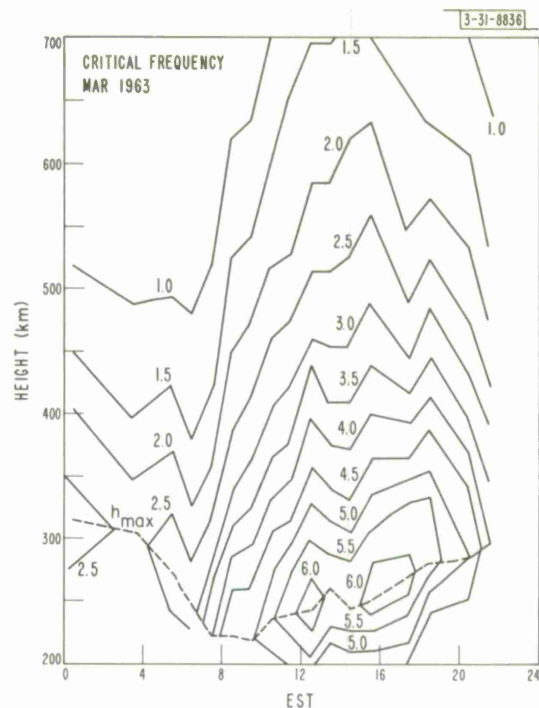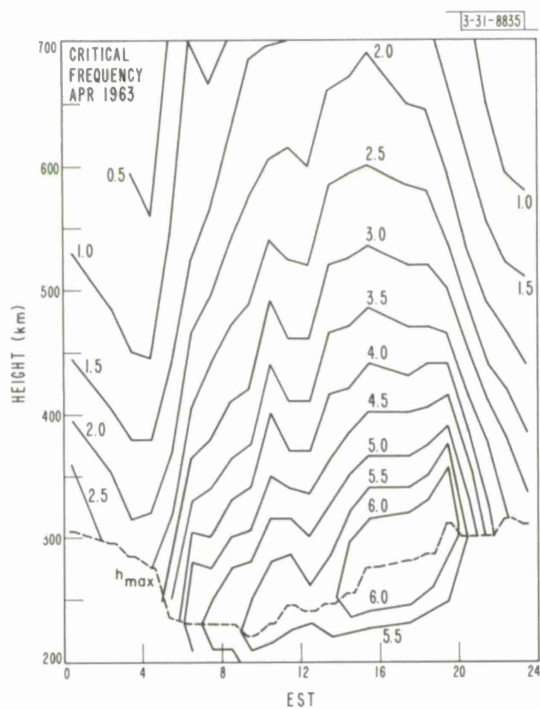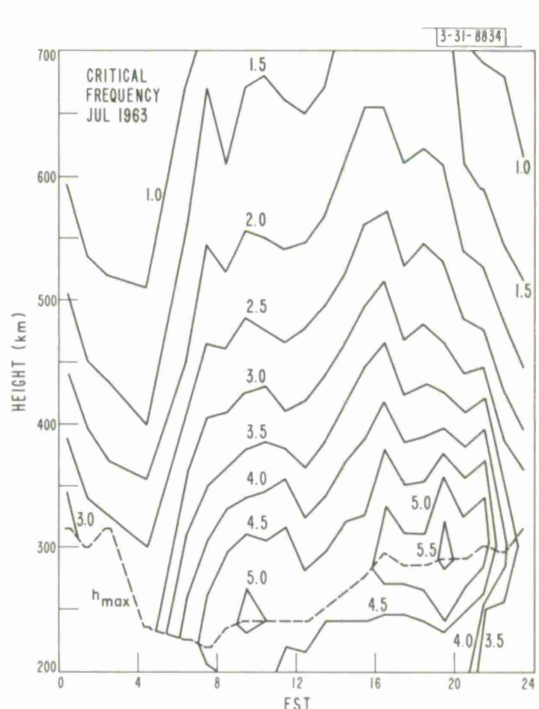
Figs. 15(a–j).   Contours of constant plasma frequency (Mcps).

Fig. 15. Continued.

(i)

(j)
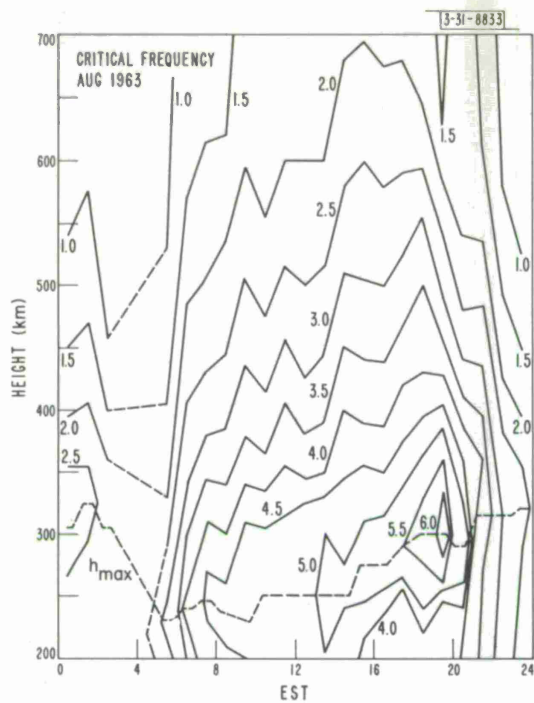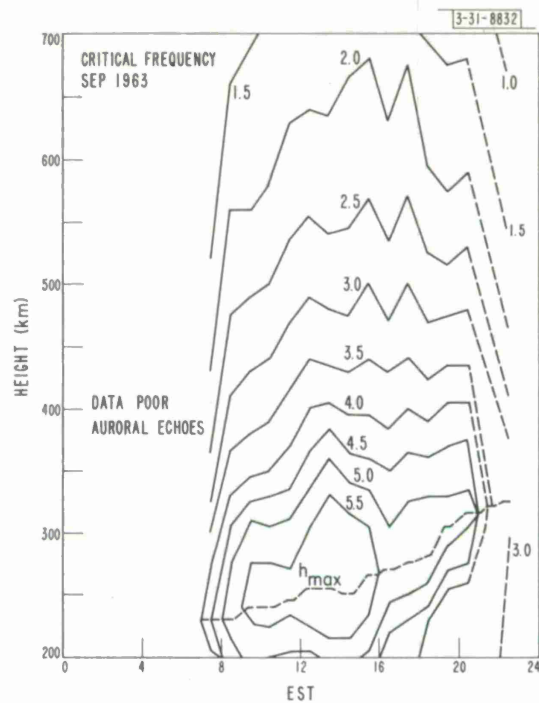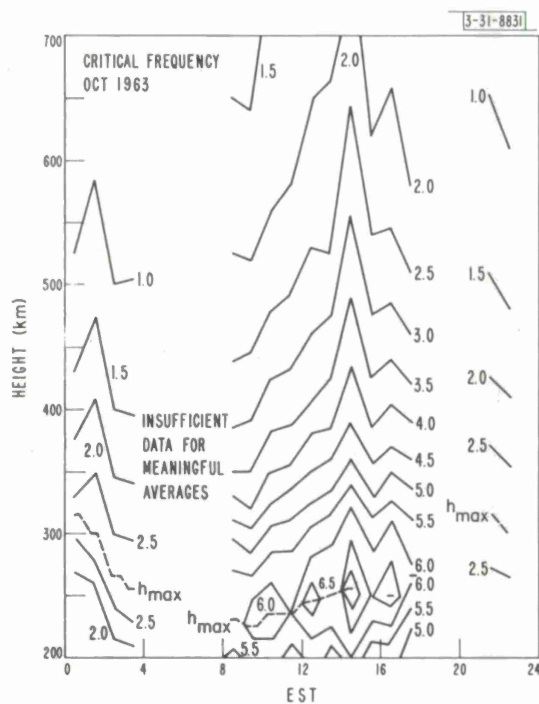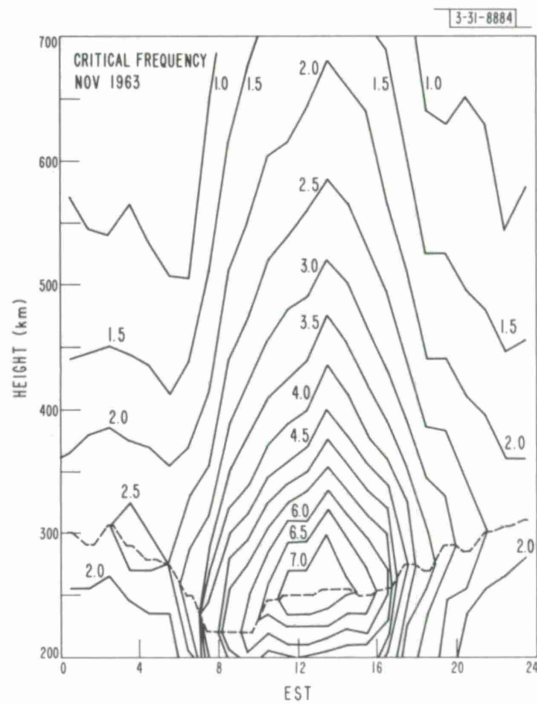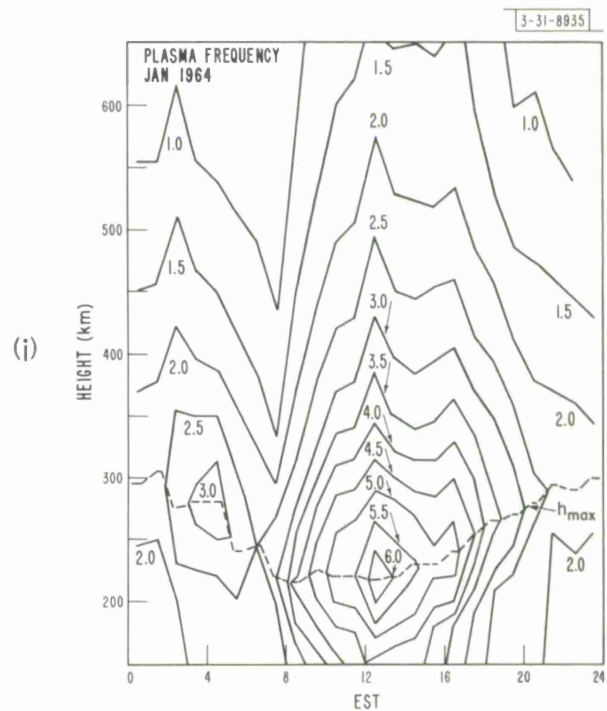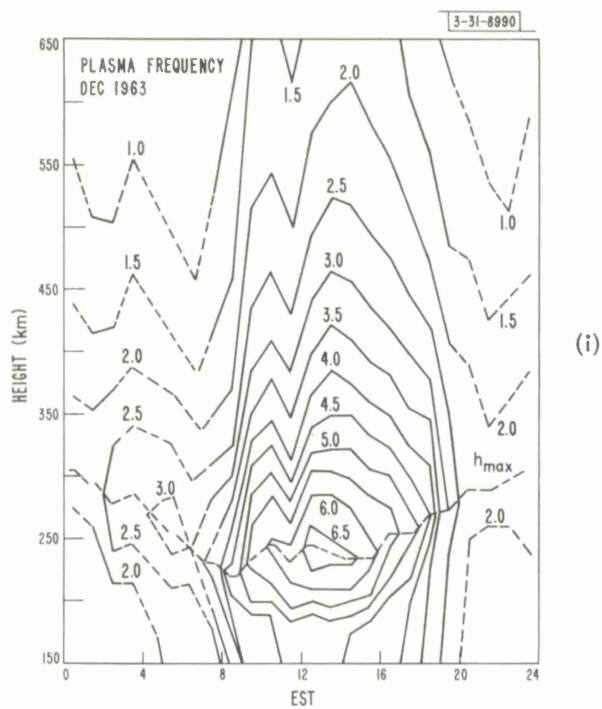
Fig. 15. Continued.
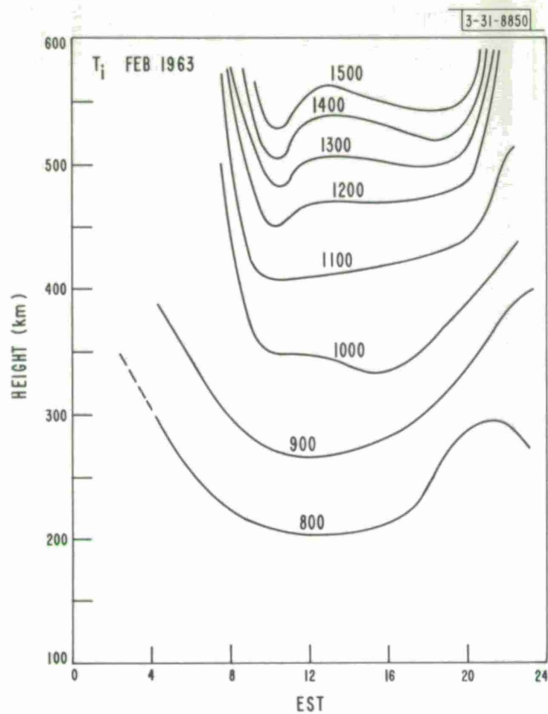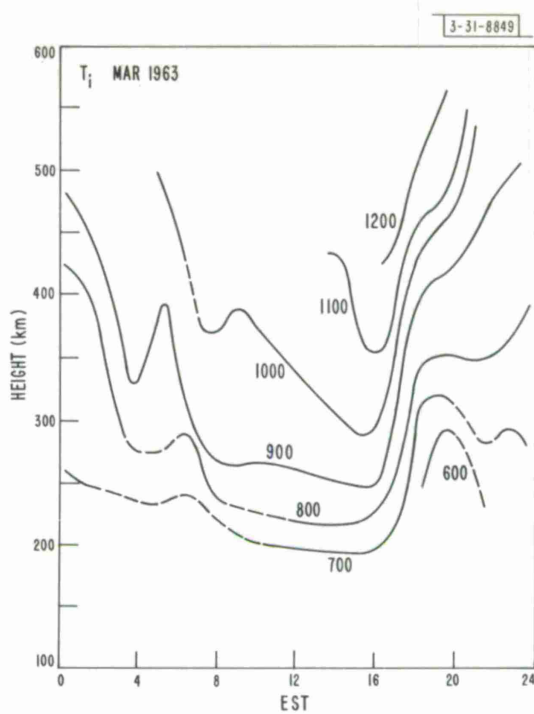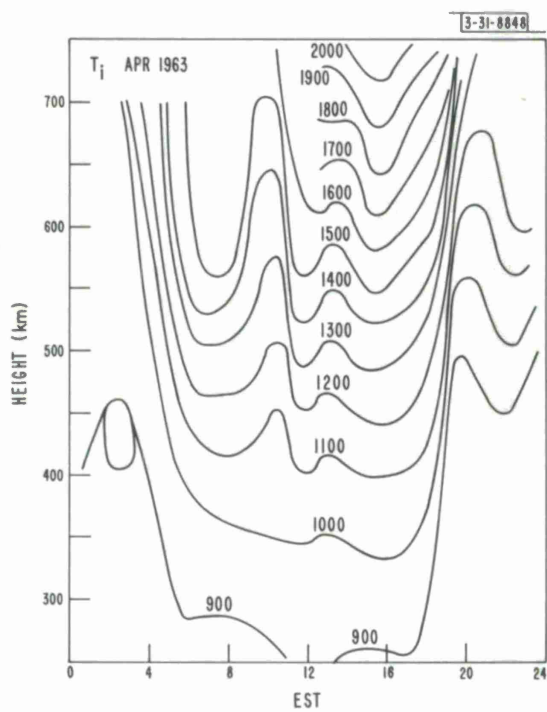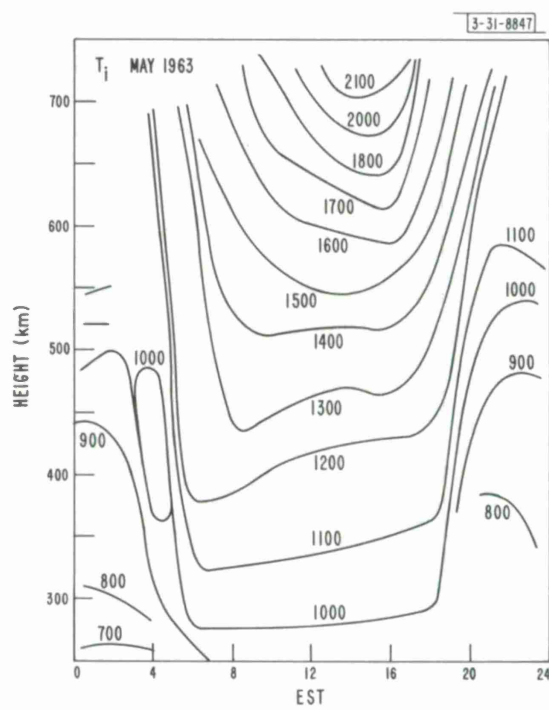
Figs. 16(a-l). Variations of T_i with time and height.
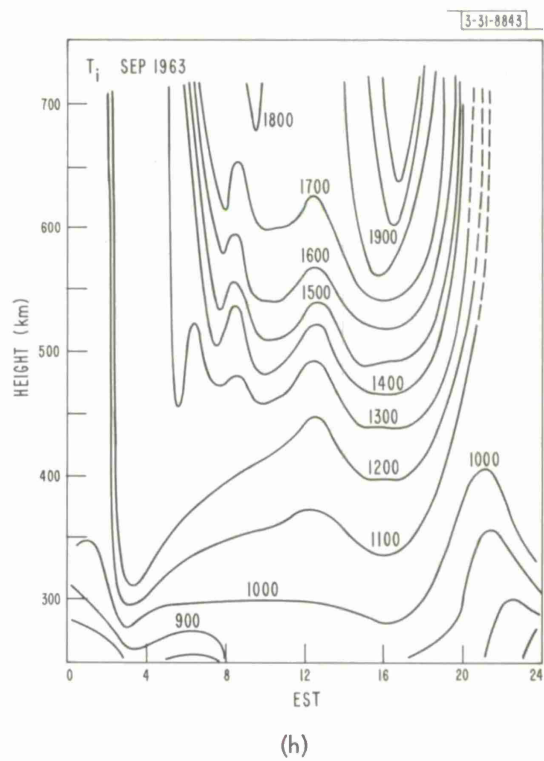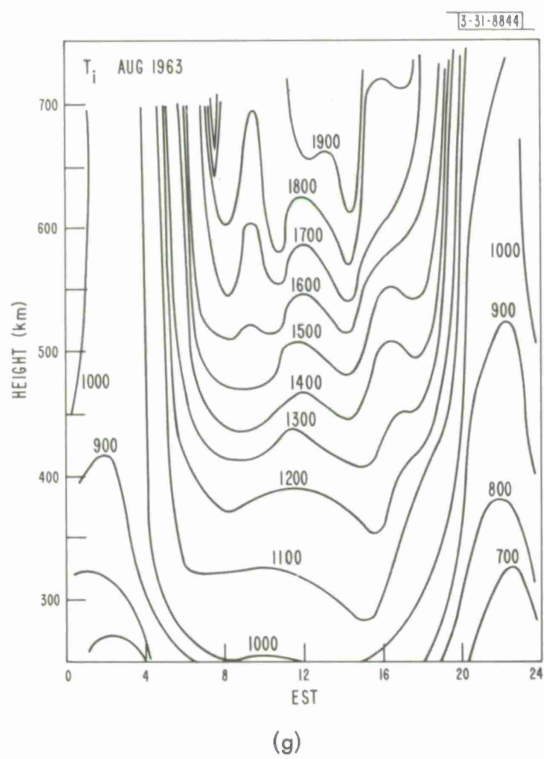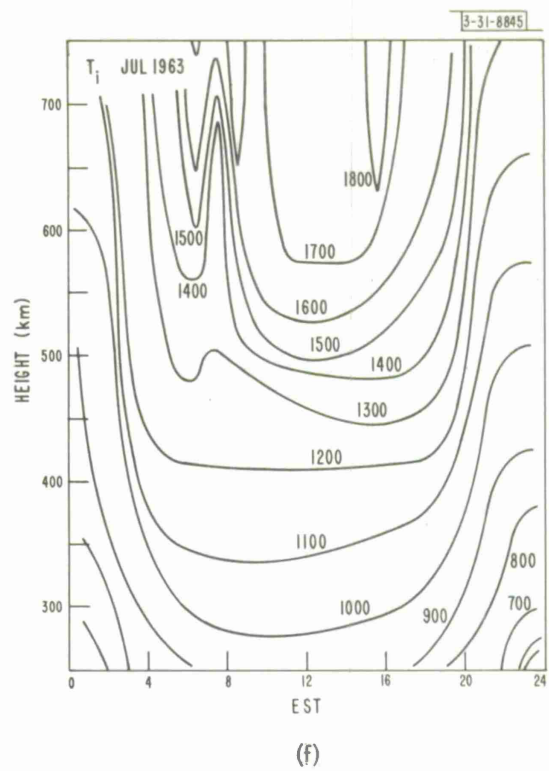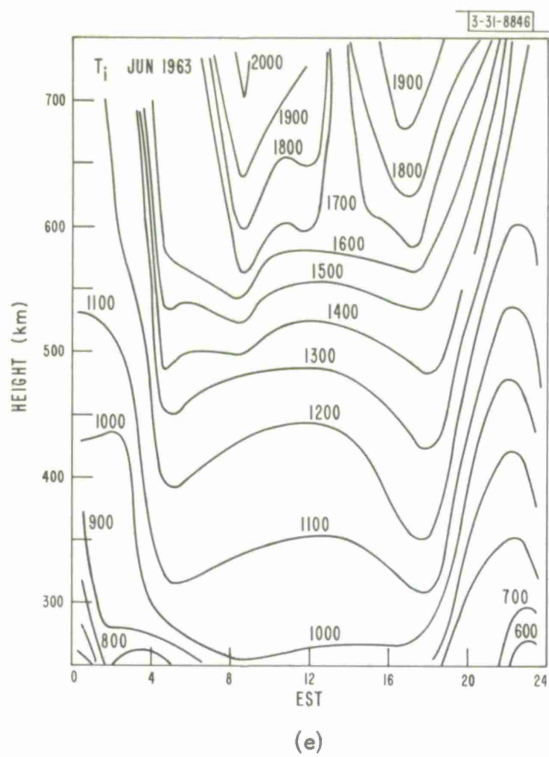
Fig. 16. Continued.
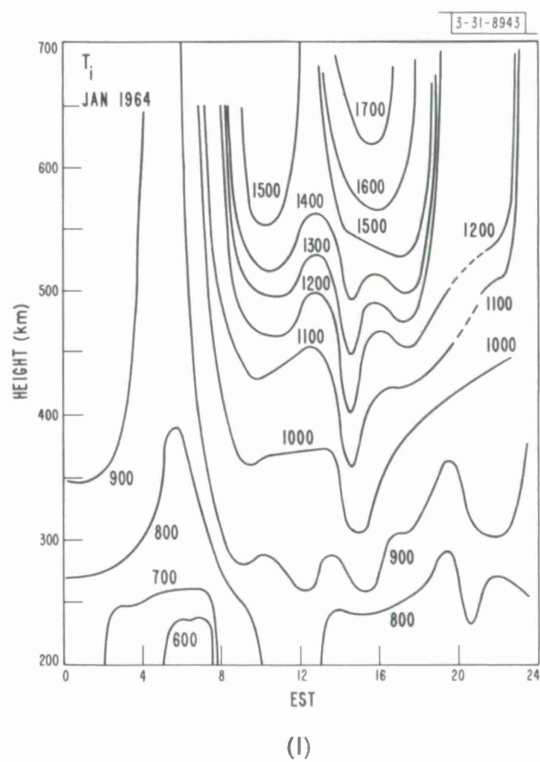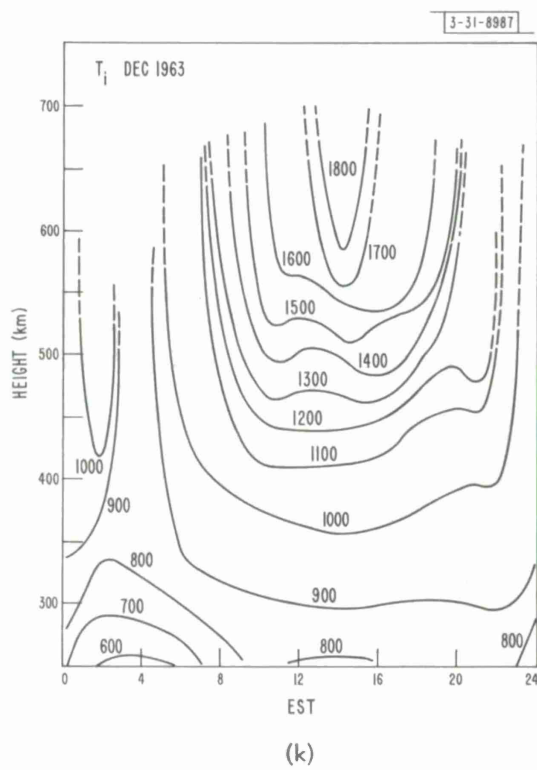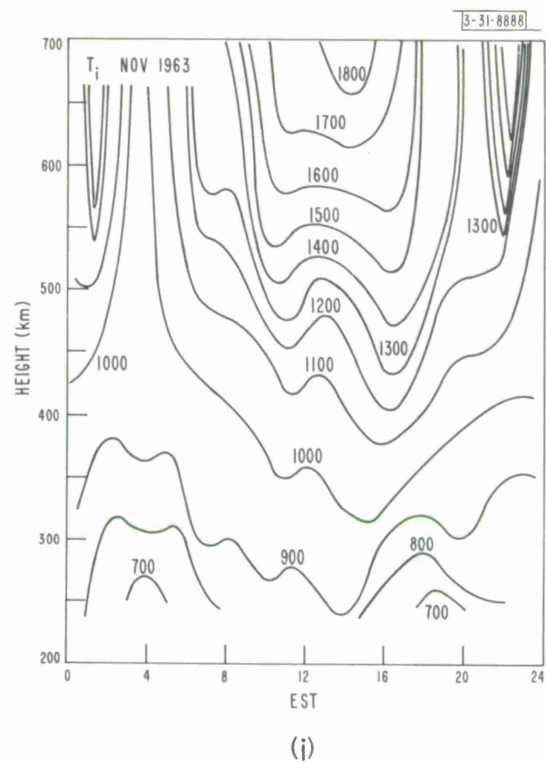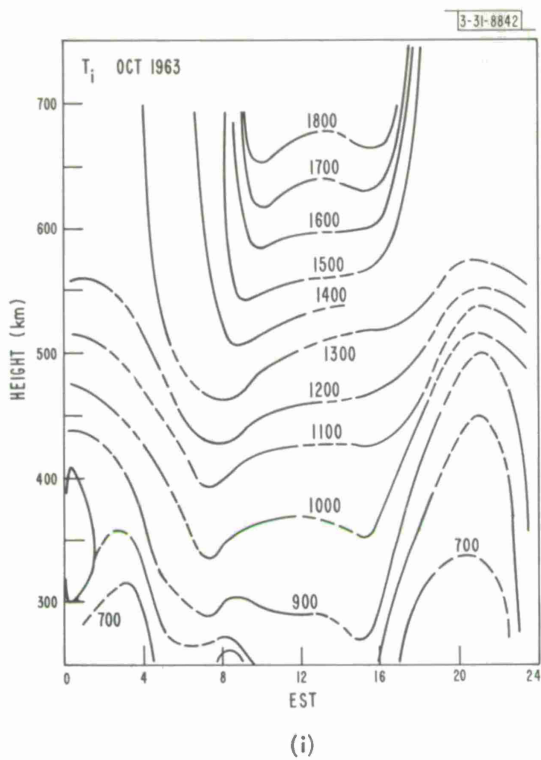
Fig. 16. Continued.
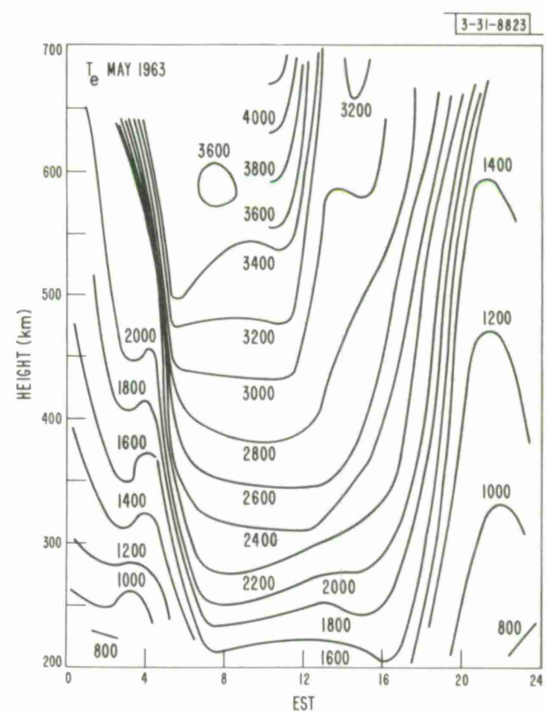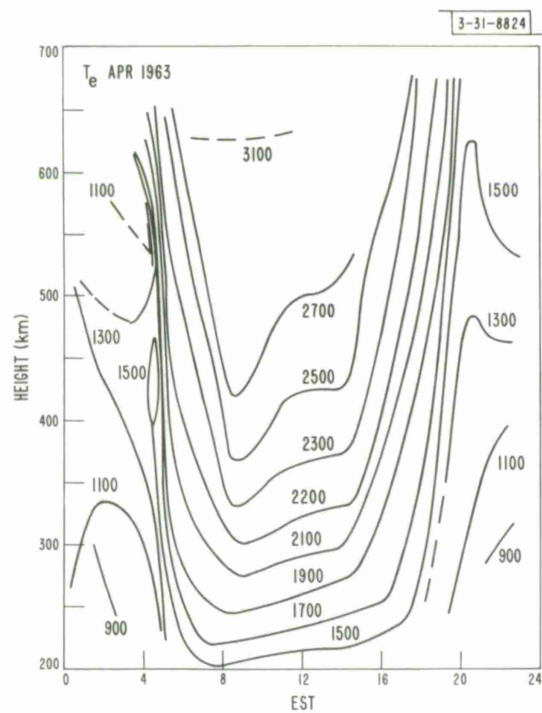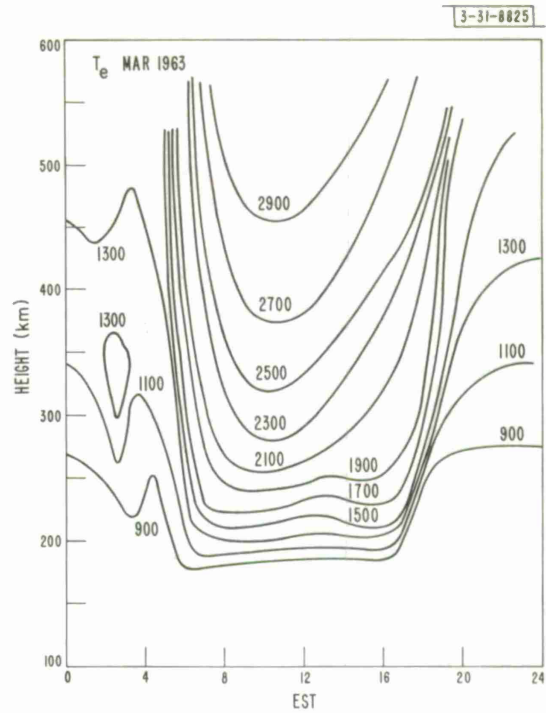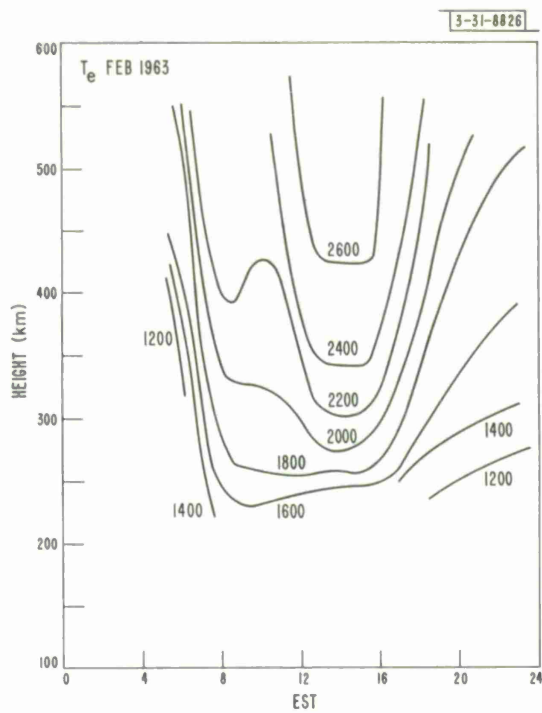
Figs. 17(a-1).   Variations of T_e with time and height.

44

Fig. 17. Continued.

45

Fig. 17. Continued.

46
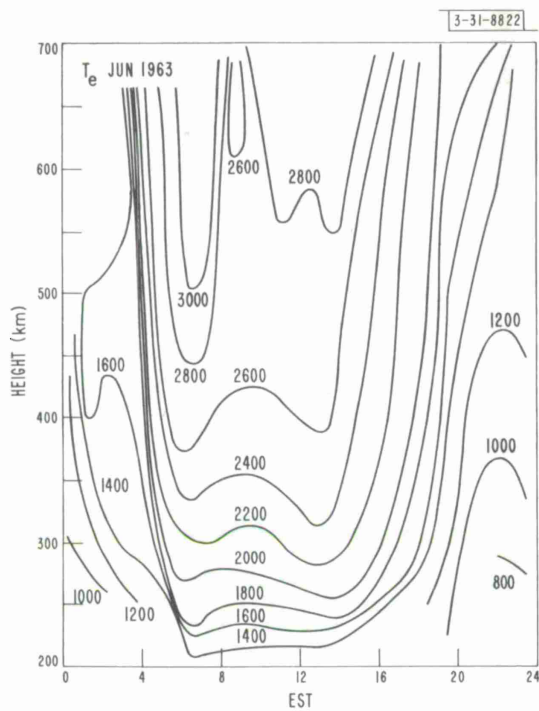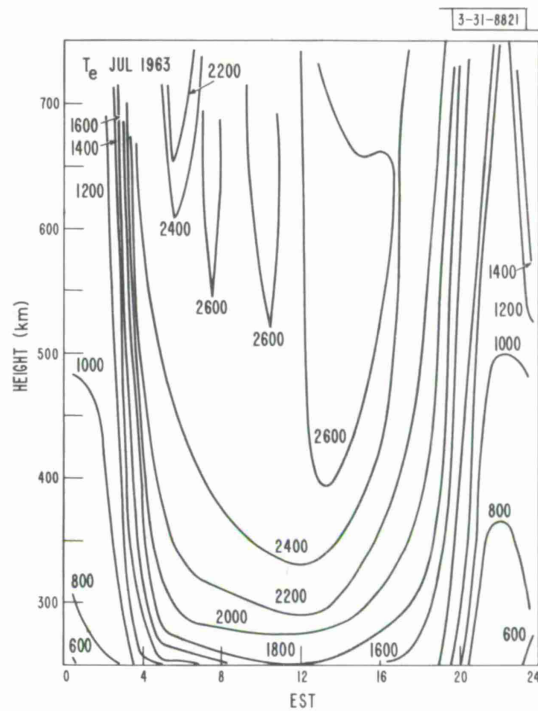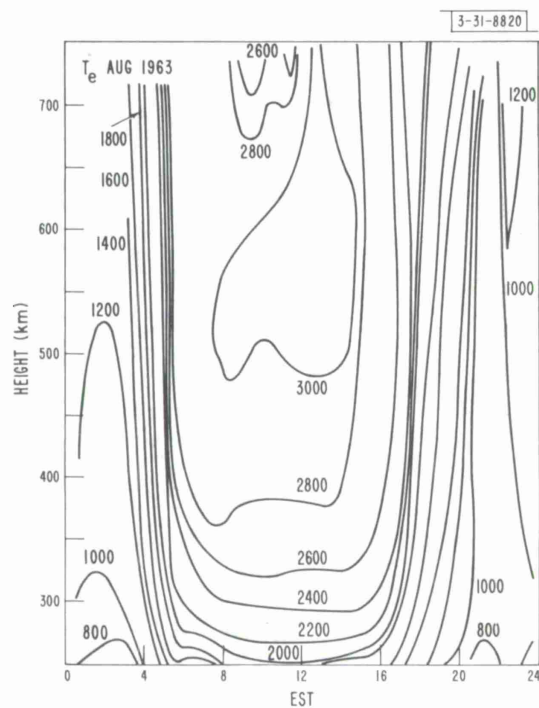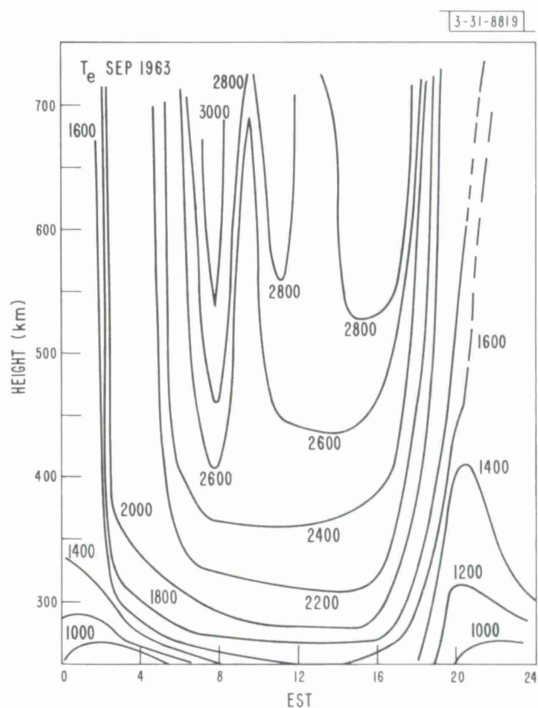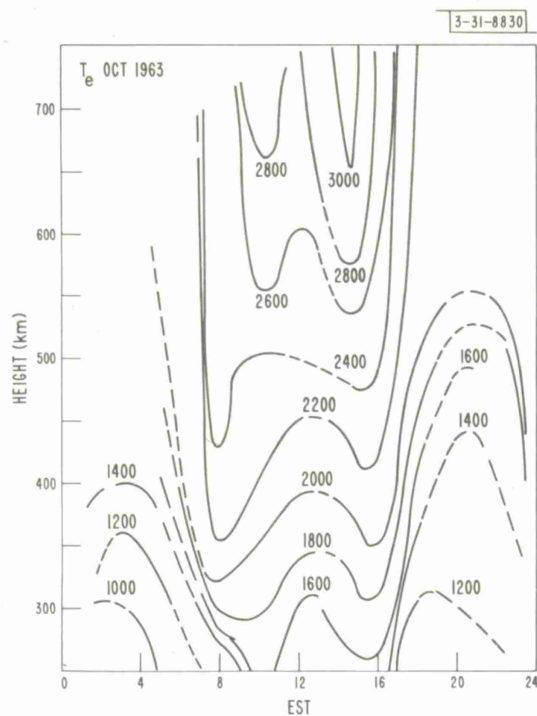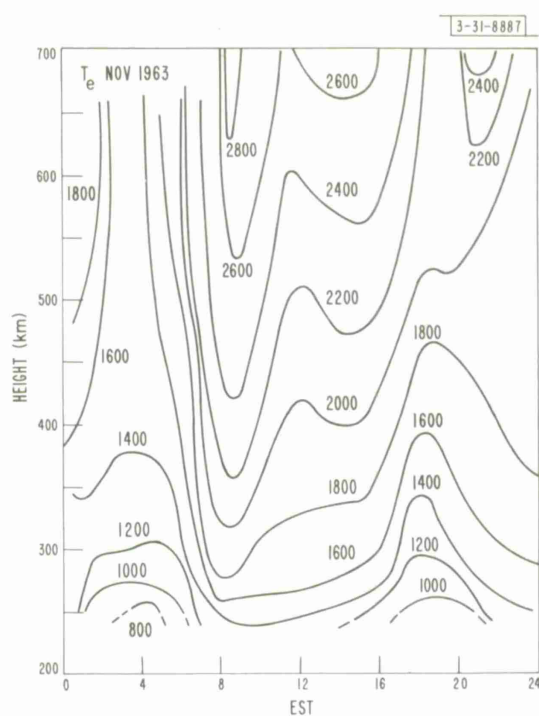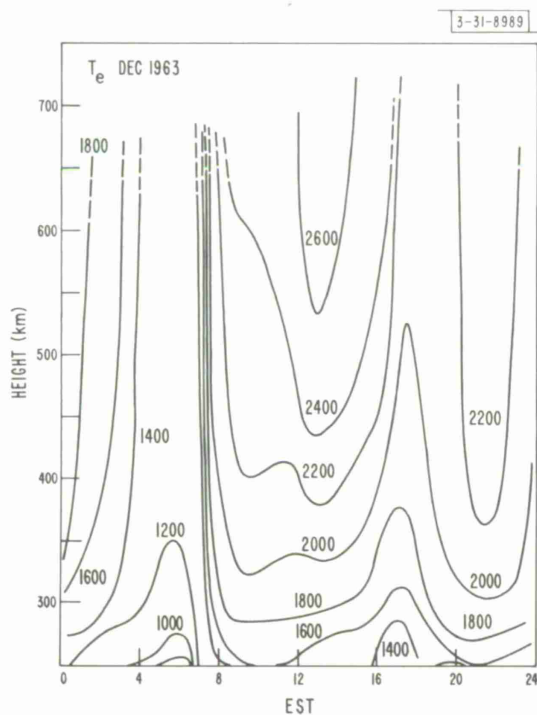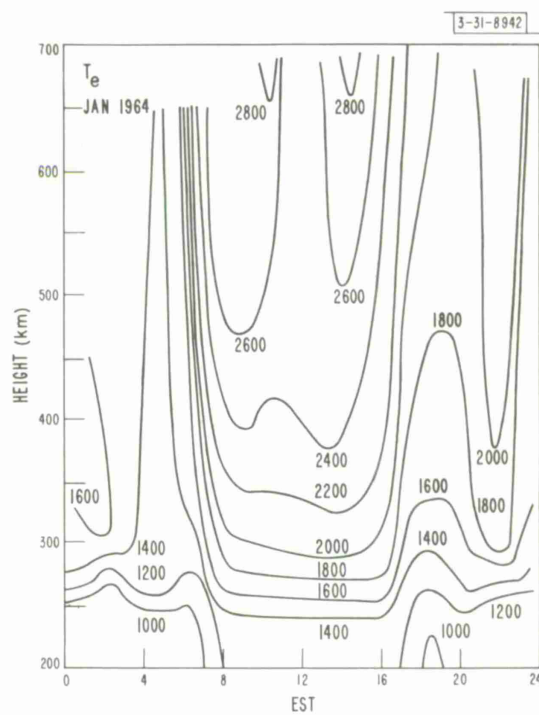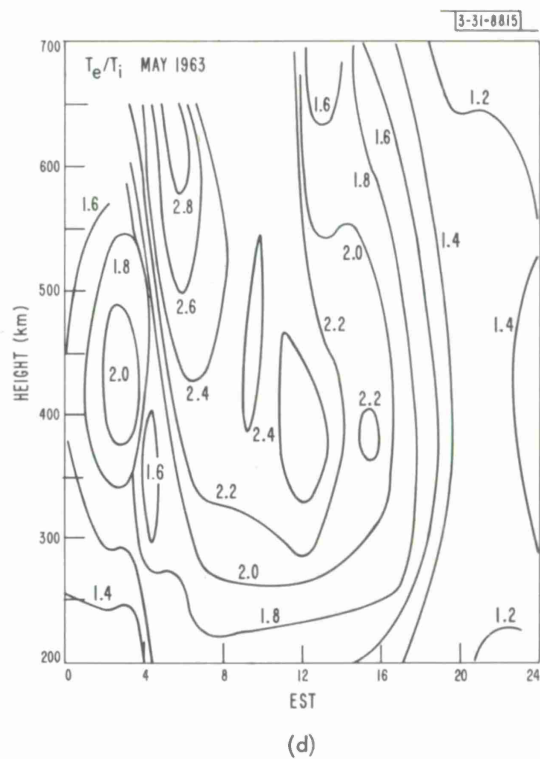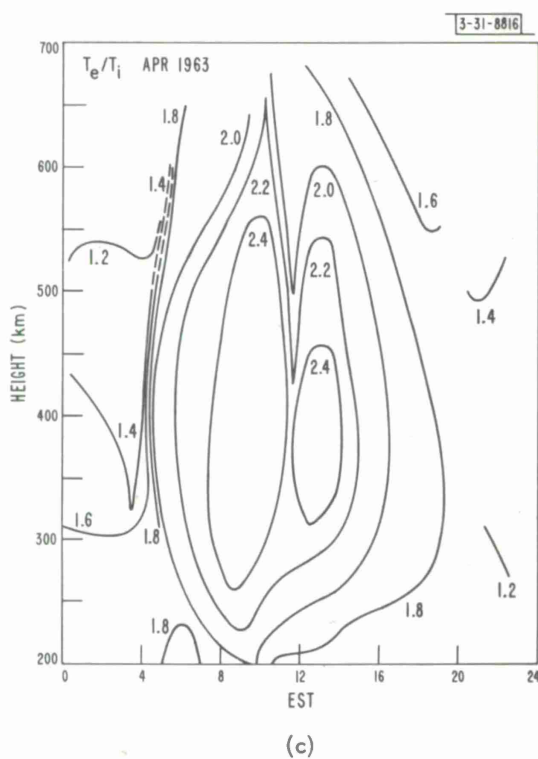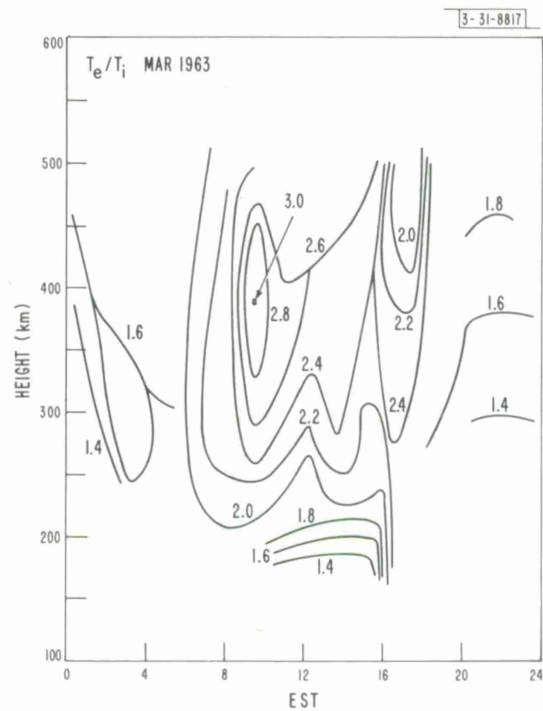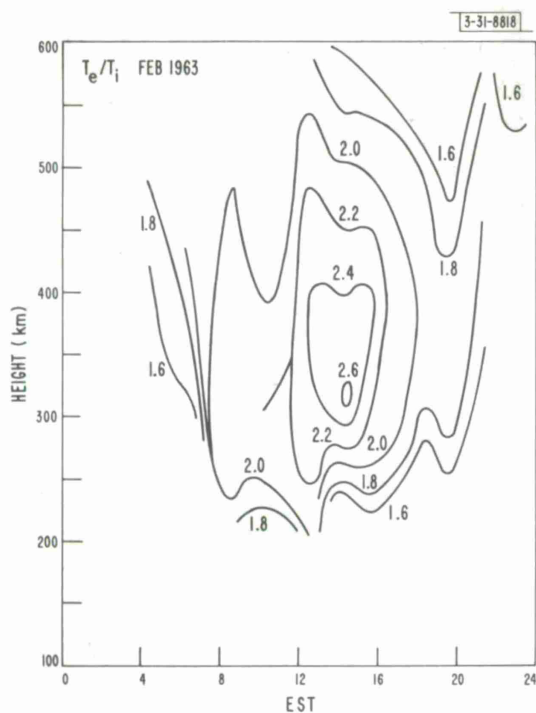
Figs. 18(a-l). Variations of ratio T_e/T_i with time and height.
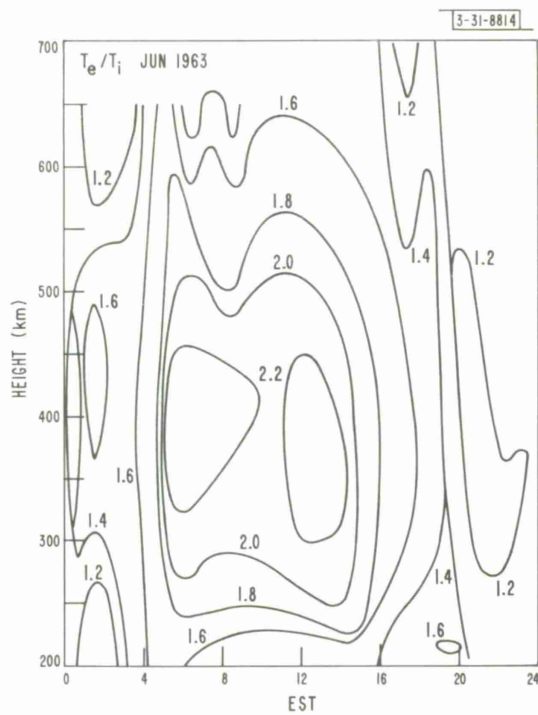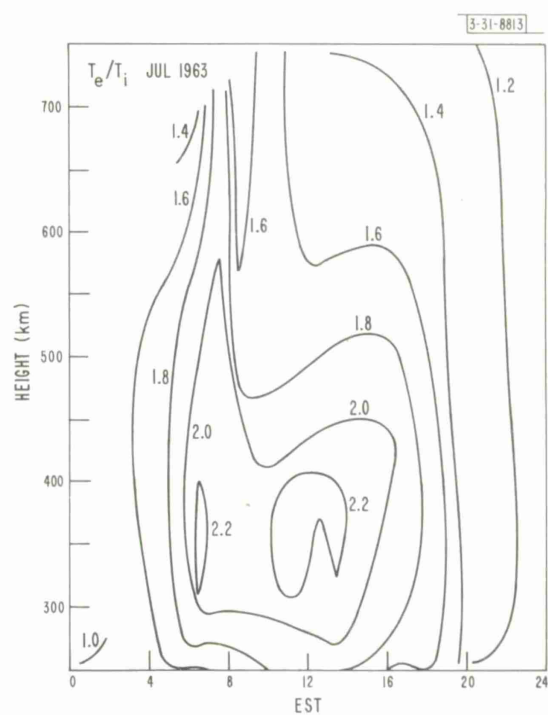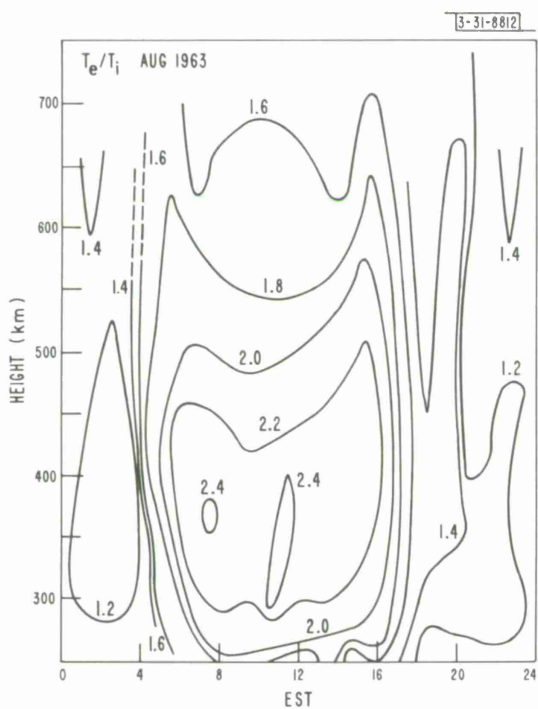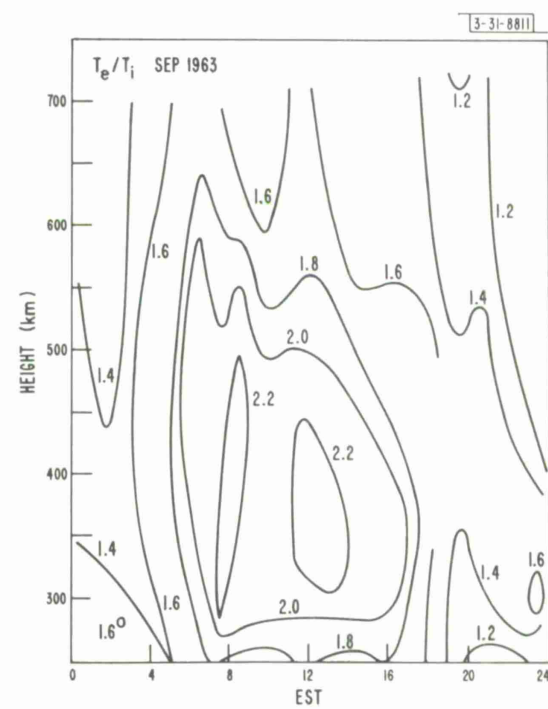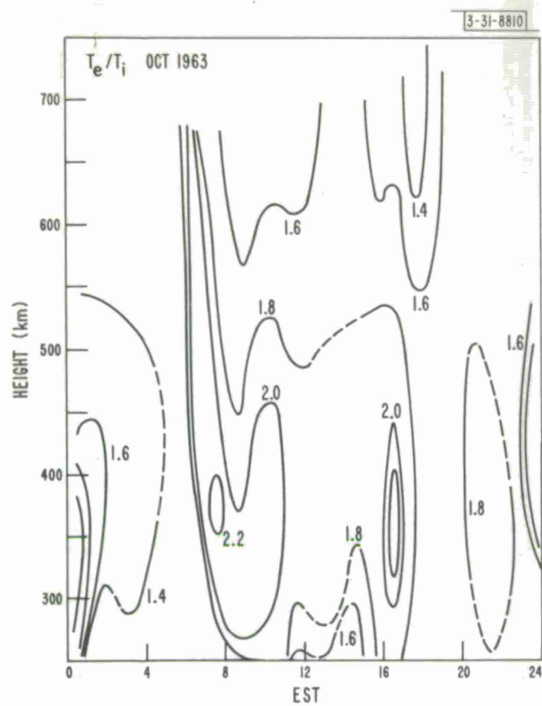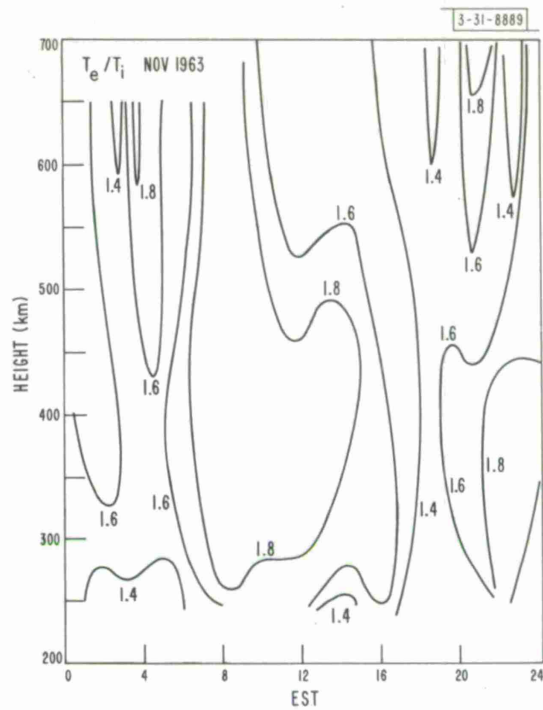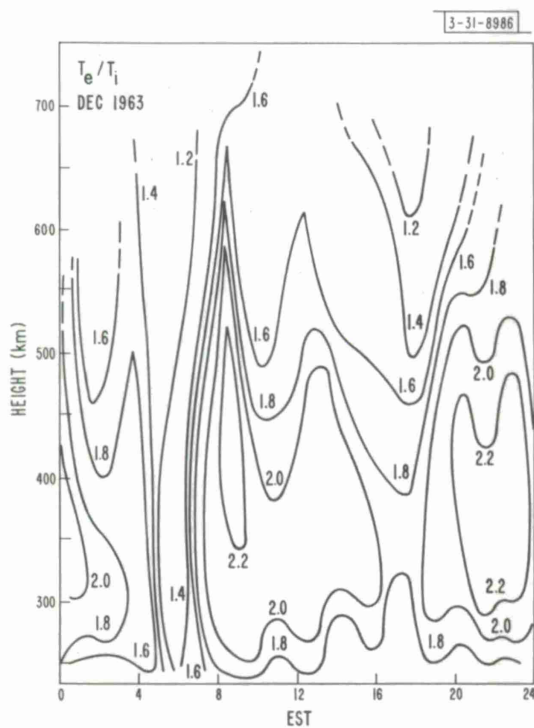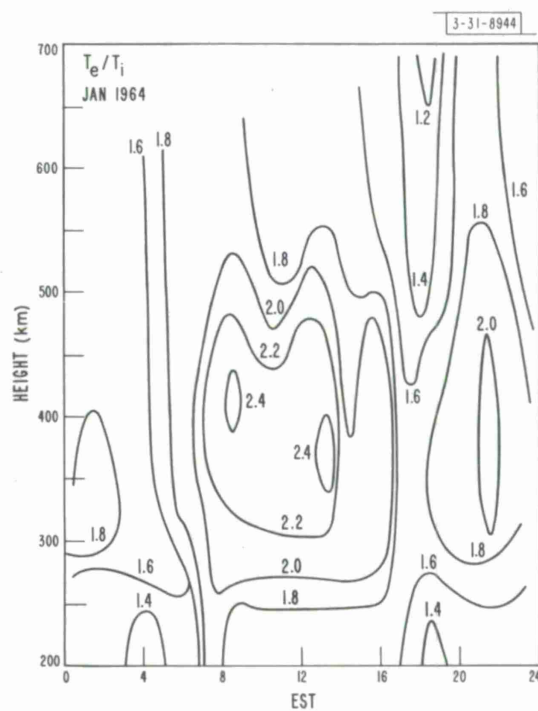
Fig. 18.   Continued.

Fig. 18. Continued.

49
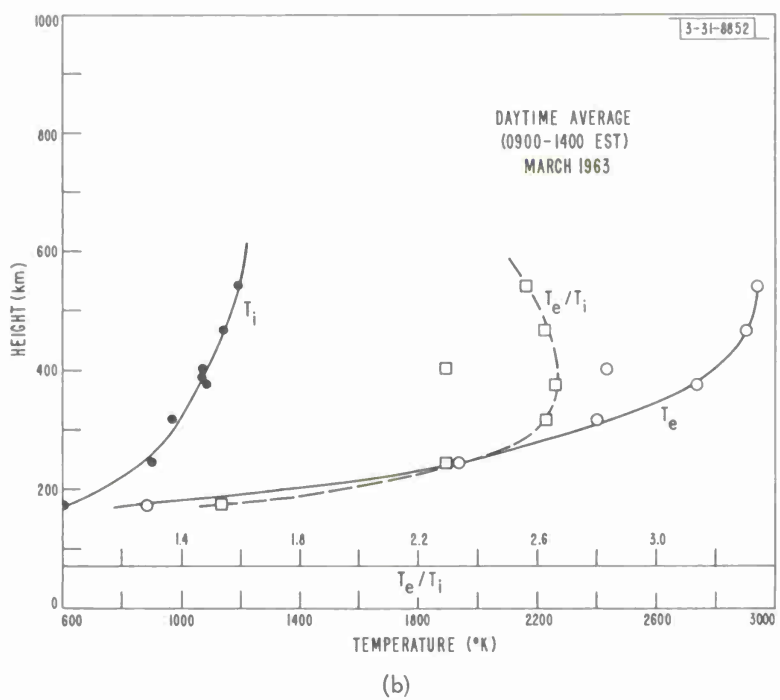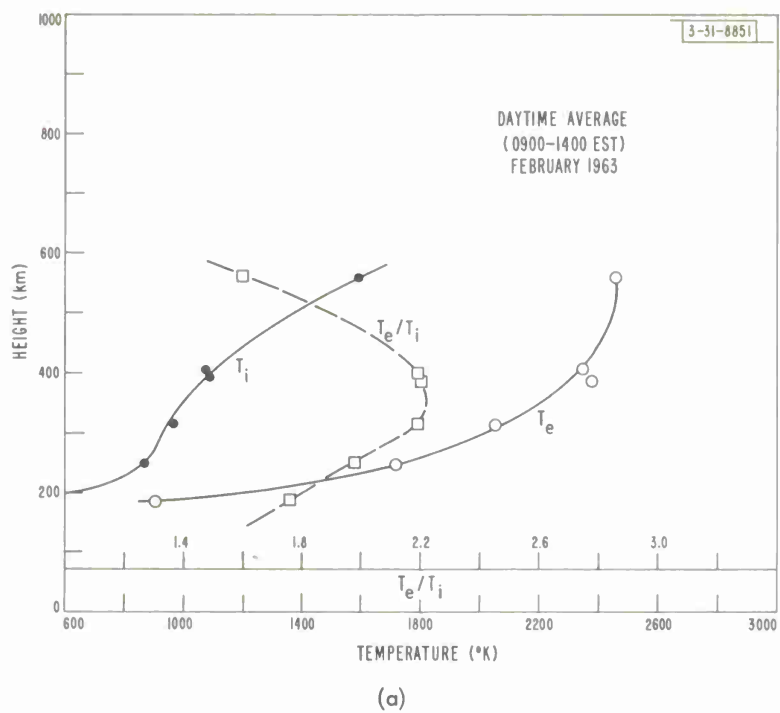
Figs. 19(a-l). Average daytime behavior of T_i, T_e, and T_e/T_i with height.

Fig. 19. Continued.

51
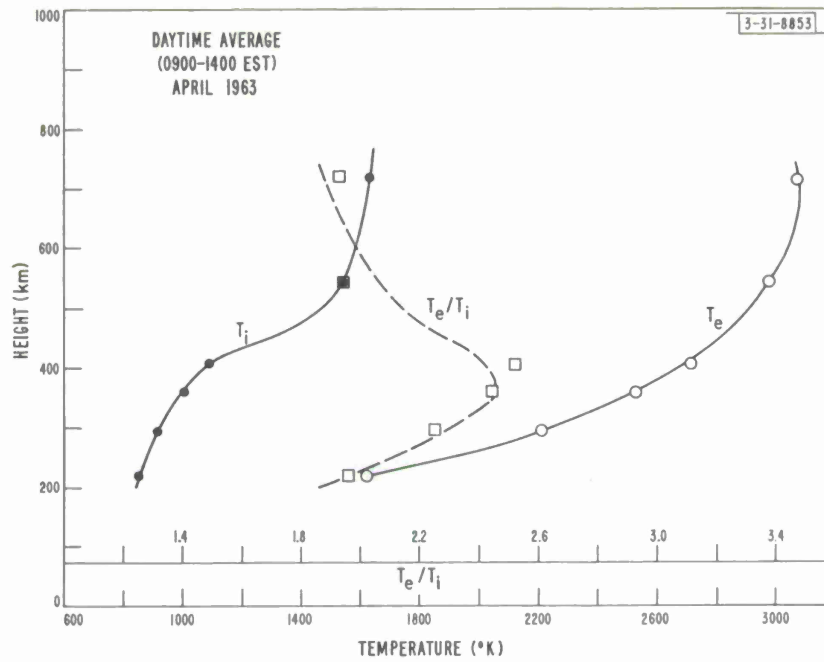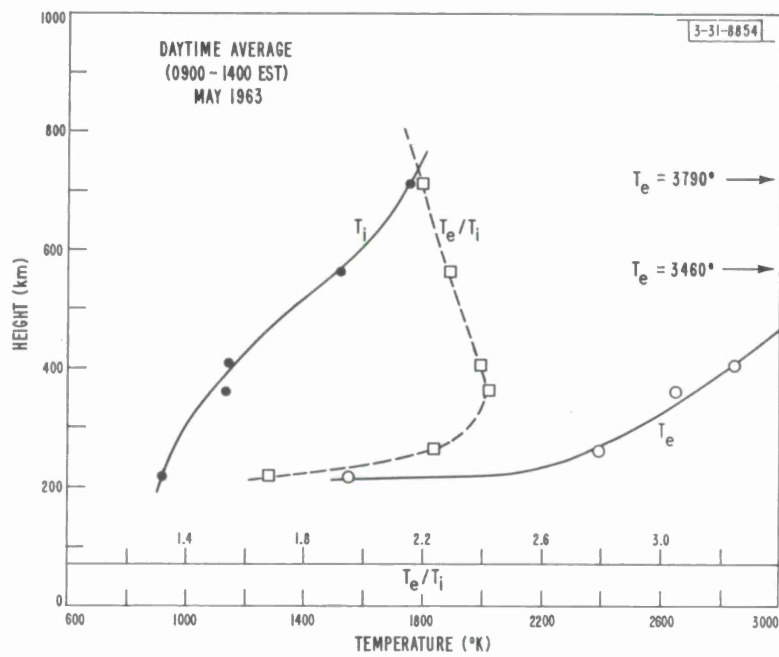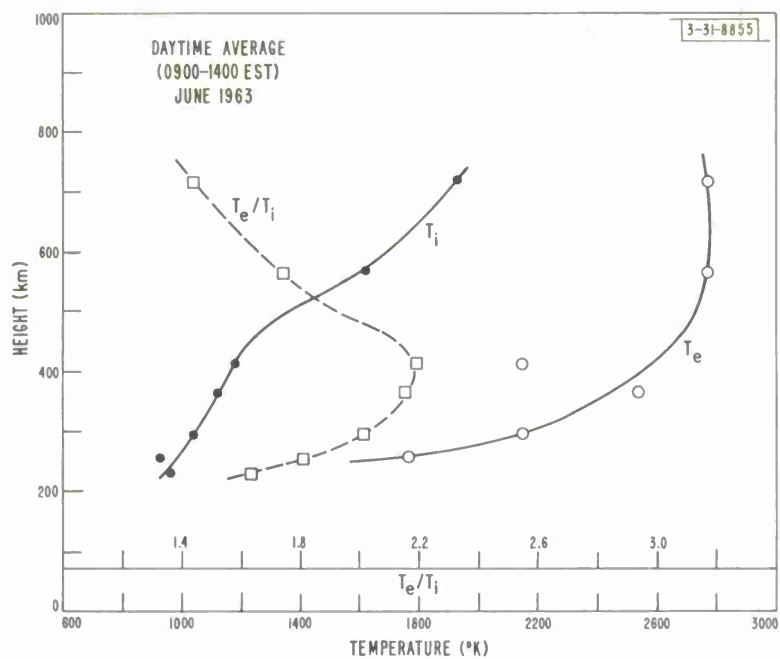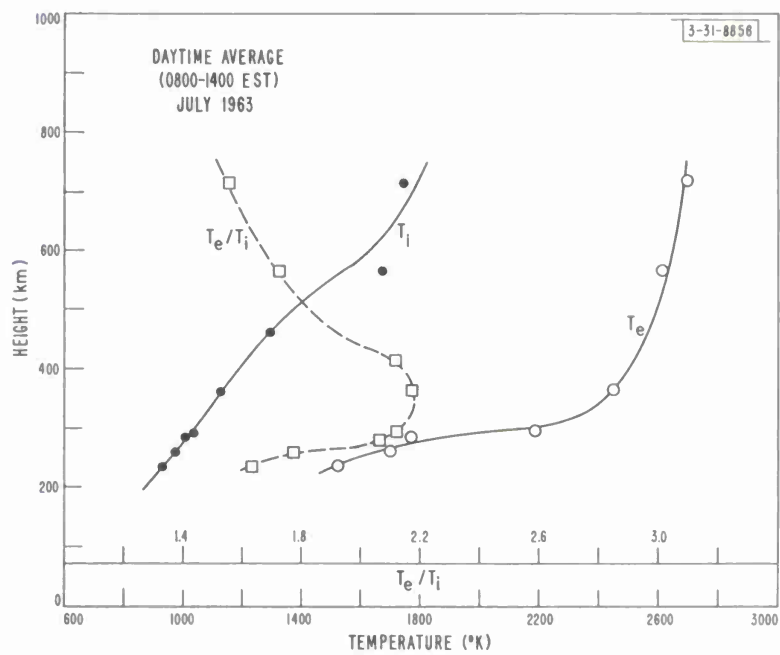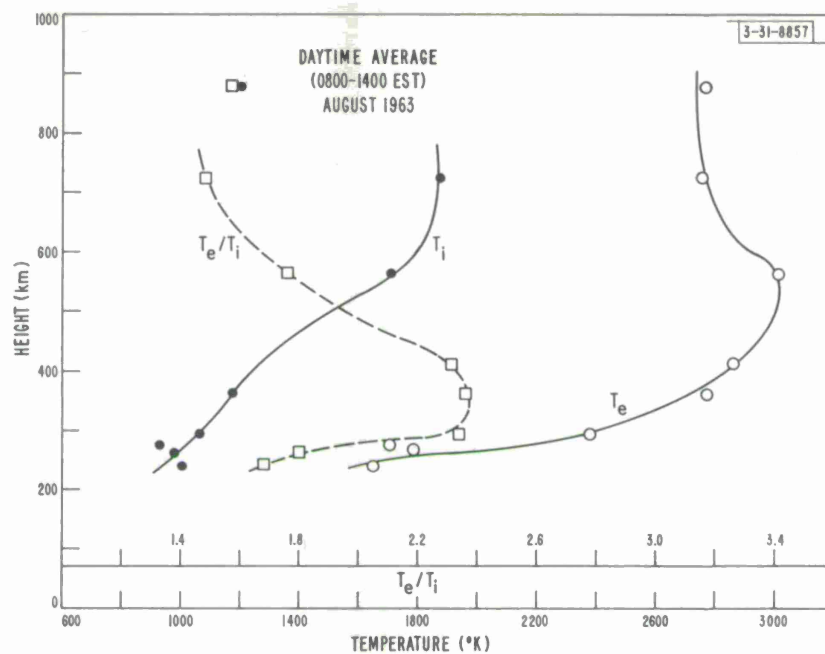
Fig. 19. Continued.

(g)
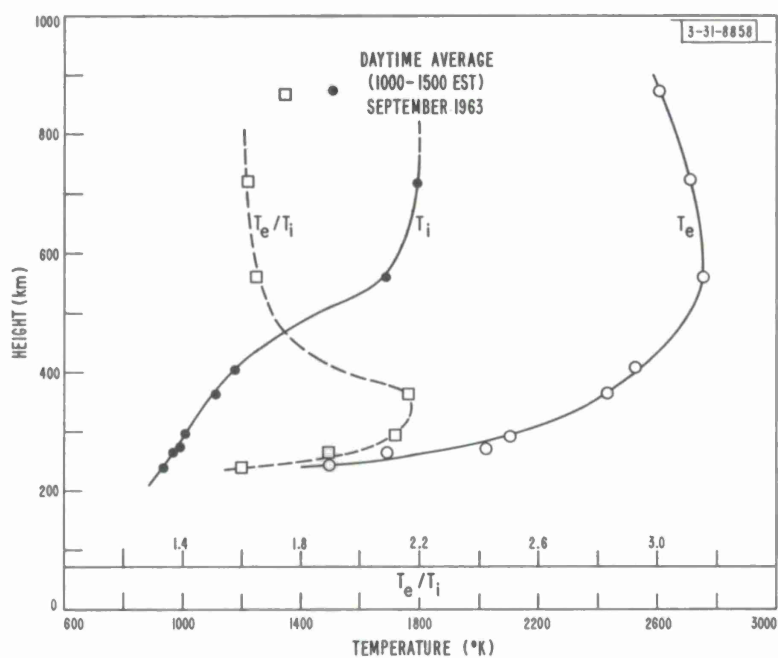
(h)
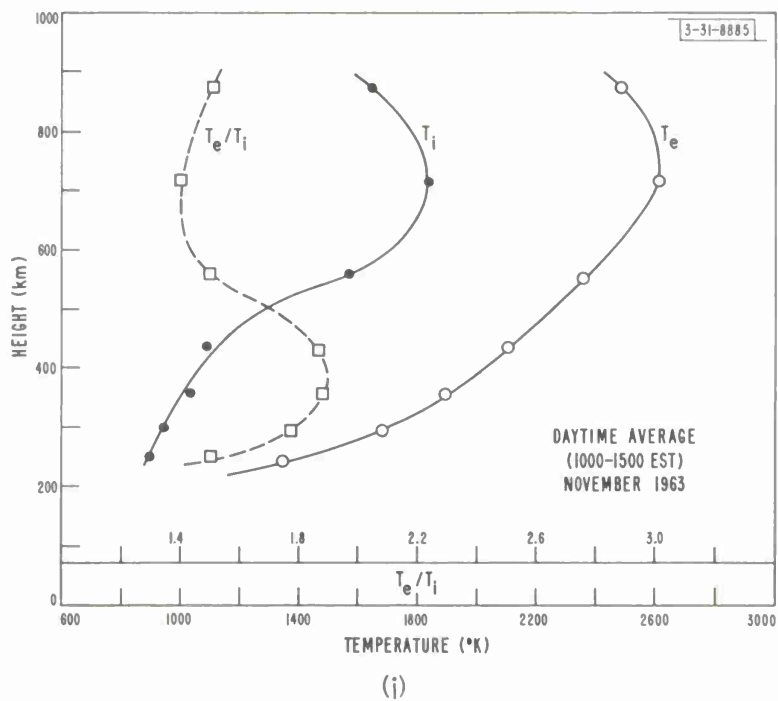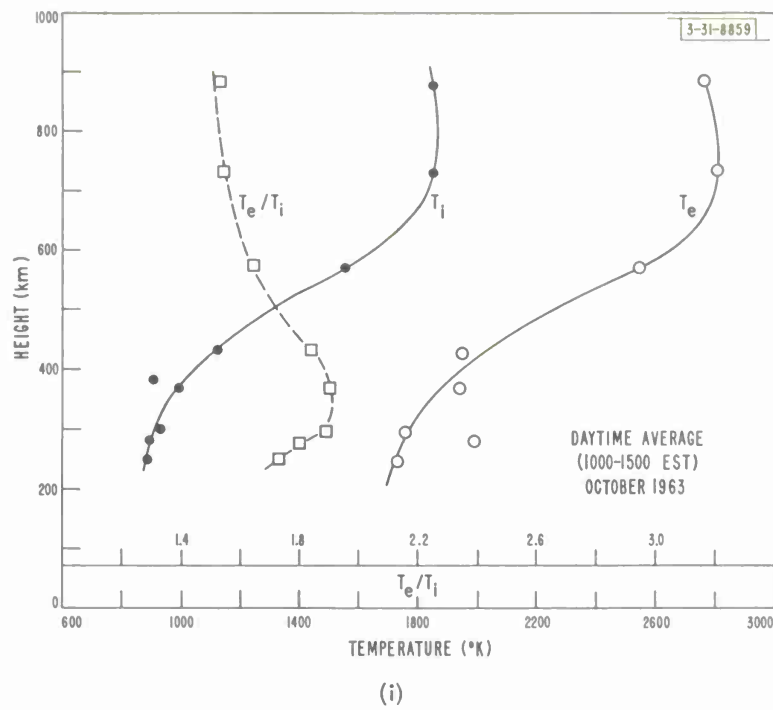
Fig. 19. Continued.

Fig. 19. Continued.

54

(k)

(l)
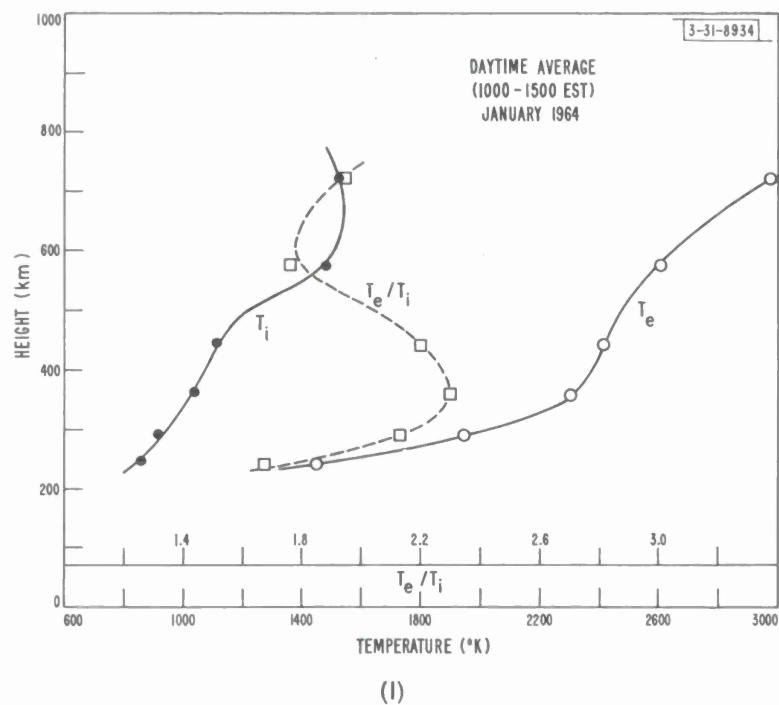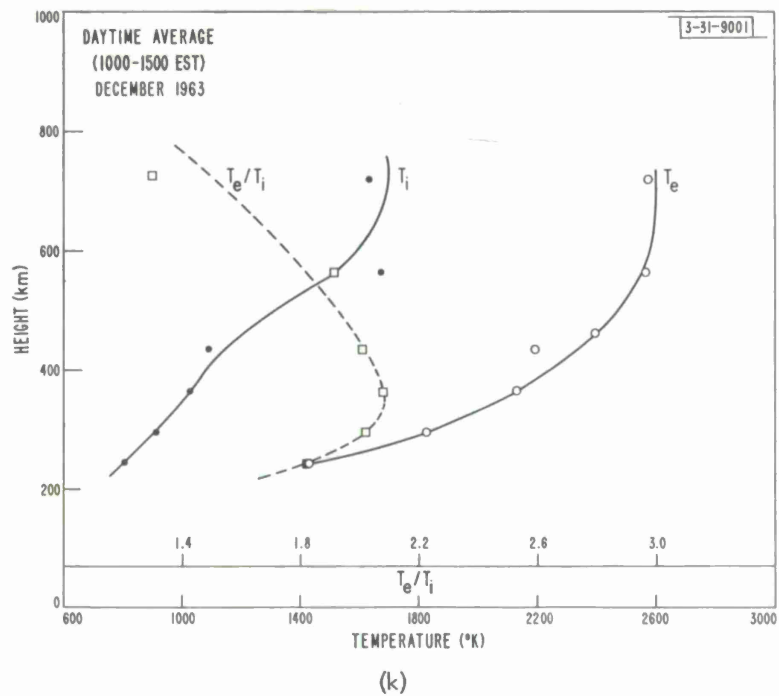
Fig. 19. Continued.
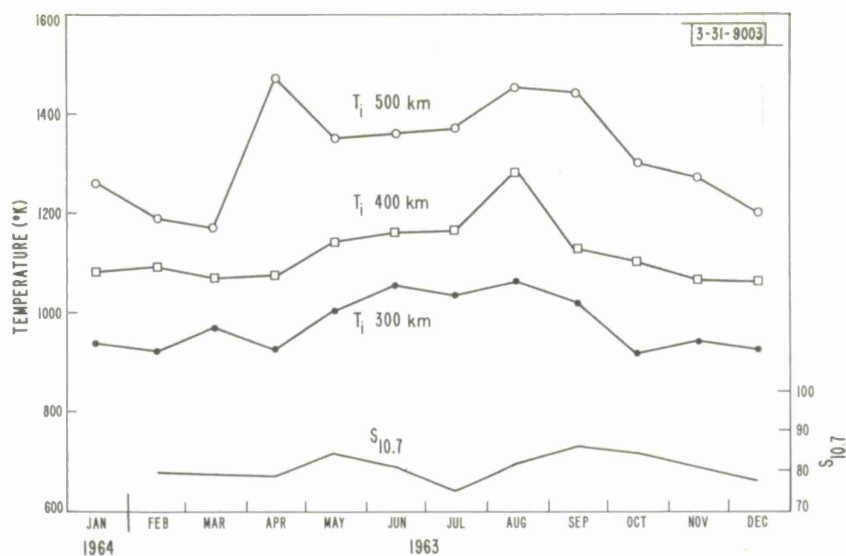
Fig. 20. Seasonal variations in average daytime values of T_i. Solar radio flux at 10.7 cm is also shown.
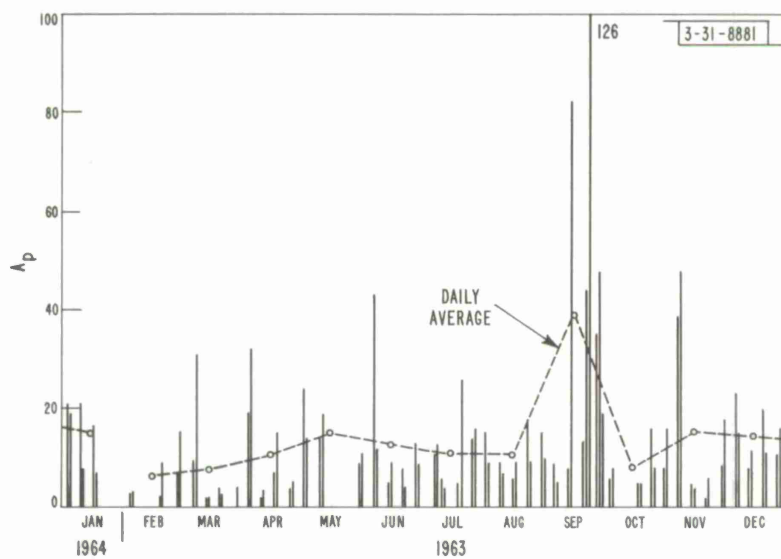
Fig. 21. Values of planetary magnetic index A_p on days when observations were conducted in 1963, together with monthly means of these values.

56
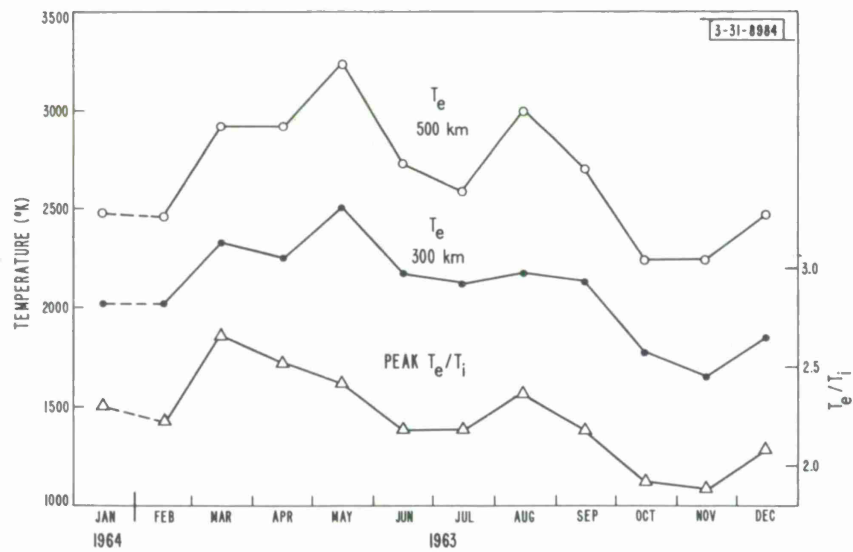
Fig. 22.   Seasonal variations in daytime T_e and T_e/T_i.
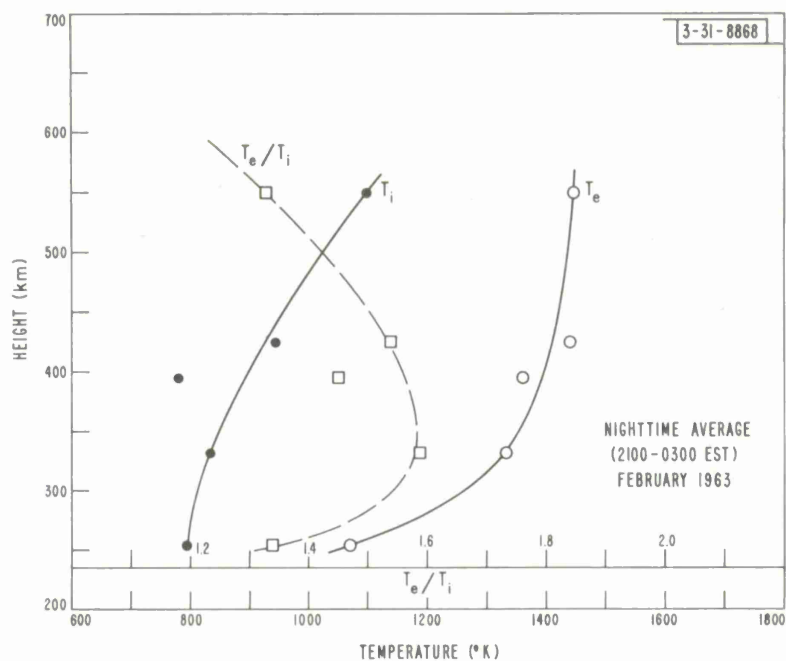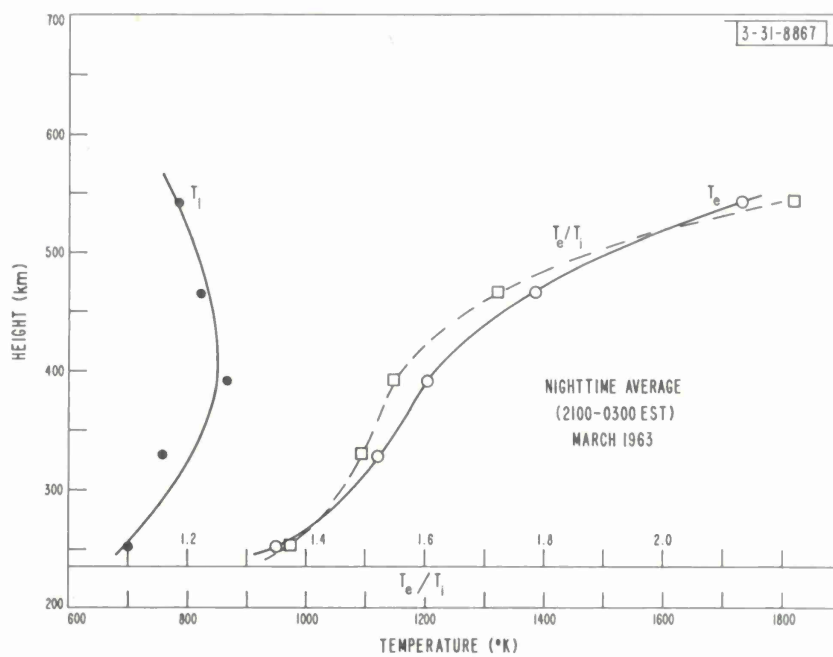
Figs. 23(a-I). Average nighttime behavior of T_i, T_e, and T_e/T_i with height.

58

(c)

(d)

Fig. 23. Continued.

(e)

(f)

Fig. 23. Continued.

60

(g)

(h)

Fig. 23. Continued.

3-31-8860

HEIGHT (km)

T_e / T_i

T_i

T_e

NIGHTTIME AVERAGE
(2200 - 0200 EST)
OCTOBER 1963

T_e / T_i

1.2 1.4 1.6 1.8 2.0

TEMPERATURE (°K)

600 800 1000 1200 1400 1600 1800

(i)

3-31-8886

HEIGHT (km)

T_e / T_i T_i T_e

NIGHTTIME AVERAGE
(2200 - 0300 EST)
NOVEMBER 1963

T_e / T_i

1.4 1.8 2.2 2.6 3.0

TEMPERATURE (°K)

600 1000 1400 1800 2200 2600 3000

(j)

Fig. 23. Continued.

62
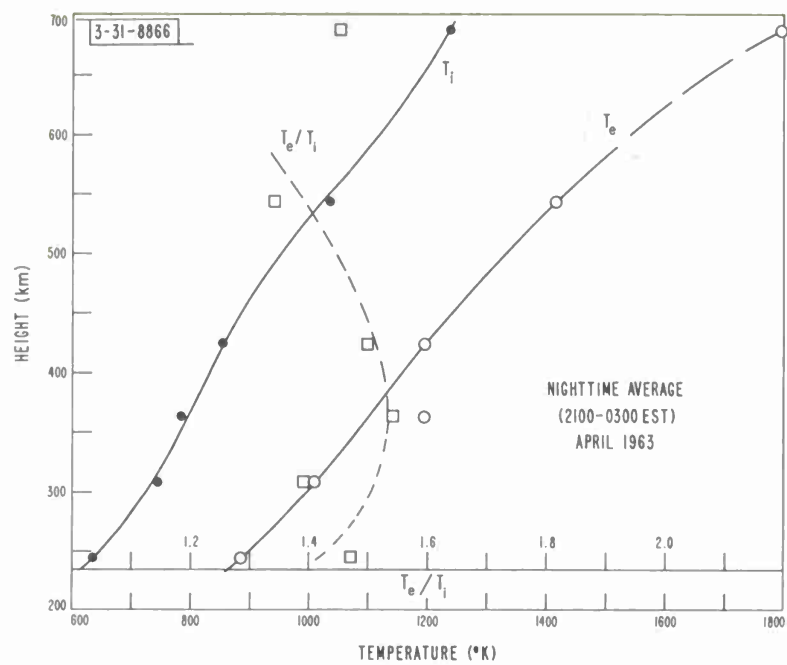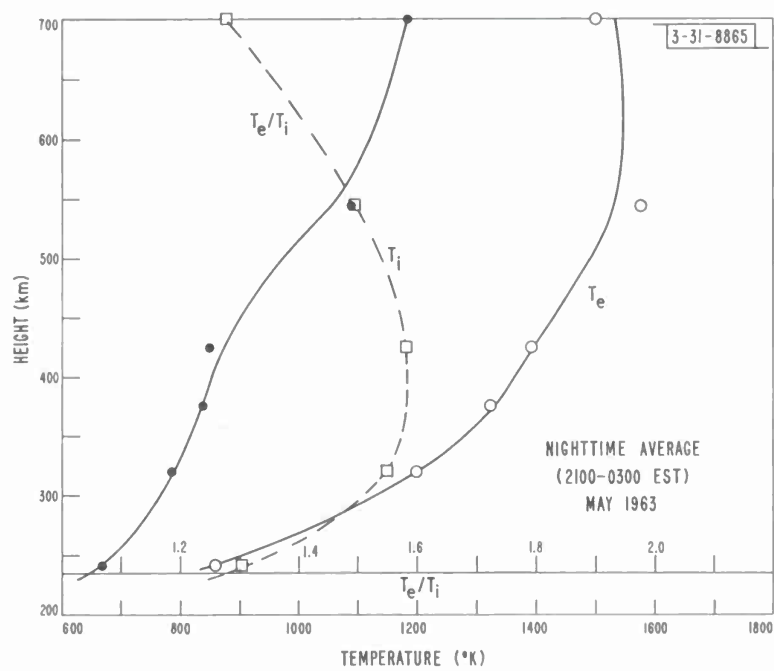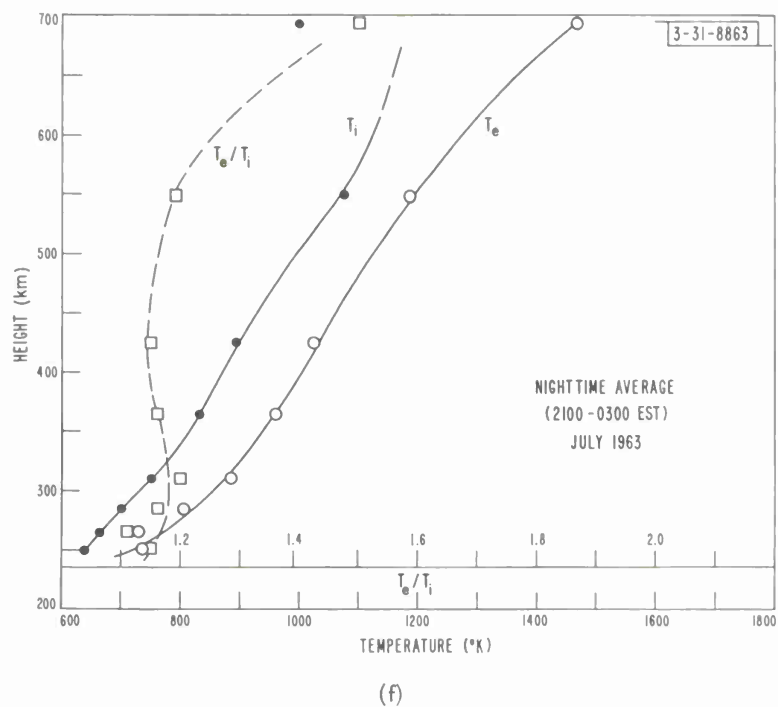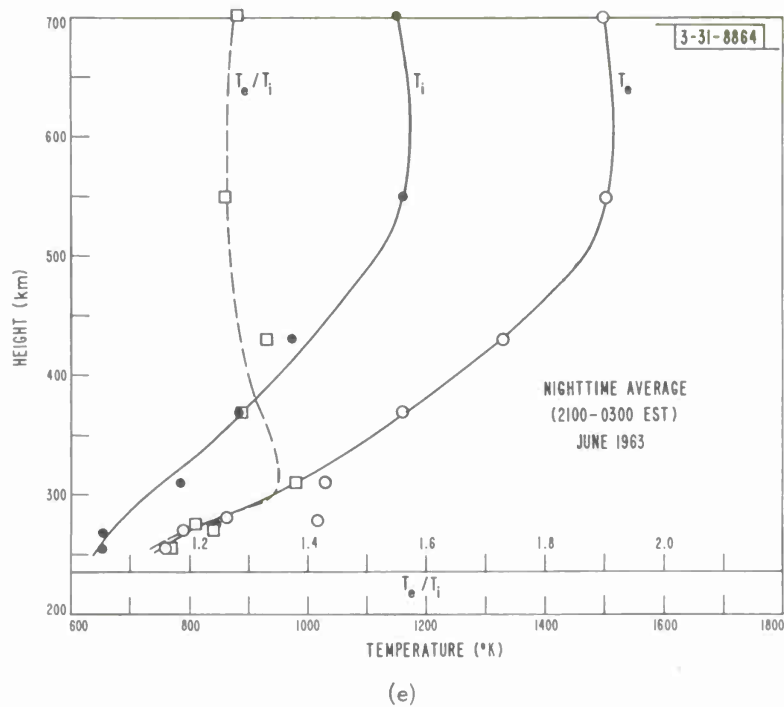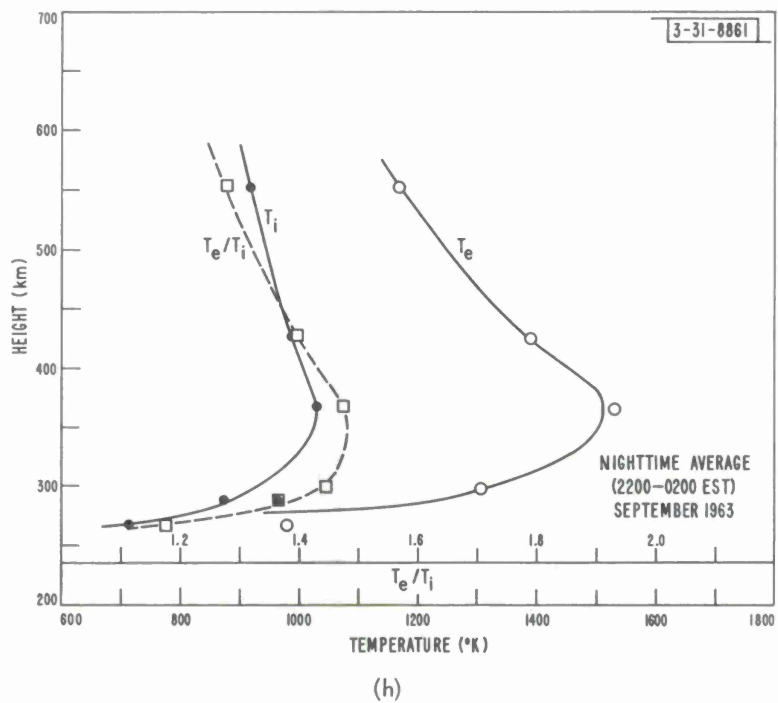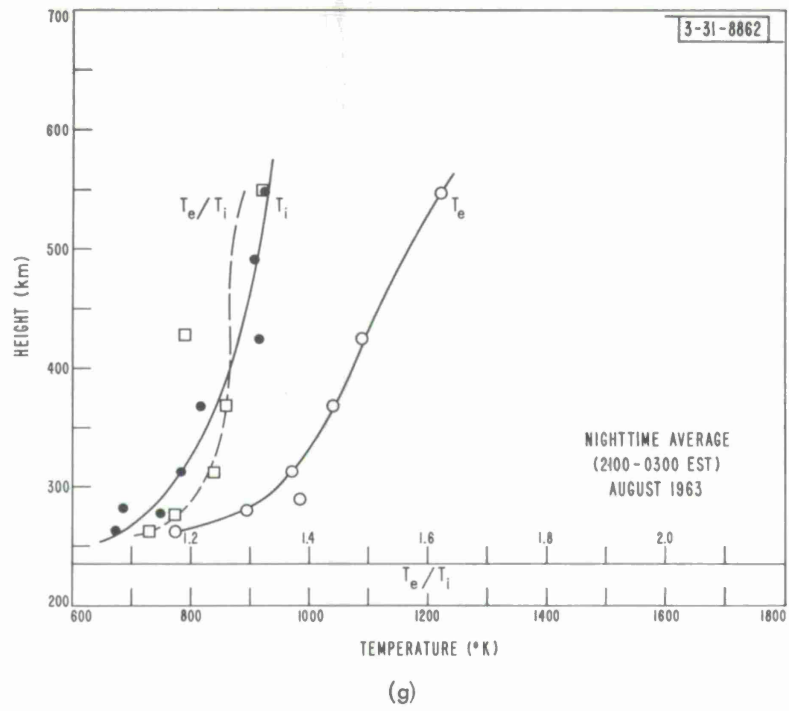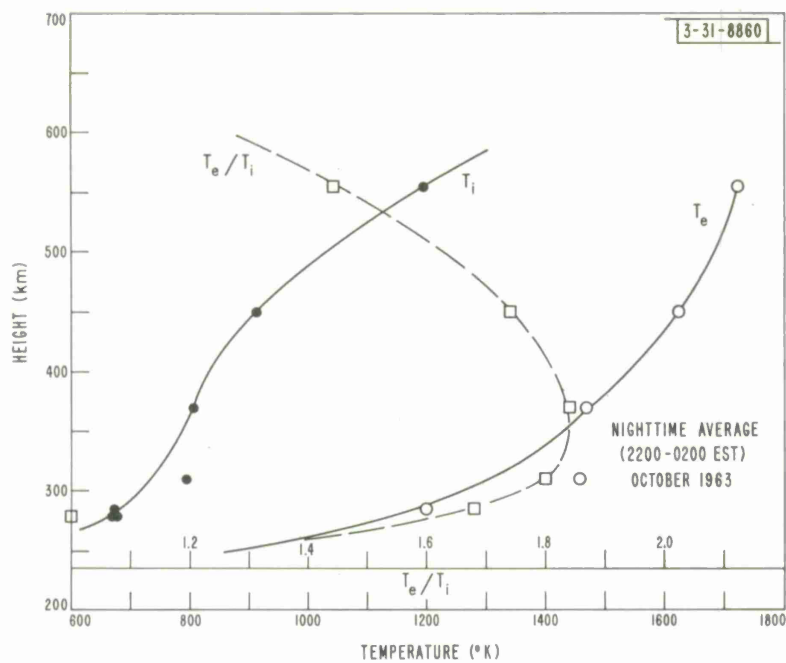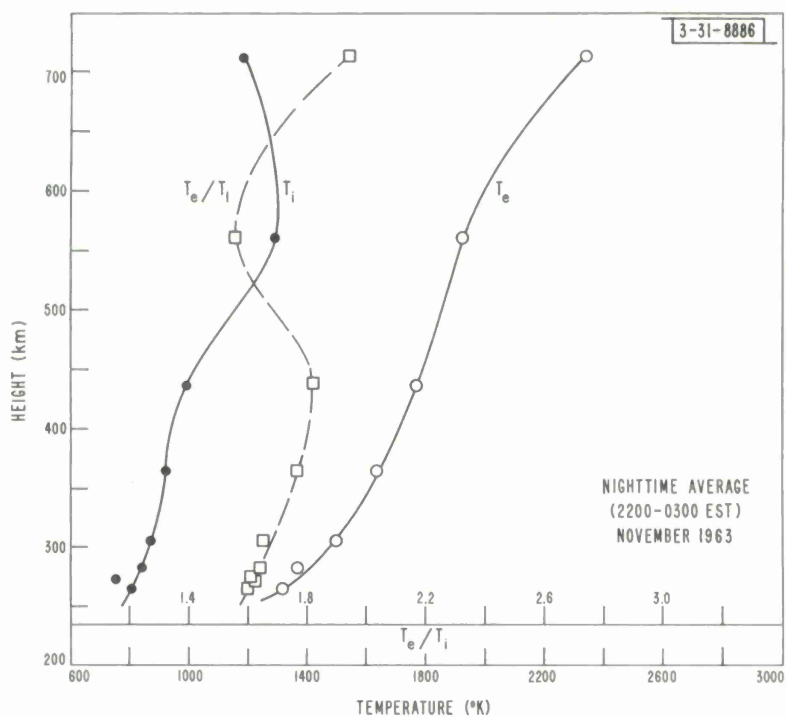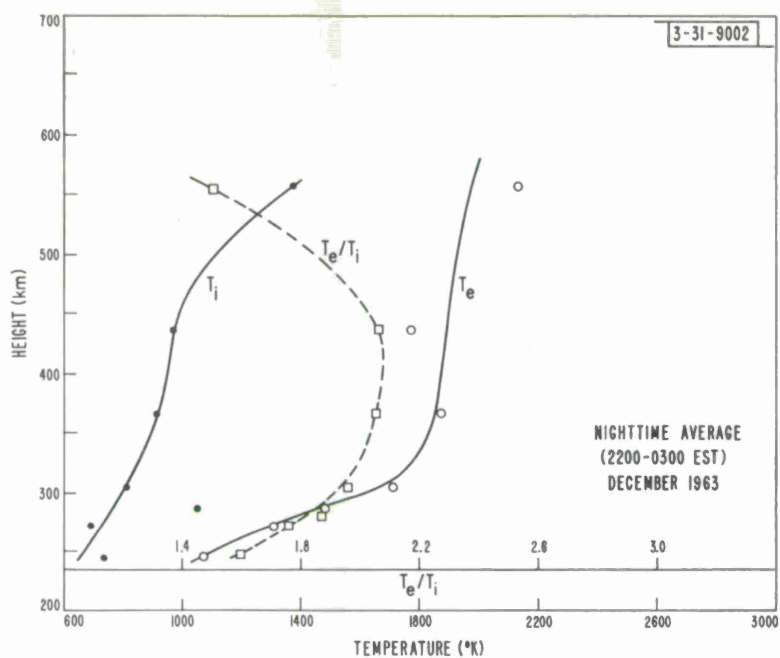
(k)

(l)

Fig. 23. Continued.

63
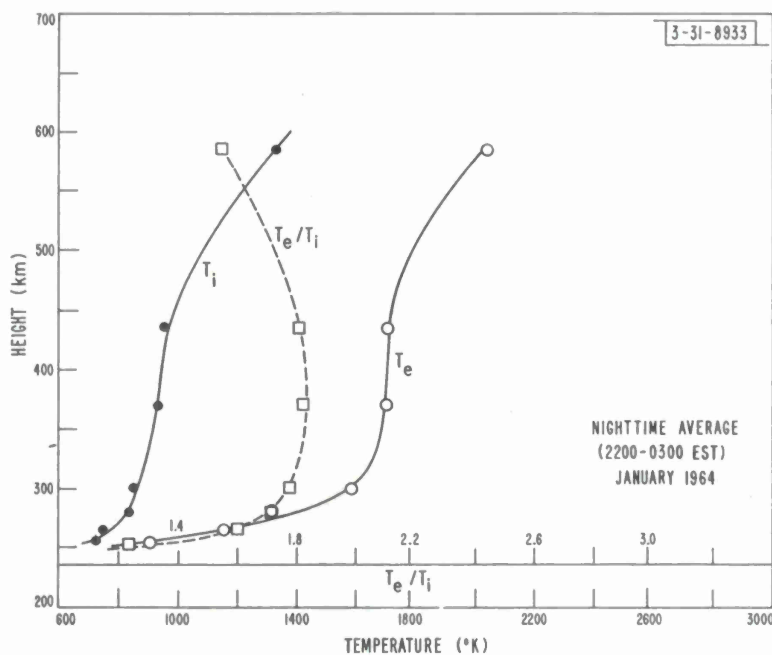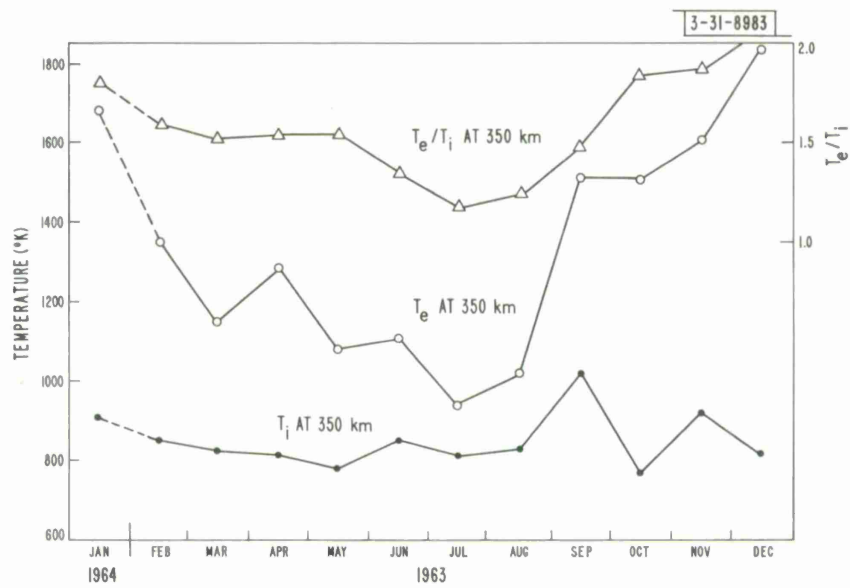
Fig. 24. Seasonal variations in nighttime T_i, T_e, and T_e/T_i at 350 km.
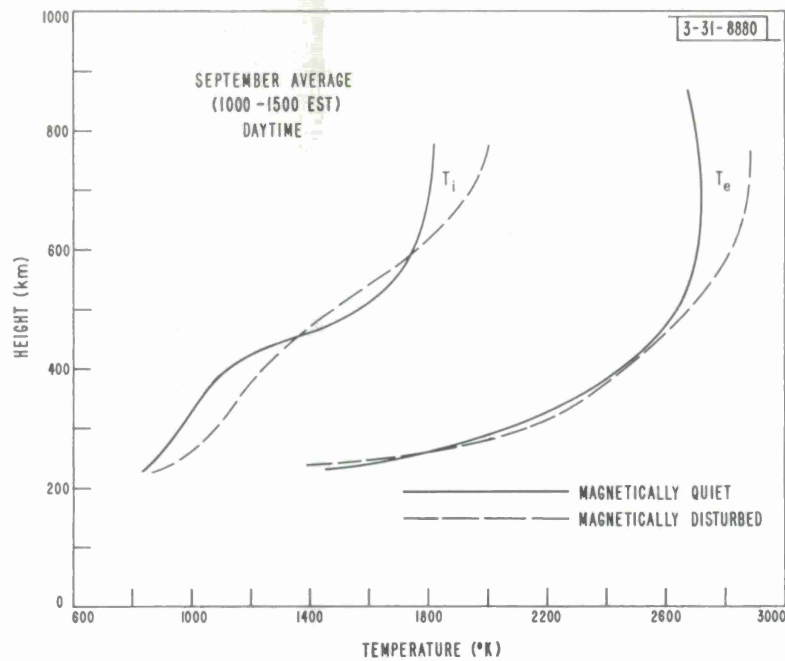
Fig. 25. Comparison of average height dependence of T_e and T_i on magnetically quiet days ($A_p \leqslant 14$) and disturbed days ($A_p \geqslant 19$) in September. As can be seen, there are no major differences.
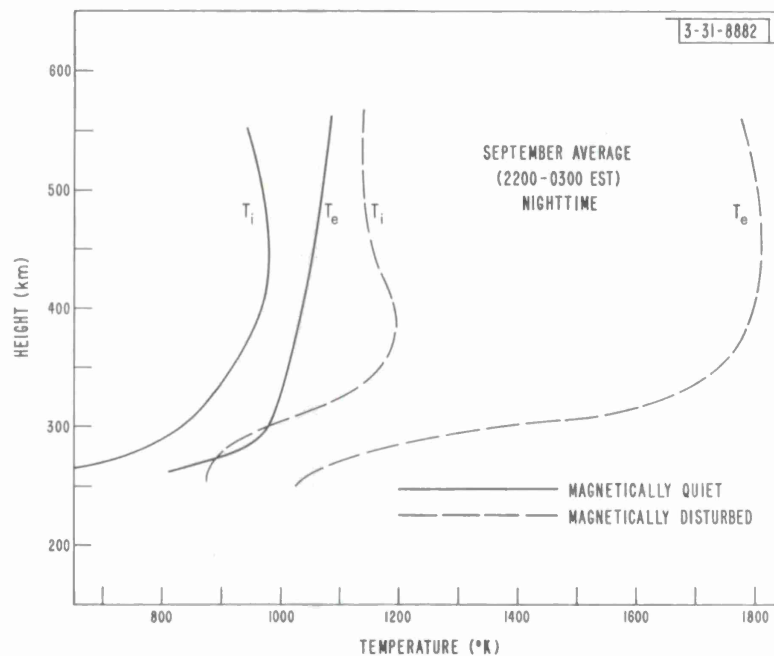
Fig. 26. Comparison of average height dependence of T_e and T_i on magnetically quiet nights ($A_p \leqslant 14$) and disturbed nights ($A_p \geqslant 19$) in September. At night, large increases associated with disturbed conditions occur in T_e and T_i.

65
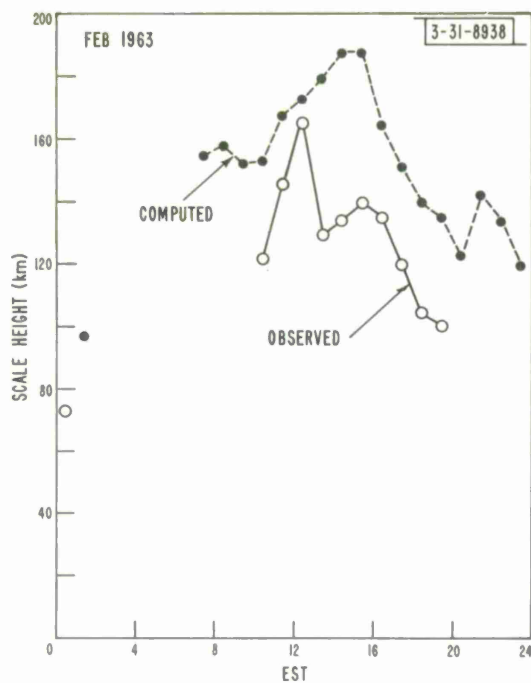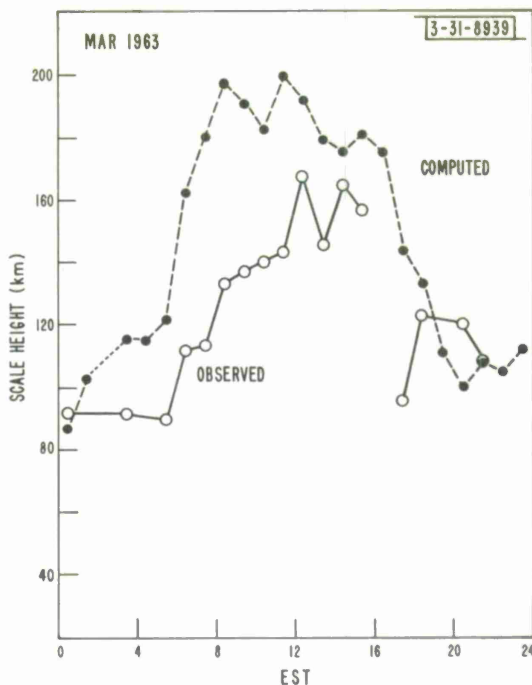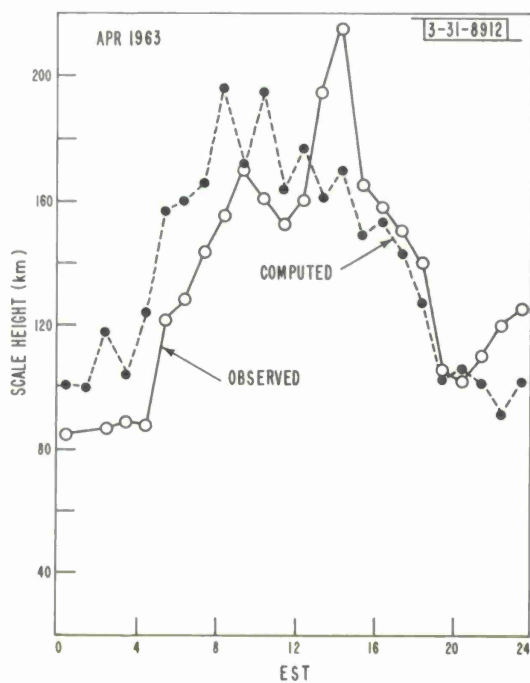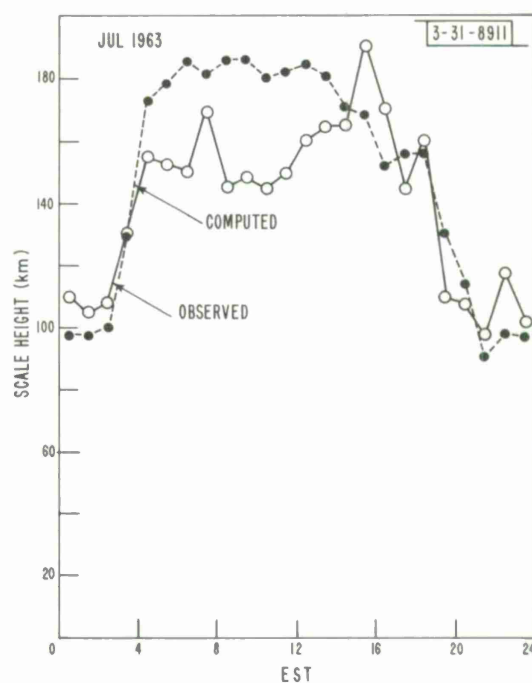
Figs. 27(a-j). Comparison of observed scale height of electron-density distribution at 400-km altitude with that computed from measured values of T_e and T_i, assuming any O^+ ions are present.
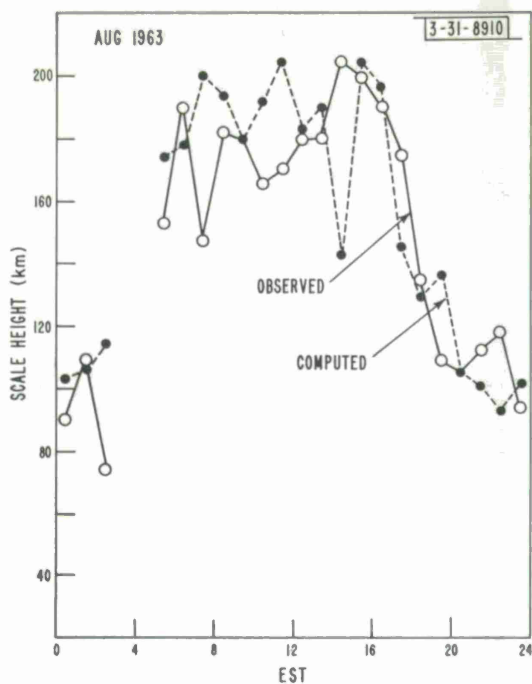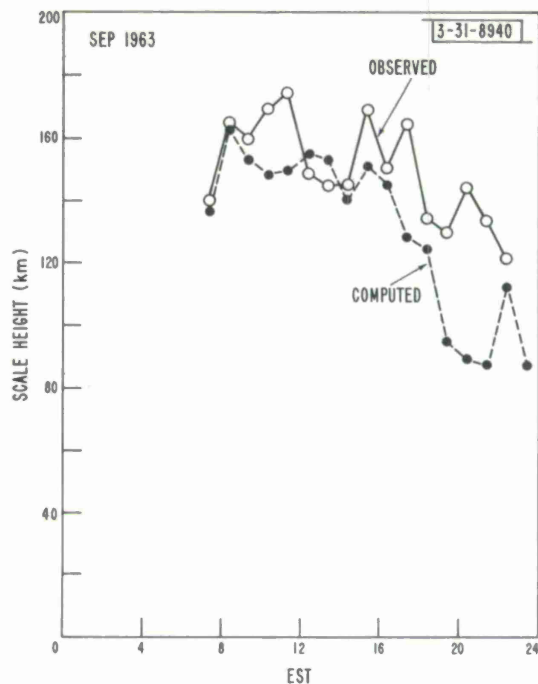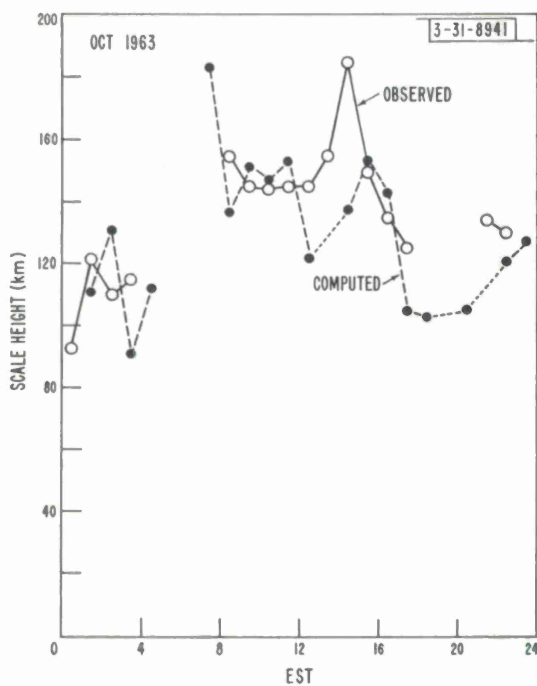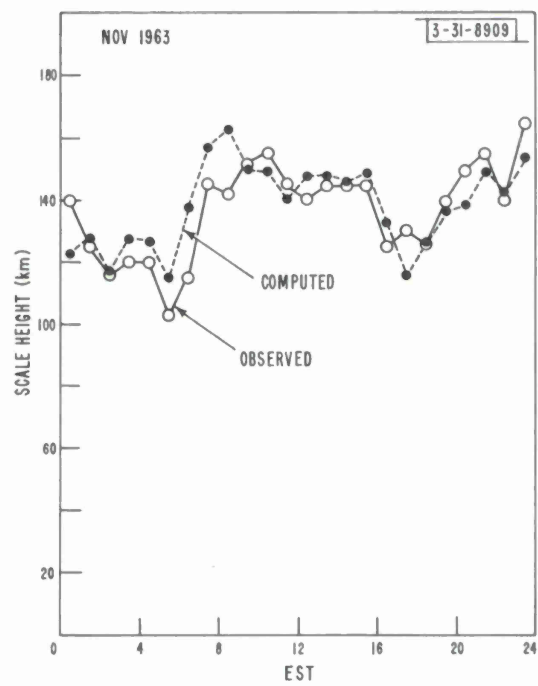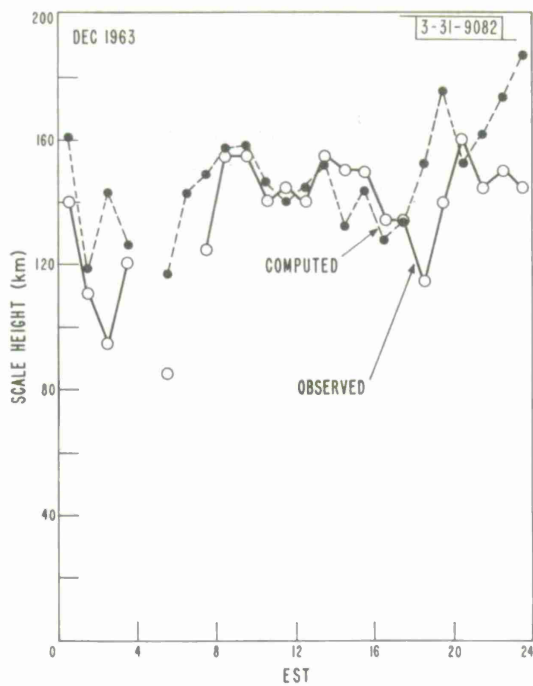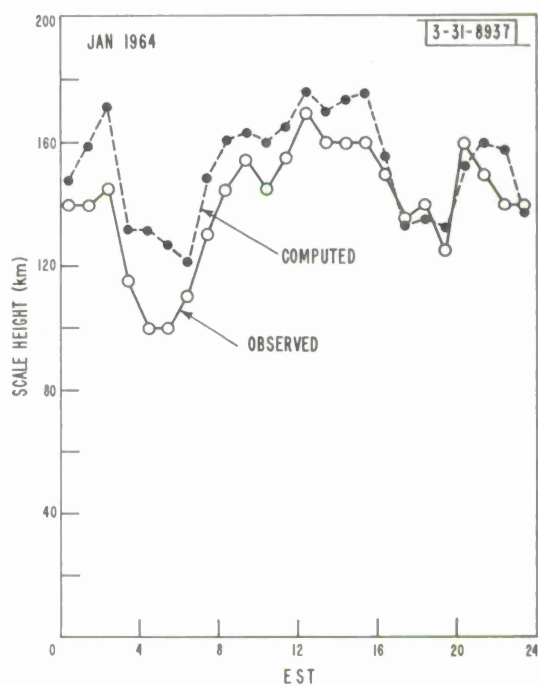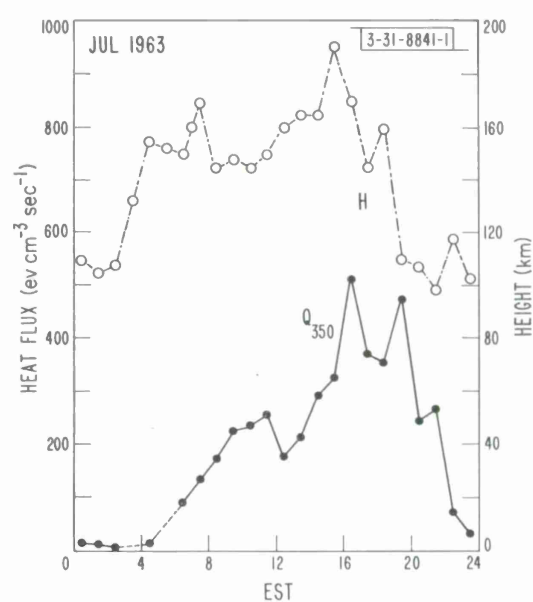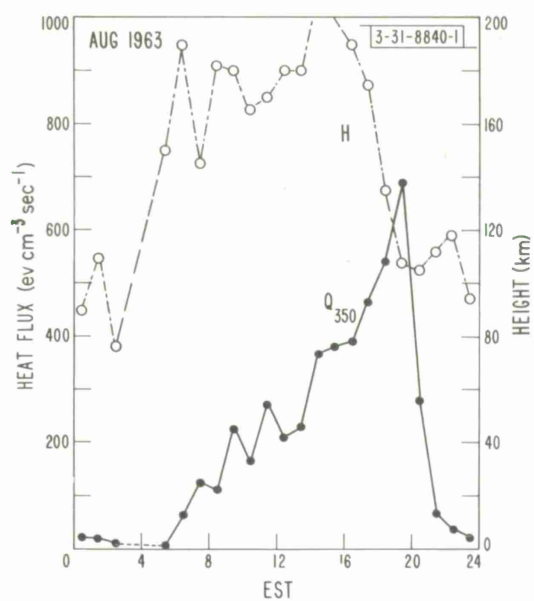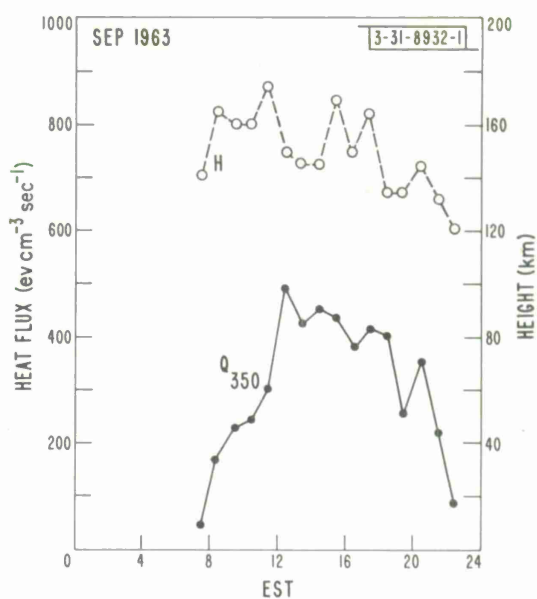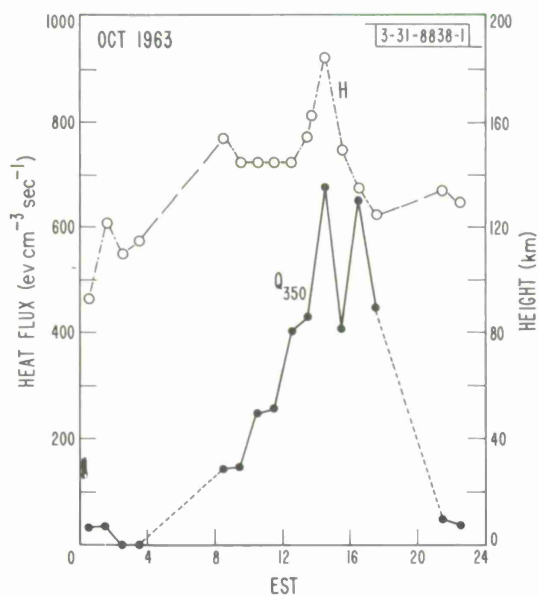
Fig. 27. Continued.
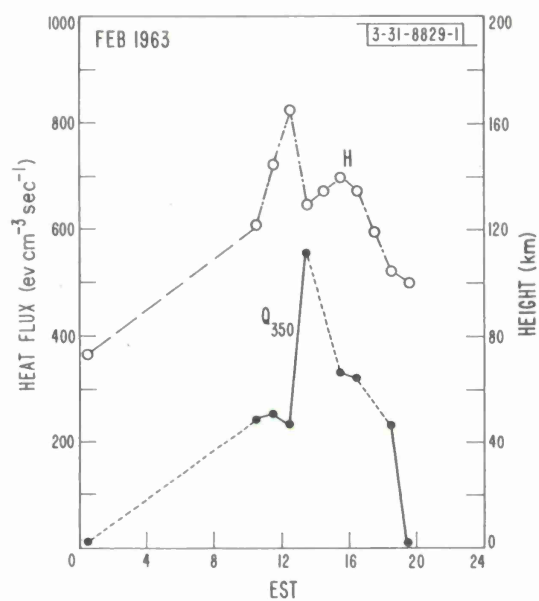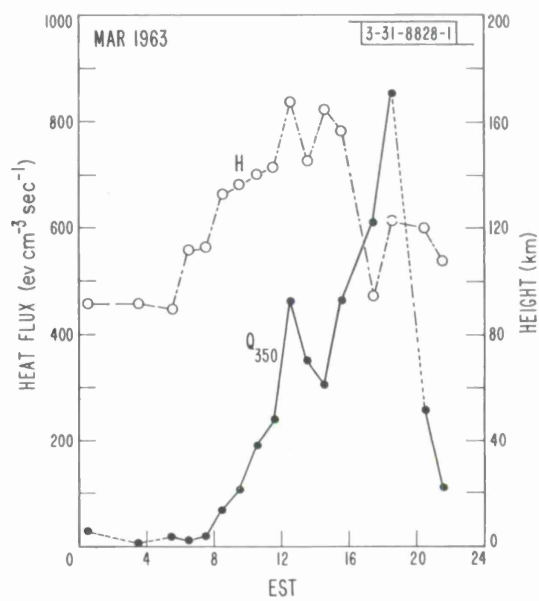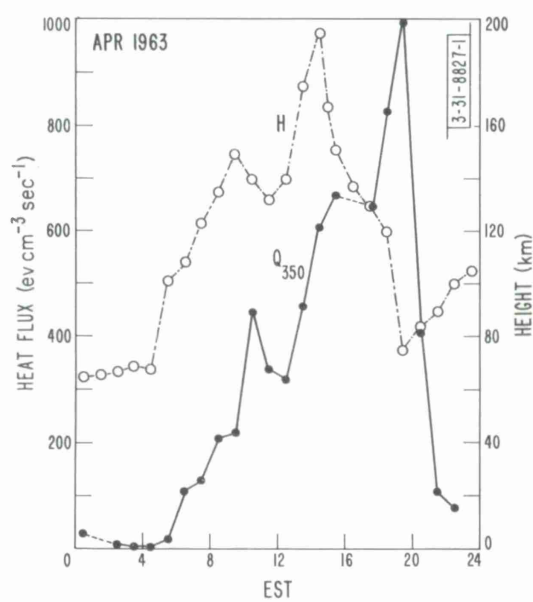
Fig. 27. Continued.

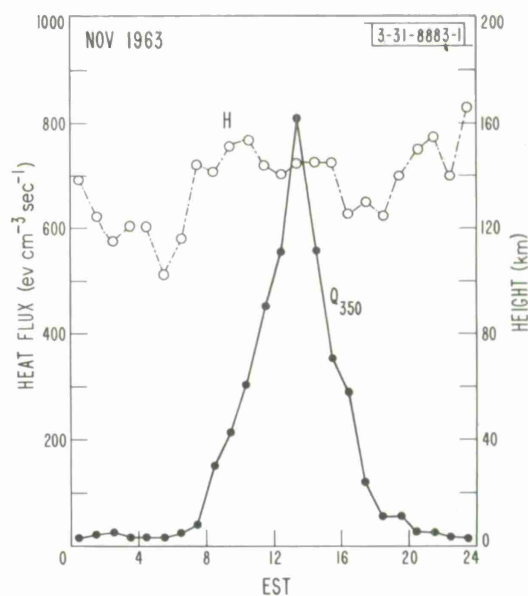Figs. 28(a-j).   Heat flux Q_{350} required to maintain temperature difference $T_e - T_i$ observed at 350 km.
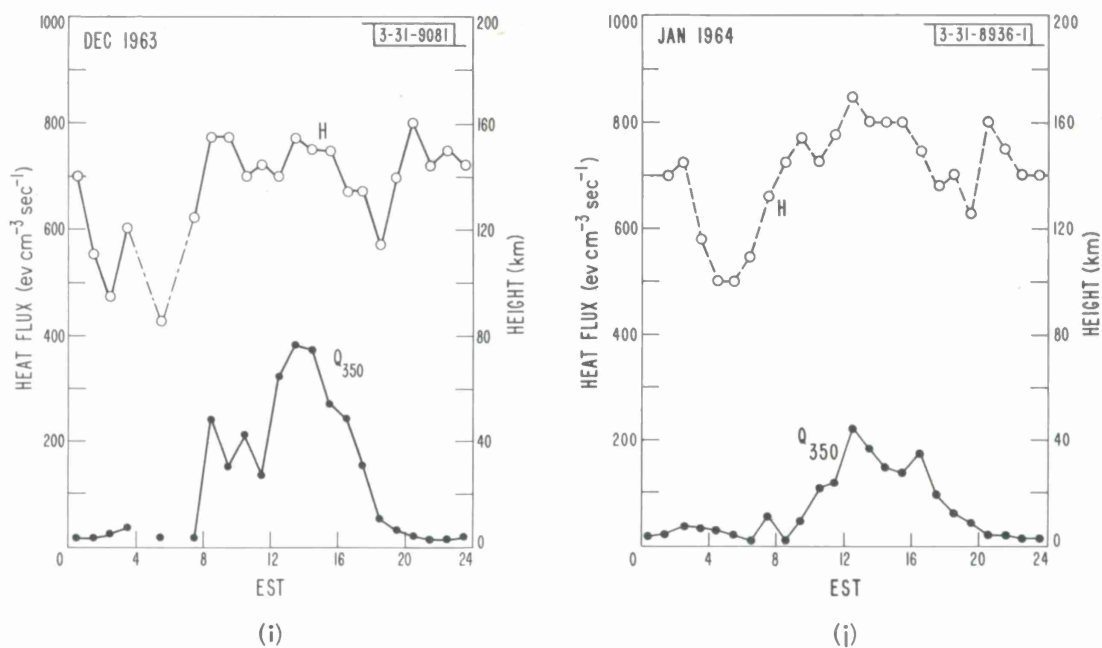
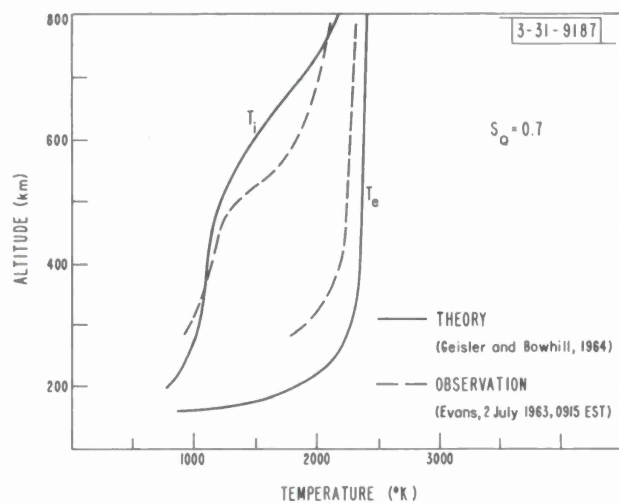Fig. 28. Continued.

Fig. 28.   Continued.

Fig. 29.   Comparison of temperature distribution with height shown in Fig. 11, with theoretical calculations by Geisler and Bowhill[60] for midday in summer at sunspot minimum.

DOCUMENT CONTROL DATA - R&D

(Security classification of title, body of abstract and indexing annotation must be entered when the overall report is classified)

1. ORIGINATING ACTIVITY (*Corporate author*)	2a. REPORT SECURITY CLASSIFICATION
Lincoln Laboratory, M.I.T.	Unclassified
	2b. GROUP
	None

3. REPORT TITLE

Ionospheric Backscatter Observations at Millstone Hill

4. DESCRIPTIVE NOTES (*Type of report and inclusive dates*)

Technical Report

5. AUTHOR(S) (*Last name, first name, initial*)

Evans, John V.

6. REPORT DATE	7a. TOTAL NO. OF PAGES	7b. NO. OF REFS
22 January 1965	76	94

8a. CONTRACT OR GRANT NO.	9a. ORIGINATOR'S REPORT NUMBER(S)
AF 19(628)-500	Technical Report 374
b. PROJECT NO.	
c. None	9b. OTHER REPORT NO(S) (*Any other numbers that may be assigned this report*)
d.	ESD-TDR-65-34

10. AVAILABILITY/LIMITATION NOTICES

11. SUPPLEMENTARY NOTES	12. SPONSORING MILITARY ACTIVITY
None	Air Force Systems Command, USAF

13. ABSTRACT

Studies of the electron-density, electron and ion temperatures in the F-region were made by means of ground-based radar observations at the Millstone Hill Radar Observatory. A 70-meter parabolic antenna directed vertically and a 2.5-Mw pulse radar operating at 440 Mcps were employed for these measurements.

Results of observations extending over a period of one year from February 1963 to January 1964 are presented. The ratio T_e/T_i achieved a maximum value $\sim$2.0 to 2.6 at a height of about 300 km soon after dawn, irrespective of the season. There was little change in height dependence in this ratio throughout the daylight hours, and at sunset the ratio fell with a time constant of the order of an hour. At night T_e/T_i was occasionally close to unity, but more often a significant difference remained in the temperatures at all heights. Ion temperature increased with height at all times, but above 500 km this may be due in part to the presence of an unknown amount of He^+ ions, which considerably affects the interpretation of the signal spectra. Electron temperatures were largely independent of height above about 300 km. Evidence is presented of ionospheric heating during magnetically disturbed conditions, but it is shown that this is only of great importance at night.

14. KEY WORDS

ionospheric scatter	signal-to-noise ratio	temperature effects
Millstone Radar	parametric amplifiers	heating
F-region	spectrum analyzers	
electron density	TR tubes	